DISSERTATION
submitted
to the
Combined Faculty for the Natural Sciences and Mathematics
of
Heidelberg University, Germany
for the degree of
Doctor of Natural Sciences

Put forward by

M. Sc.-Math.: Vladislav Olkhovskiy

Born in: Jekaterinburg

Oral
examination:..............................................................................................................

# Modeling and Simulation of the Aqueous Humor Flow for Healthy, Glaucomatous and Treated Eyes with Stokes and Darcy Equations

Advisor: Prof. Dr. Elfriede Friedmann

## Zusammenfassung

Im Alter erkranken manche Menschen an Glaukom. In einigen Fällen kann Glaukom zum Erblinden führen. Der Hauptfaktor für die Entwicklung des Sehverlustes ist der erhöhte Augeninnendruck und die Senkung des Augeninnendrucks ist im Moment die einzige Therapiemöglichkeit mit nachgewiesener Effektivität. Um das Verhalten des Kammerwasserflusses und des Augeninnendrucks in der Vorderkammer des menschlichen Auges zu verstehen, wird ein mathematisches Modell entwickelt. Das Modell ist durch Stokes und Darcy Gleichungen gegeben. Die Stokes-Gleichung beschreibt den Kammerwasserfluss in der Vorderkammer und die Darcy-Gleichung im Trabekelwerk, welches ein poröses Medium ist. Anhand der Darcy Gleichung wird der Druck im Trabekelwerk ermittelt. Dann wird der Mittelwert des Drucks im Trabekelwerk erfasst und als Robin Randbedingung in der Stokes Gleichung gestellt. Die charakteristischen Größen sind durch die Einflussrate des Kammerwassers am Ziliarkörper, den Druck der episkleralen Venen gegeben und es wird angenommen, dass die Cornea, die Augenlinse, die Iris und die Zonulafasern keine Flüssigkeiten durchlassen. Es werden Geometrien für gesunde, pathologische und behandelte Augen betrachtet. Die numerischen Simulationen mit der Finite Elemente Methode werden vorgestellt. In den Simulationen werden gemischte Finite Elemente verwendet und die Lösungen der Gleichungen mit der deal.ii Software ermittelt. Die Ergebnisse der Simulationen liefern Vorhersagen für medizinische Anwendungen wie Trabekulektomie, Stent-Einsatz beim Glaukom sowie Kataraktoperation. Außerdem werden spezifische Parametertests gemacht und es werden Abhängigkeiten zwischen der Änderung des Drucks und dem entsprechenden Parameterwert des Modells erfasst. Beispielsweise konnte mit dem Modell gezeigt werden, dass im Falle der partiellen Verstopfung des Trabekelwerks und eines Ausgangsaugeninnendrucks von 28.37 mmHg und einer Trabekulektomie in dem verstopften Abschnitt der Augeninnendruck um 18.32% gesenkt werden kann. Außerdem wird anhand des Modells ein linearer Zusammenhang zwischen dem Augeninnendruck und dem episkleralen Venendruck gewonnen.

# Abstract

In old age some people fall ill with glaucoma. In some cases glaucoma can lead to blindness. The primary risk factor for the development of the vision loss in glaucoma is an increased intraocular pressure (IOP) and lowering the IOP is currently the only therapeutic option with proven efficiency. To understand the behavior of the aqueous humor flow and of the IOP in the anterior chamber of the human eye, a mathematical model is developed. This model is given by Stokes and Darcy equations. The Stokes equation describes the aqueous humor flow in the anterior chamber and the Darcy equation describes the pressure in the trabecular meshwork which is a porous medium. With the help of the Darcy equation the mean pressure value in the Darcy domain is computed. This mean pressure value is incorporated into the Robin boundary condition of the Stokes equation. The characteristic physical properties are given by the inflow rate of the aqueous humor at the ciliary body, the pressure of the episcleral veins and it is assumed that the cornea, the lens, the iris and the zonules are impermeable. Geometries for healthy, pathological and treated eyes are considered. Numerical simulations using the Finite Element method are performed in three dimensions. In the computation, mixed finite elements (e.g. Taylor Hood finite elements for the Stokes equation) are used and the solutions of the equations are generated with deal.ii software. The simulations cover the dependence of the IOP to specific changes of certain model and geometric parameters. Moreover, medical applications concerning IOP changes due to cataract surgery, stent insertion as well as trabeculectomy are discussed. For instance, the model shows a postoperative decrease in IOP about 18.32% in a case of partial occlusion of the trabecular meshwork and the initial IOP of 28.37 mmHg. In addition, the model illustrates linear dependence between the episcleral venous pressure and the IOP.

## Mathematical novelty

In this thesis, a mathematical model is developed. This model is given by Stokes and Darcy equations. The Stokes equation describes the aqueous humor flow in the anterior chamber and the Darcy equation describes the pressure in the trabecular meshwork. With the help of the Darcy equation the mean pressure value in the trabecular meshwork is computed. This mean pressure value is incorporated into the Robin boundary condition of the Stokes equation. Then, the Stokes equation is solved and the mean intraocular pressure is determined. The characteristic physical properties are given by the inflow rate of the aqueous humor at the ciliary body, the pressure of the episcleral veins and it is assumed that the cornea, the lens, the iris and the zonules are impermeable. The existence and uniqueness of solutions of the model is shown. Theory about finite elements and discretization concerning Stokes and Darcy equations is adapted to the model.

# Contents

# Introduction

With the help of the eyes humans perceive upwards of 70% of information (e.g., reading and studying, enjoying the beauty of nature, communication with facial expressions). Thus, good vision and healthy eyes are significant for the quality of living. Since the age of Babylon people have been starting to develop methods to heal eye diseases. One of the eye diseases is glaucoma. Quingley [QB06] and Tham [TLW$^+$14] estimate that worldwide there were approximately 60.5 million people with glaucoma in 2010, increasing to 79.6 million by 2020 and to 111.8 million by 2040. Glaucoma is a disease that damages the optic nerve and leads to blindness. The damage of the optic nerve can be a consequence of elevated pressure within the eye, a neurodegenerative disease or other diseases in the body. This thesis considers glaucoma connected with elevated pressure within the eye, since it is seen as the primary risk factor for the development of the vision loss and lowering of the pressure within the eye (which is called intraocular pressure (IOP)) is currently the only therapeutic option with proven efficiency (see for example [HLB$^+$02]). To understand the reasons for the increased IOP, the flow of the aqueous humor in the anterior chamber and the trabecular meshwork will be studied. There are *several models describing the flow through the the anterior chamber and the trabecular meshwork.*

In [FO$^+$14] the aqueous humor flow in the anterior chamber is modeled using Navier Stokes - Darcy coupling. In this article, the influence of the aqueous humor production rate on the IOP as well as of the aqueous humor drainage on the IOP is considered. Moreover, drug delivery through the cornea from a therapeutic lens to the anterior chamber of the eye is modeled. The last model consists of three coupled systems of partial differential equations linked by interface conditions: drug diffusion in the therapeutic lens; diffusion and metabolic consumption in the cornea; diffusion, convection and metabolic consumption in the anterior chamber of the eye. The simulations are performed in two dimensions.

In [VR$^+$12] a 3D computational fluid dynamic model of the eye based on the anatomy of a real human eye is presented. This model is based on stacks of micrographs from human eye slides from which digital processing of the images of the eye structure and 3D reconstruction of the model is performed. The following model is based on the Navier Stokes equation and Boussinesq approximation for temperature in the anterior chamber and on the Darcy equation in the trabecular meshwork. Glaucoma surgery cases are also considered. Trabeculectomy is modeled as a hole of $400\mu$m in diameter located in the irido-corneal angle in the anterior chamber. Moreover, insertion of glaucoma drainage implants ExPRESS$^{\text{TM}}V50$ (Ex-PRESS, Alcon Inc.) is also considered. The simulations are performed with ANSYS CFX. The simulation results are compared with experimental data. In this article, no mathematical proof for correctness of the computation is shown.

In [CE13] computational results for the pressure in the anterior chamber and the trabecular meshwork of a human eye are presented. The fluid flow is assumed to be axisymmetric and modeled as a coupled system of the Stokes and Darcy fluid flow equations, representing the flow in the anterior chamber and in the trabecular meshwork, respectively. In this paper, the 3D problem in cylindrical coordinates is reduced to the problem in 2D. Furthermore, computations for varying angles between the base of the iris and the trabecular meshwork are given. The limit of this model is the prescribed outflow condition of the aqueous humor.

In [Kum03] numerical simulations of the aqueous humor dynamics in the anterior chamber of the human eye are presented. The basic flow and transport mechanisms are delineated. The geometry of the anterior chamber is given by a part of a sphere, the natural lens by a half-ellipsoid, the cornea by a rigid shell and the iris is modeled as a rigid elliptical disc of uniform thickness with a circular hole. The model is given by steady three-dimensional incompressible Navier-Stokes equations with the inclusion of buoyancy terms for natural convection and Darcy pressure drop terms in the porous zone. The density appearing in the buoyancy term is assumed to satisfy the Boussinesq approximation. Healthy case, angle closure glaucoma, pupillary block and iridectomy are considered.

There are also *further works dealing with fluid mechanics in the human eye*. In [CG02] and in [ADF06] the buoyancy-driven flow arising from the temperature difference between the anterior surface of the cornea and the iris is considered. The authors use Boussinesq model to describe the aqueous humor flow. Using non-dimensionalization technique, the model is simplified and analytic solutions for the simplified equations are computed. In [ON07] the effect of the aqueous humor flow on the temperature distribution inside the eye is investigated. In [MH07] the aqueous humor outflow resistance in the juxtacanalicular tissue (JCT) of the human eye is studied. In that work, JCT is treated as a heterogeneous tissue with a variable permeability. Further aspects are studied in [HBT02], where passive mechanical interaction between the aqueous humor and the iris is modeled and in [AS06], where aqueous humor outflow through the trabecular meshwork is described. In [AS06] a strain-dependent permeability function is incorporated into Darcy's law which is coupled to the force balance for the bulk material.

In [MAGA14] , the physiology of aqueous humor dynamic in the anterior chamber due to rapid eye movement (REM) is considered. Here, a harmonic model for the REM was developed and a dependence between REM amplitudes and velocity is shown. In [WO16], the fluid and structure coupling of the interaction between the aqueous humor and iris is analyzed.

In this thesis, the aqueous humor flow in the anterior chamber is described. The flow and pressure distribution in the anterior chamber is modeled with the help of Stokes and Darcy equations. The Stokes equation describes the flow in the anterior chamber and the Darcy equation describes the flow in the trabecular meshwork. The characteristic physical properties are given by the inflow rate of the aqueous humor at the ciliary body, the pressure of the episcleral veins and it is assumed that the cornea, the lens, the iris and the zonules are impermeable. In the current moment, it is the first finite element simulation in 3D for the aqueous humor flow in the anterior chamber based on sound mathematical approach. Moreover, it is an alternative model to Stokes-Darcy model with a Beavers Joseph Saffman condition on the interface. In this thesis, the Darcy equation is solved first. Then, the mean intraocular pressure in the trabecular meshwork is computed. Afterwards, this mean value is incorporated in the Robin boundary condition of the Stokes equation and the Stokes equation is solved afterwards. This coupling strategy answers the question about how the resistance of the pores in the trabecular meshwork influences the IOP in the anterior chamber. This question is very common in literature (in particular in medicine and engineering) and this thesis gives an answer from the mathematical point of view. Furthermore, parameter dependence between the IOP and different model parameters like the episcleral venous pressure, the viscosity of the aqueous humor, the production rate of the aqueous humor, the permeability of the trabecular meshwork, the thickness of the lens, the radius of the pupil opening as well as the position of the body are shown. Moreover, the model covers the change of the IOP after scleral lens wear as well as surgical interventions like trabeculectomy, insertion of stents and cataract surgery. The following thesis has the following *structure*. In section two medical background is introduced. The structure of the eye is discussed, the flow path of the aqueous humor flow is illustrated. In this section, glaucoma with possible treatment options is mentioned. In the third section, mathematical notation and function spaces are repeated. In the forth section a mathematical model is derived and described. Fifth section deals with the well posedness of the model and the existence and uniqueness of solutions of the model equations. Moreover, concepts of the Finite Element method are presented and the Finite Element method is applied to the model. Section six describes the geometry, the implementation of the model and the medical applications (trabeculectomy, cataract surgery and the effect of specific parameters on the IOP).

# 1 Medical background

This chapter gives a summary of medical knowledge to understand the model of this thesis. First, the structure of the eye is explained. This section shows how main parts of the eye are interacting to maintain vision and how they are positioned inside of the human eye. Next, aqueous humor flow is illustrated. In particular, the path of the aqueous humor flow is described and characteristics and function of aqueous humor are presented. Then, the structure of the trabecular meshwork is considered. This chapter ends with glaucoma and therapeutic methods for healing glaucoma. Especially, changes of the characteristics of the trabecular meshwork are considered during glaucoma.

## 1.1 Structure of the Eye

The detailed description of the structure and physiology of the human eye can be found in [Lev11]. In this section, only basic terminology is introduced. The eye is an organ which is capable of transducing photons into neural signals. The eye consists of the anterior chamber, the posterior chamber and the vitreous chamber. 1/6th of the total surface of the eye (which is also a surface of the anterior chamber) is covered by a clear, transparent skin called cornea and the remaining 5/6th of the surface area are covered by a white, opaque sclera [Lev11]. The cornea is one of the eye's refractive structures and it has two key optical properties - light refraction and light transmission [Lev11]. The sclera serves more of a biomechanical function and is analogous to the housing of the camera and lens [Lev11]. The iris lies at the border between the anterior and the posterior chamber. The iris is a thin, circular structure of the eye controlling the size of the pupil and consequently the amount of light reaching the retina. Behind the iris, there is the lens. The lens is a transparent ellipsoidal structure in the eye helping to refract light to be focused on the retina. The lens functions to change the focal distance of the eye so that it can focus on objects at various distances, thus allowing a sharp real image of the object of interest to be formed on the retina. This adjustment of the lens is known as accommodation [Lev11]. The space between the lens and the retina of the eyeball is called vitreous chamber. The vitreous chamber is filled with a transparent, colorless, gelatinous gel called the vitreous humor. The vitreous humor is stagnant. Thus, if blood cells or other byproducts of inflammation get into it, they will retain there. In contrast to the vitreous humor, the fluid in the anterior chamber (which is called the aqueous humor), is continuously replenished. The aqueous humor is described in the next section.

## 1.2 Aqueous humor flow

The aqueous humor is a clear, colorless fluid consisting of 98 % of water, $0.5 - 1\%$ of proteins as well as other organic and inorganic ions, amino acids, oxygen, carbon dioxide, carbohydrates, urea [FJ09]. Its density is given by $\rho = 1\text{g/cm}^3$ and its kinematic viscosity by $\nu = 70 \cdot 10^{-6}\text{m}^2/\text{s}$ [FJ09]. The aqueous humor flow performs different physiological functions. On the one hand, the positive pressure that it generates ensures accurate positioning of the optical elements of the eye and hence clarity of vision. On the other hand, aqueous humor supplies nutrients and removes waste products from the avascular lens and the central cornea. [SE11] The aqueous humor originates in the ciliary body and flows along the iris through the pupil into the anterior chamber. The amount of aqueous humor secretion in the ciliary body is approximately $2.5\,\frac{\text{mm}^3}{\text{min}}$ according to [PW17]. The major part of the aqueous humor flow (which is about 85% of the aqueous humor) drains from the anterior chamber via the trabecular meshwork (which is called the conventional outflow) [JT10]. Because the flow is not able to traverse the intact iris [FJ09], the other part of the flow circulates along the iris and flows through the pupil into the posterior chamber. Some of the aqueous humor (about 10%) leaves through ciliary body and some of the aqueous humor penetrates zonules (about 5%) and enters the vitreous chamber (unconventional outflow). The aqueous flow is driven by a gradient of hydrostatic pressure between the eye and the episcleral veins [FJ09]. The production of aqueous humor flow is dependent on the circadian rhythm. In the night, the production of the aqueous humor is reduced by 40 percent. Otherwise, the aqueous humor production maintains constant [Gre12]. In this thesis, the focus lies on the outflow via the trabecular meshwork. Thus, the next section will introduce this structure of the eye in more detail.

## 1.3 Trabecular meshwork

The trabecular meshwork consists out of three tissues: uveal meshwork, corneoscleral meshwork and the juxtacanalicular meshwork. The uveal meshwork is formed by prolongation of connective tissue arising from the iris and ciliary body stromas [LGG03a]. It is consisting of a set of beams organized into an irregular netlike structure [FJ09]. The uveal meshwork is a porous structure with numerous openings varying in size between 25 and 75 $\mu$m [JT10]. The corneoscleral meshwork extends from the uveal meshwork ca. 100 $\mu$m in the direction of flow towards Schlemm's canal. The corneal meshwork consists of a number of interconnected sheets. These sheets, like the cores of the uveal meshwork beams, have an avascular core of collagen and elastin [FJ09]. Due to large intracellular spaces of uveal and corneoscleral meshworks the aqueous humor resistance in these regions is low [LGG03b] and may be neglected in the model.
Juxtacanalicular meshwork is also known as endothelial meshwork or cribriform region. It has large, apparently empty spaces and is typically 2 to 15 $\mu$m thick [JT10]. The cells

of this region are fibroblast in appearance, but are not determined yet. Juxtacanalicular meshwork is composed of a loose connective matrix which is porous under typical flow conditions. Its extracellular matrix consists of collagen, elastin, glycoproteins and proteoglycans [FJ09]. Juxtacanalicular meshwork might cause significant resistance, however it is not supported by hydrodynamic considerations, see [SE11] and the references therein. Bulk of the aqueous humor pressure drop occurs near the inner wall of Schlemm's canal, but no further quantitative conclusions are possible [JT10]. If the pores in the trabecular meshwork are obstructed, the IOP increases. The increase of IOP might lead to glaucoma.

## 1.4 Glaucoma

Glaucoma is a group of eye diseases which result in damage to the optic nerve with respective effects in the visual field [Gre12]. The increased intraocular pressure is considered as the primary risk factor for glaucoma. The intraocular pressure is created by the aqueous humor flow and the outflow is adjusted in the trabecular meshwork. The normal intraocular pressure is $15.5 \pm 2.75\,\mathrm{mmHg}$ meaning that the normal values amount to the range between 10 and 21 mmHg [Gre12]. There are primary glaucoma and secondary glaucoma. Primary glaucoma occurs spontaneously. Secondary glaucoma is a consequence of other eye diseases or generalized diseases. About 90 percent of primary glaucoma are open angle glaucoma, less than 5 percent are closed-angle glaucoma.

This chapter is structured as follows. Firstly, the consequences of increased intraocular pressure (IOP) are described. Then, different types of glaucoma are explained. In the end of the chapter, therapies are discussed.

### Consequences of increased IOP

To understand one of the principles how glaucoma occurs, retinal ganglion cells are introduced. Retinal ganglion cell is a type of neuron located near the inner surface of the retina of the eye. The retinal ganglion cell receives information from photoreceptors and transmits image-forming and non-image forming visual information from the retina to several regions in the human brain. If these cells die, people loose eyesight. There are multiple theories explaining how the elevated intraocular pressure causes the death of retinal ganglion cells (see [SE11] and the references therein). The following mechanism is shown in [AH74], [BMB+07] and [MBJ77]. Retinal ganglion cells require axonal transport, a cellular process for movement of mitochondria, lipids, vesicles and proteins, to remain viable. During this cellular process the vesicles are transported along the nerve fibers, named axons, by motor proteins. These motors require energy for their task. Their energy is coming from adenosine triphosphate (ATP) molecules, which are released from mitochondria located along the axon. ATP is distributed along the axon

by a combination of diffusive and, in the presence of the flow, convective effects. If the supply of ATP is sufficiently depleted then active axonal transport will be reduced or stopped. Without enough supply ganglion cells die.
In some cases the reason for glaucoma lies in the low blood circulation in the optic nerve or a disparity between the blood flow in the optic nerve and the intraocular pressure. The disproportion of the aqueous humor generation and outflow is common for all types of glaucoma. In this thesis it is differentiated between primary open-angle glaucoma, primary closed-angle glaucoma and secondary glaucoma.

### Primary open-angle glaucoma

Primary angle glaucoma is a slowly progressive, in most cases bilateral eye disease of an older individual. The characteristic symptoms are optic disk cupping, restrictions in the visual field and an open iridocorneal angle. In the case of primary open-angle glaucoma, the trabecular meshwork is clogged up with plaque material. Thus, the aqueous flow resistance elevates and the intraocular pressure increases, see [SE11] and [Gre12]. When the intraocular pressure is lower than 21 mmHg and there are restrictions in the visual field, an open iridocorneal angle and optic disk cupping, the disease is called normal-tension glaucoma.

### Primary closed-angle glaucoma

During primary closed-angle glaucoma the iris moves anteriorly from its normal position reducing or eliminating the gap between it and the cornea. This can lead to a complete occlusion of the outflow with attendant dramatic increases of IOP [SE11]. There are different types of closed-angle glaucoma. If there is an acute shift of the iridocorneal angle generated by the basis of the iris, closed-angle glaucoma is called acute closed-angle glaucoma. Characteristics are a closed iridocorneal angle and relatively large lens, which is typical for older individuals. Predisposition for this glaucoma can be observed by

- flattening of the anterior chamber
- narrow iridocorneal angle
- bulged iris

Pupillary block is also a common reason for closed-angle glaucoma. It occurs in the case of flattening of the anterior chamber and if the back of the iris is lying tense to the lens. In this case, the flow of the aqueous humor through the pupil is blocked. Thus, there is a pressure drop between the posterior chamber and the anterior chamber. Further types of closed angle glaucoma can be found in [PW17] and [Gre12]. The review of scientific research in primary closed angle glaucoma can be found in [SDC+17].

### Secondary glaucoma

Secondary glaucoma is a consequence of other eye diseases or generalized diseases. Like in primary glaucoma, the increasing intraocular pressure and obstructions of the flow in the trabecular meshwork are the main factors for its cause. Classification of possible secondary glaucoma can be found in [PW17] and [Gre12]. Most glaucoma types are open angle glaucoma. Thus, therapeutic options for open angle glaucoma are considered here.

### Therapies

The only known efficient therapeutic option in open angle glaucoma is to decrease the intraocular pressure. There are three possibilities to realize it [Gre12]:

- Treatment with medication
- Treatment with a laser (laser trabeculoplasty)
- Surgical intervention (trabeculectomy, shunt implantation, micro-invasive glaucoma surgery)

According to European guidelines [EGS17], the first choice of an ophthalmologist is the treatment with medication [HARCH19b]. In more severe cases, laser trabeculoplasty is often completed alongside or after medications ([HARCH19b] and citations therein). In later stages of the disease, surgical interventions like shunt implantation or trabeculectomy are considered [SB11], [HARCH19b]. Common medication for glaucoma are eye drops. Eye drops can reduce the generation of the aqueous humor or they can lower the outflow resistance of the trabecular meshwork. In particular, eye drops are often used to treat chronic primary closed-angle glaucoma. You can find a list of medicaments for glaucoma treatment below [Gre12], [TRS13]:

1. Medicaments to force miosis of the pupil: Pilocarpin, Glaucotat etc.
2. Medicaments to reduce the aqueous humor production:
   - for Beta-blockers (Timolol, Propranolol) preparations like Arutimol, Chibrotimoptol, Betaman are used.
   - for Adrenalin derivates D-Epifrin can be used.
   - for the local carbonic anhydrase inhibitors Trusopt is used.
   - for combinations between Beta-blockers and carbonic anhydrase inhibitors Cosopt is used.
3. Medicament to reduce the intraocular fluid production and to lower the outflow resistance of the trabecular meshwork: Prostaglandin agonist Xalatan

4. Medicament to reduce the intraocular fluid production and to better the blood circulation in the optical nerve: $\alpha$-2-agonist Alphagan.

If the intraocular pressure does not decrease or if the patient is eye drop intolerant, a surgery or a laser treatment is necessary. In this thesis, only surgery in the trabecular meshwork will be considered. Most popular choices for surgical interventions in the trabecular meshwork are trabeculectomy and micro-invasive glaucoma surgery using stent implantation.

### Trabeculectomy

The goal of trabeculectomy is to relieve the intraocular pressure by removing a part of the trabecular meshwork and adjacent structures. This is achieved by making a small hole in the sclera, covered by a thin trap-door in it. The aqueous humor drains through the trap-door to a small reservoir or bleb just under the eye surface, hidden by the eyelid. The trap-door is sutured in a way that prevents aqueous humor from draining too quickly. This surgical technique was developed by Cairns. Trabeculectomy is used to treat adult patients suffering from open-angle glaucoma and chronic closed-angle glaucoma [NMBW$^+$95]. Medical studies on trabeculectomy can be found in [JMG$^+$05], [GSF$^+$09] and [FPS03]. Since trabeculectomy requires a strict postoperative follow-up and brings with it a range of intra- and postoperative complications [GHB$^+$12], surgeons search for alternatives. Micro-invasive glaucoma surgery is a promising alternative to trabeculectomy.

### Micro-invasive glaucoma surgery

A large portion of the glaucoma population − particularly in eyes that need additional intervention beyond medication and/or lasers, but that do not yet warrant the risks of trabeculectomy, may profit from micro-invasive glaucoma surgery. Micro-invasive glaucoma surgery (MIGS) offers such a treatment, as it has shown consistent reductions in IOP and medication burden, while also maintaining favorable longterm safety (see [HARCH19b], [HARCH18], [MMH$^+$18] and citations therein). During micro-invasive surgery a MIGS implant is inserted into the trabecular meshwork. The implant allows fluid to pass through it. The details about implantation can be found in [LS17]. MIGS implants are for example XEN®45, (Allergan plc, Dublin, Ireland) gel stent, iStent® Trabecular Micro-Bypass (Glaukos Corp., San Clemente, CA, USA; FDA 2012, CE 2004 or iStent *inject*® Trabecular Micro-Bypass (Glaukos; FDA 2018, CE 2010), which includes two trabecular stents designed to reduce IOP by bolstering aqueous outflow through the trabecular meshwork into Schlemm's canal. The stents look like small tubes or cylinders. In [HARCH19b], [HARCH18], [MMH$^+$18], [HARCH19a] clinical studies on stents from above are illustrated.

# 2 Mathematical preliminaries

In order to understand the derivation of the model and its mathematical analysis, the main results and notation will be repeated in following chapter. Following [Lax02], [Eva15], [RA03], [LM72], [Tem77] and [Bor16] the mathematical notation and function spaces are introduced.

## 2.1 Basic notation

**Definition 2.1.** *In Euclidean space $\mathbb{R}^n$ the canonical basis is given by $e_1 = (1, 0, ..., 0)$, $e_2 = (0, 1, ..., 0)$, ... , $e_n = (0, 0, ..., 1)$ and $x = (x_1, x_2, ..., x_n)$ denotes some point in the space. The differential operator*

$$\frac{\partial}{\partial x_i} \quad (1 \leq i \leq n)$$

*will be written $D_i$ and if $\alpha = (\alpha_1, ..., \alpha_n)$ is a multi-index, $D^\alpha$ will be the differentiation operator*

$$D^\alpha = D_1^{\alpha_1} ... D_n^{\alpha_n} = \frac{\partial^{[\alpha]}}{\partial x_1^{\alpha_1} ... \partial x_n^{\alpha_n}},$$

*where*

$$[\alpha] = \alpha_1 + \alpha_2 + ... + \alpha_n.$$

*If $\alpha_i = 0$ for some $i$, $D_i^{\alpha_i}$ is the identity operator.*

**Definition 2.2.** *Let $\Omega \subset \mathbb{R}^n$ be an open bounded set. Let $x = (x_1, x_2, ..., x_n)$ denote some point in space. Differential operators for vector fields $u : \mathbb{R}^d \to \mathbb{R}^n$ with $u = (u_1(x), u_2(x), ..., u_d(x))$ are defined as follows:*

$$\begin{aligned} \nabla u &= \begin{pmatrix} \frac{\partial u_1}{\partial x_1} & \cdots & \frac{\partial u_1}{\partial x_n} \\ \frac{\partial u_2}{\partial x_1} & \cdots & \frac{\partial u_2}{\partial x_n} \\ \vdots & \cdots & \vdots \\ \frac{\partial u_d}{\partial x_1} & \cdots & \frac{\partial u_d}{\partial x_n} \end{pmatrix} && \textit{(gradient)}, \\ \nabla \cdot u &= \sum_{i=1}^{n} \frac{\partial u_i(x)}{\partial x_i} && \textit{(divergence)} \end{aligned}$$

*For a tensor field $\sigma : \mathbb{R}^n \to \mathbb{R}^{n \times n}$, the divergence is a vector defined column-wise as*

$$\nabla \cdot \sigma = (\sum_{i=1}^{n} \frac{\partial \sigma_{ij}}{\partial x_i})_{j=1,...,n}.$$

*The Laplacian is the divergence of the gradient*

$$\Delta u := \nabla \cdot (\nabla u).$$

Let $\Omega$ be a domain of $\mathbb{R}^n$. The space of continuous, real-valued functions on $\Omega$ which admit continuous partial derivatives up to order $m \in \mathbb{N}$ is denoted by $C^m(\Omega)$. The space of smooth functions on $\Omega$ is denoted by $C^\infty(\Omega)$. Lebesgue-spaces of order $p$ are denoted as $L^p(\Omega)$ for $1 \leq p \leq \infty$ and $H^s(\Omega)$ is the Sobolev space of order $s$ with $s \in \mathbb{R}$, $s \geq 0$ and $H^0(\Omega) := L^2(\Omega)$. The case $p = \infty$ is not considered in this thesis, thus only spaces $L^p(\Omega)$ for $1 \leq p < \infty$ are explained below:

- $L^p(\Omega)$ is the set of all measurable functions $f : \Omega \to \mathbb{R}^n$ such that for the norm $||\cdot||_{L^p(\Omega)}$ there holds

$$||f||^p_{L^p(\Omega)} := \int_\Omega |f(x)|^p \, dx < \infty.$$

- $L^2(\Omega)$ is a Hilbert space if the scalar product is considered

$$(f, g)_{L^2(\Omega)} := \int_\Omega f(x)g(x) \, dx \qquad f, g \in L^2(\Omega).$$

- For $\phi \in C^\infty(\Omega)$ the norms $||\cdot||_{H^k(\Omega)}$ are defined by

$$||\phi||^2_{H^k(\Omega)} := \sum_{\alpha \in \mathbb{N}^n, |\alpha|_1 \leq k} \int_\Omega |D^\alpha \phi(x)|^2 \, dx.$$

  The space $H^k(\Omega)$ is defined as the completion of $C^\infty(\Omega)$ with respect to aforementioned norm:

$$H^k(\Omega) := \overline{C^\infty(\Omega)}^{||\cdot||_{H^k}}.$$

  The Sobolev space with zero trace on the boundary are denoted as

$$H^k_0(\Omega) = \{\phi \in H^k(\Omega) \,|\, \phi_{\partial\Omega} = 0\}.$$

**Definition 2.3.** *$H^{-1}(\Omega)$ denotes the dual space to $H^1_0(\Omega)$.*

In other words $f$ belongs to $H^{-1}(\Omega)$ provided $f$ is a bounded linear functional on $H^1_0(\Omega)$. The space $H^1_0(\Omega)$ is not identified with its dual. Instead, it holds [Eva15]

$$H^1_0(\Omega) \subset L^2(\Omega) \subset H^{-1}(\Omega).$$

## 2.2 Trace operators

To be able to evaluate partial differential equations at boundaries or a part of a boundary of a certain domain, trace theorems [LM72] are introduced.
In order to study mixed finite element methods, the space $H^{\mathrm{div}}$ is useful.

$$H^{\mathrm{div}}(\Omega) := \{q \,|\, q \in (L^2(\Omega))^d, \, \nabla \cdot q \in L^2(\Omega)\}$$

Its norm is given by

$$||q||^2_{H^{\mathrm{div}}(\Omega)} = ||q||^2_{L^2(\Omega)} + ||\nabla \cdot q||^2_{L^2(\Omega)}.$$

Then, it is possible to define the normal trace of $q$ on $\Gamma$, $q \cdot n|_\Gamma$.

**Definition 2.4.** *The mappings*

$$\begin{aligned} \gamma : C^\infty(\Omega) \to C^\infty(\Gamma),\, \gamma(v) &= v_{|\Gamma}, \\ \gamma_n : C^\infty(\Omega)^d \to C^\infty(\Gamma),\, \gamma_n(v) &= (v \cdot n)_{|\Gamma} \end{aligned}$$

*may be continuously extended to $H^1(\Omega)$ or $H^{div}(\Omega)$, respectively.*

**Theorem 2.5.** *The trace operators*

$$\gamma : H^1(\Omega) \to H^{\frac{1}{2}}(\Gamma), \quad \gamma_n : H^{div} \to H^{-\frac{1}{2}}(\Gamma)$$

*are linear, bounded and surjective. Consequently, there exist constants $c_\gamma, c_{\gamma_n} > 0$ such that*

$$\begin{aligned} ||v||_{H^{\frac{1}{2}}(\Gamma)} &\leq c_\gamma ||v||_{H^1(\Omega)}, \quad \forall v \in H^1(\Omega) \\ ||v||_{H^{-\frac{1}{2}}(\Gamma)} &\leq c_{\gamma_n} ||v||_{H^{div}(\Omega)}, \quad \forall v \in H^{div}(\Omega) \end{aligned}$$

*Proof.* See theorem 8.3 in [LM72]. The surjectivity of trace in $H^{\mathrm{div}}$ is also explained in [BBF13]. □

With this definitions, the Green formula can be introduced.

**Theorem 2.6.** *Let $u \in H^{div}(\Omega)$ and $n : \partial\Omega \to \mathbb{R}^d$ the normal field of the boundary. Then it holds*

$$\int_\Omega (\nabla \cdot u(x)) v(x)\, dx + \int_\Omega \nabla v(x) \cdot u(x) = \int_{\partial\Omega} (u(x) \cdot n(x)) v(x)\, dx, \quad \forall v \in H^1(\Omega).$$

*Proof.* see [BBF13]. □

Green formulas are useful in order deal with term conversions in weak formulations of partial differential equations.
The next section covers the theorems from functional analysis implying existence and uniqueness of solutions of the model in this thesis.

## 2.3 Lax Milgram theorem

Let $H$ be a Hilbert space. Let $y$ be fixed, $(x, y) = l(x)$ is a linear functional of $x$, that means a linear mapping of $H$ into $\mathbb{R}$.Furthermore, according to the Schwarz inequality, $l(x)$ is *bounded* by a constant multiple of $||x||$.

**Theorem 2.7. Riesz-Frechet representation theorem**
*Let $l(x)$ be a linear functional on a Hilbert space $H$ that is bounded:*

$$l(x) \leq c||x|| \tag{1}$$

*Then there exists $y \in H$ such that*

$$l(x) = (x, y)$$

*The point $y$ is uniquely determined.*

*Proof.* See [Lax02] □

In particular, the Riesz Frechet theorem implies that each Hilbert space $H$ may be identified with its dual space $H^*$. In other words: for any $f \in H^*$ there exists one and only one $u \in H$, such that $\forall v \in H$ holds

$$\begin{aligned} < f, v >_H &= (u, v)_H \\ ||f||_{H^*} &= ||u||_H \end{aligned}$$

**Theorem 2.8. Lax Milgram theorem**
*Let $H$ be a real-valued Hilbert space, and $B(x, y)$ a function of two vectors with the following properties:*

- *$B(x, y)$ is for fixed $y$ a linear function of $x$, for fixed $x$ a linear function of $y$.*
- *$B$ is bounded: there is a constant $c$ such that for all $x$ and $y$ in $H$:*

  $$|B(x, y)| \leq c||x||||y||$$

- *There is a positive constant $b$ such that*

  $$|B(y, y)| \geq b||y||^2$$

  *This property is often called* coercivity.

*Then, every linear functional $l$ on $H$ is bounded and of the form*

$$l(x) = B(x, y), \qquad y \text{ a uniquely determined vector in } H.$$

*Proof.* See [Lax02]. □

In order to verify that the assumptions of Lax Milgram theorem hold, Poincare inequality may be helpful.

**Theorem 2.9. Poincaré inequality**
*Let $v \in H_0^1(\Omega)$. Then, there exists $d_\Omega > 0$ such that*

$$||v||_{L^2(\Omega)} \leq d_\Omega ||\nabla v||_{L^2(\Omega)},$$

*where $d_\Omega$ is diameter of the domain $\Omega$.*

*Proof.* See [Ran17]. More general versions of this theorem may be found in [GRS07] and in [GGZ74]. □

# 3 Mathematical Model

In the following section the model of the aqueous humor flow in the anterior chamber and in the trabecular meshwork is presented. First, the well known Stokes Darcy coupling is introduced and the actual model is derived. After this, the connection between the new model and the application is explained.

## 3.1 Stokes Darcy Coupling

Stokes Darcy coupling with a Beavers Joseph Saffman condition at the interface is a well known model to describe the flow between the free fluid domain and a porous medium (see for example [LSP03], [ESP75] and many more). The coupling of Stokes and Darcy flow is a problem with a wide range of applications covering models of the groundwater flow [CGW10],[DMQ02], the flow of blood through arterial vessels [DZ11] and the flow inside of industrial filters [HWNW09]. In [CE13] the Stokes-Darcy model is considered to simulate the flow in the anterior chamber and in the trabecular meshwork.

Let $\mathbb{T}(u,p) = 2\nu\mathbb{D}(u) - pI$. Then, the strong formulation of the Stokes equation without boundary conditions is given by:

$$-\nabla \cdot \mathbb{T}(u,p) = f \text{ in } \Omega_{\mathrm{f}}$$

$$-\nabla \cdot u = 0 \text{ in } \Omega_{\mathrm{f}},$$

where $\Omega_{\mathrm{f}} \subset \mathbb{R}^d$ with $d = 2,3$ is the fluid domain and where $u$ denotes the velocity, $p$ the pressure, $f$ the force, and $\nu$ the viscosity of the aqueous humor. The primal form of the Darcy equation without boundary conditions is given by:

$$-\nabla \cdot (\frac{K}{\nu}\nabla p) = f \text{ in } \Omega_{\mathrm{p}},$$

where $\Omega_{\mathrm{p}} \subset \mathbb{R}^d$ with $d = 2,3$ is the porous domain (trabecular meshwork), where $K$ is a permeability constant, $\nu$ the viscosity, $p$ the pressure and $f$ the force.

The Beavers Joseph Saffman conditions on the interface $\Gamma = \partial\Omega_{\mathrm{p}} \cap \partial\Omega_{\mathrm{f}}$ are

$$\begin{aligned} u_f \cdot n &= -(K\nabla p) \cdot n && (2)\\ -n \cdot \mathbb{T}(u,p) \cdot n &= p_{\mathrm{D}} && (3)\\ u \cdot \tau + \alpha \cdot \tau \cdot \mathbb{T}(u,p) \cdot n &= 0. && (4) \end{aligned}$$

The first equation describes the continuity of normal velocities, the second equation illustrates the balance of normal forces and the third condition is motivated by experiments conducted by Beavers Joseph and Saffman [BJ67], [Saf71]. A mathematical justification of the Beavers Joseph Saffman condition can be found in [JM96],[JM00].

In [CGHW10] the well-posedness of a coupled Stokes-Darcy model with BJS interface boundary conditions under the assumption of small coefficient in boundary condition (4) is shown. Badea, Discacciati and Quarteroni [BDQ10] analyze the Navier-Stokes/Darcy coupling using domain decomposition methods and Steklov-Poincaré interface equation. In [LSY03] a weak formulation of Stokes and Darcy coupling with Beavers Joseph Saffman condition is considered and the existence and uniqueness of solutions is proved.
There are multiple numerical approaches to solve the Stokes Darcy problem. On the one hand, there are direct monolithic, or single domain methods which aim at solving the coupled system in a single step. Examples of finite element based approaches in this class may be found in [BH07], [GOS11], [MTW02], [UNGD08], [XXX08]. Furthermore, there are other techniques like mortar finite elements, DG schemes and mixed finite elements to solve a Stokes-Darcy problem. Mortar finite elements for the Stokes-Darcy coupling are described in [EJS11]. Strongly conservative method using discontinuous Galerkin techniques in the Stokes subdomain and a mixed method in the Darcy subdomain is considered in [KR09]. In [RY04] a discontinuous Galerkin method for the Stokes subdomain and a finite element method in the Darcy subdomain is used. In [LSY03] a continuous finite element scheme coupled with mixed finite elements for the Stokes Darcy problem with BJS conditions is analyzed. On the other hand, there are decoupled, domain decomposition, or multidomain approaches which solve the coupled problem with a subdomain iterative procedure based, at each iteration, on the solution of Stokes and Darcy problem separately. These approaches can be found in [CJW14] and [Dis05]. At a first glance, iterative methods require multiple solutions of the subproblems. However, the decoupled techniques allow to use specialized efficient solvers for Stokes and Darcy problems, respectively, which results in efficient procedures. Beyond this techniques, there is a two-grid method which is explained in [MX07].
In the current thesis, a simplified decoupled approach is used. In contrast to [Dis05] where you solve Stokes and Darcy equation separately and update the interface condition in each iteration step, the Stokes and Darcy equations are solved only once. In this work, the Darcy equation is solved first and the mean value of the pressure in the porous domain is determined. Then, this mean value of the pressure is incorporated into the specific Robin boundary condition in the Stokes equation and the Stokes equation is solved. This ansatz saves the computation time and it may be used for applications where the fluid domain is much larger than the porous domain.
The next section shows how the Robin boundary condition in the Stokes equation is constructed and how the model is derived.

## 3.2 Derivation of the Model

To derive a model, a weak formulation of the Stokes and the Darcy equations is computed.

### Weak formulations and BJS conditions

Writing $\Gamma \cup \Gamma_{\mathrm{D}} = \partial\Omega_{\mathrm{f}}$, $\Gamma_{\mathrm{out}} \cup \Gamma_{\mathrm{wall}} \cup \Gamma = \partial\Omega_{\mathrm{p}}$, denoting the interface with $\Gamma$ and introducing the spaces

$$\begin{aligned} H^1_\phi(\Gamma_{\mathrm{D}}, \Omega_{\mathrm{f}}) &:= \{v \in H^1(\Omega) \,:\, v = \phi \text{ on } \Gamma_{\mathrm{D}}\}, \\ Q_{\mathrm{S}} &:= L^2(\Omega_{\mathrm{f}}), \\ Q_{\mathrm{D}} &:= \{\phi \in H^1(\Omega_{\mathrm{p}}) \,:\, \phi = p_0 \text{ on } \Gamma_{\mathrm{out}}\}, \end{aligned}$$

the weak formulation of *Stokes equation* is obtained by partial integration: Find $(u,p) \in H^1_\phi(\Gamma, \Omega_{\mathrm{f}}) \times Q_{\mathrm{S}}$ such that it holds for all $(v,q) \in H^1_\phi(\Gamma, \Omega_{\mathrm{f}}) \times Q_{\mathrm{S}}$

$$(2\nu\mathbb{D}(u), \mathbb{D}(v))_{L^2(\Omega_{\mathrm{f}})} - (p, \nabla\cdot v)_{L^2(\Omega_{\mathrm{f}})} - (\mathbb{T}(u,p)\cdot n, v)_{L^2(\partial\Omega_{\mathrm{f}})} + (\nabla\cdot u, q)_{L^2(\Omega_{\mathrm{f}})} = (f, v)_{L^2(\Omega_{\mathrm{f}})}.$$

The weak formulation of the *primal Darcy equation* is: Find $p \in Q_{\mathrm{D}}$ such that it holds for all $w \in Q_{\mathrm{D}}$

$$\frac{K}{\nu}(\nabla p, \nabla w)_{L^2(\Omega_{\mathrm{p}})} = -(\frac{K}{\nu}\nabla p \cdot n, w)_{L^2(\partial\Omega_{\mathrm{p}})} + (f, w)_{L^2(\Omega_{\mathrm{p}})}.$$

### Coupled weak formulation

Similarly to [CJW14] *Stokes Darcy equation* is given by:
Find $(u, p, \phi_p) \in H^1_\phi(\Gamma, \Omega_{\mathrm{f}}) \times Q_{\mathrm{S}} \times Q_{\mathrm{D}}$ such that it holds for all $(v, q, \chi) \in H^1_\phi(\Gamma, \Omega_{\mathrm{f}}) \times Q_{\mathrm{S}} \times Q_{\mathrm{D}}$:

$$\begin{aligned} a_{\mathrm{f}}(u,v) + b_{\mathrm{f}}(v,p) - (\mathbb{T}(u,p)\cdot n, v)_{L^2(\Gamma)} &= (f,v)_{L^2(\Omega_{\mathrm{f}})} \\ b_{\mathrm{f}}(u,q) &= 0 \\ a_{\mathrm{p}}(\phi_p, \chi) + (K\nabla\phi_p \cdot n, \chi)_{L^2(\Gamma)} &= (f, \chi)_{L^2(\Omega_{\mathrm{p}})}, \end{aligned}$$

where

$$\begin{aligned} a_{\mathrm{f}}(u,v) &= (2\nu\mathbb{D}(u), \mathbb{D}(v))_{L^2(\Omega_{\mathrm{f}})} \\ b_{\mathrm{f}}(v,p) &= -(\nabla\cdot v, p)_{L^2(\Omega_{\mathrm{f}})} \\ a_{\mathrm{p}}(\phi_p, \chi) &= (K\nabla\phi_p, \nabla\chi)_{L^2(\Omega_{\mathrm{p}})}. \end{aligned}$$

Now, rewrite

$$\begin{aligned}(-\mathbb{T}(u,p)\cdot n, v)_{L^2(\Gamma)} &= (-n\cdot\mathbb{T}(u,p)\cdot n, v\cdot n)_{L^2(\Gamma)} - \sum_{i=1}^{d-1}(\tau_i\cdot\mathbb{T}(u,p)\cdot n, v\cdot\tau_i)_{L^2(\Gamma)} \\ &= (p_{\mathrm{D}}, v\cdot n)_{L^2(\Gamma)} + \sum_{i=1}^{d-1}(\frac{1}{\alpha}u\cdot\tau_i, v\cdot\tau_i)_{L^2(\Gamma)}\end{aligned}$$

with the use of (3) and (4).
With the help of (2) the *Coupling of the Stokes and Darcy equation* is obtained:
Find $(u,p,\phi_p)\in H^1_\phi(\Gamma,\Omega_{\mathrm{f}})\times Q_{\mathrm{S}}\times Q_{\mathrm{D}}$ such that it holds for all $(v,q,\chi)\in H^1_\phi(\Gamma,\Omega_{\mathrm{f}})\times Q_{\mathrm{S}}\times Q_{\mathrm{D}}$:

$$\begin{aligned}a_{\mathrm{f}}(u,v)+b_{\mathrm{f}}(v,p)+(p_{\mathrm{D}},v\cdot n)_{L^2(\Gamma)}+\sum_{i=1}^{d-1}(\frac{1}{\alpha}u\cdot\tau_i, v\cdot\tau_i)_{L^2(\Gamma)} &= (f,v)_{L^2(\Omega_{\mathrm{f}})} && (5)\\ b_{\mathrm{f}}(u,q) &= 0 && (6)\\ a_{\mathrm{p}}(\phi_p,\chi)+(u_{\mathrm{f}}\cdot n,\chi)_{L^2(\Gamma)} &= (f,\chi)_{L^2(\Omega_{\mathrm{p}})}, && (7)\end{aligned}$$

where $p_{\mathrm{D}}$ is the pressure in the Darcy domain (at the interface) and $\alpha=\alpha_0\cdot\sqrt{\frac{K}{\mu\cdot g}}$.
The volume of the anterior chamber is about $160\pm 30\,\mathrm{mm}^3$ according to measurements from [RKA06], the volume of the anterior and posterior chamber is about $404\,\mathrm{mm}^3$ according to estimation from simulations and the volume of the trabecular meshwork is approximated by $11.84\,\mathrm{mm}^3 = 36.1283\mathrm{mm}\cdot 0.4\mathrm{mm}\cdot 0.824\mathrm{mm}$, where 36.1283 mm is the length of the trabecular meshwork (= circumference of the iris root), 0.4 mm the height and 0.824 mm the depth of the trabecular meshwork [MH07], [LL+16]. The ratio between these two volumes is approximately 1:34. Moreover, the ratio between the interface area and the surface area is 1:18 according to computations. Consequently, the Darcy domain is much smaller than the Stokes domain in the application. Thus, the following strategy is applied:

- Solve the Darcy equation first (with data from measurements for the inflow rate)
- Solve the Stokes equation using $p_{\mathrm{D}}=\frac{1}{|\Omega_{\mathrm{p}}|}\int_{\Omega_{\mathrm{p}}}p(x)\,dx$, where $p(x)$ is the solution of the Darcy equation.

This ansatz reduces the Darcy equation to a Robin boundary condition in the Stokes equation. In fact, the Darcy equation is transformed into one dimension with the help of this technique. The weak formulation for the model is:
Find $(u,p)\in H^1_\phi(\Gamma,\Omega_{\mathrm{f}})\times Q_{\mathrm{S}}$ such that it holds for all $(v,q)\in H^1_\phi(\Gamma,\Omega_{\mathrm{f}})\times Q_{\mathrm{S}}$:

$$\begin{aligned}a_{\mathrm{f}}(u,v)+\sum_{i=1}^{d-1}(\frac{1}{\alpha}u\cdot\tau_i, v\cdot\tau_i)_{L^2(\Gamma)}+b_{\mathrm{f}}(v,p) &= (f,v)_{L^2(\Omega_{\mathrm{f}})}-(p_{\mathrm{D}},v\cdot n)_{L^2(\Gamma)}\\ b_{\mathrm{f}}(u,q) &= 0\end{aligned}$$

with $p_{\mathrm{D}} = \frac{1}{|\Omega_{\mathrm{p}}|} \int_{\Omega_{\mathrm{p}}} p(x)\, dx$ and $p(x)$ is computed using the solution of
Find $p \in Q_{\mathrm{D}}$ such that it holds for all $q \in Q_{\mathrm{D}}$

$$a_{\mathrm{p}}(p, q) = (f, q)_{L^2(\Omega_{\mathrm{p}})} - (u_{\mathrm{in}}^{\mathrm{TW}} \cdot n, q)_{L^2(\Gamma)}.$$

The next chapter describes the application and the model in more detail.

## 3.3 Description of the Model

To describe the model in more comprehensive way, the strong formulation is introduced. The flow in the free fluid domain is given by the Stokes equation with a Robin boundary condition:

$$\begin{aligned} -\nabla \cdot \mathbb{T}(u, p) &= f \text{ in } \Omega_{\mathrm{f}} \\ \nabla \cdot u &= 0 \text{ in } \Omega_{\mathrm{f}} \\ u &= u_{\mathrm{in}}^{\mathrm{CB}} \text{ on } \Gamma_{\mathrm{in}} \\ u &= 0 \text{ on } \Gamma_{\mathrm{ns}} \\ n \cdot \mathbb{T}(u, p) \cdot n &= p_0 \text{ on } \Gamma_{\mathrm{out}} \\ n \cdot \mathbb{T}(u, p) \cdot \tau &= \tilde{\alpha} u \cdot \tau \text{ on } \Gamma_{\mathrm{out}}, \end{aligned} \tag{8}$$

where $\Omega_{\mathrm{f}} \subset \mathbb{R}^d$ with $d = 2, 3$ is the domain illustrating the anterior and posterior chamber and where $u$ denotes the velocity, $p$ the pressure, $f$ the gravitational force, $u_{\mathrm{in}}^{\mathrm{CB}}$ the inflow velocity at the ciliary body, $p_0$ the pressure (resistance) of the trabecular meshwork and $\nu$ the viscosity of the aqueous humor. $\Gamma_{\mathrm{out}}$ describes the outflow boundary located at the iridocorneal angle, $\Gamma_{\mathrm{in}}$ the inflow boundary located at the ciliary body and $\Gamma_{\mathrm{ns}}$ the boundary with no slip condition which applies for the lens, zonules, cornea and iris. The boundary is given by $\Gamma_{\mathsf{Stokes}} = \Gamma_{\mathrm{ns}} \cup \Gamma_{\mathrm{in}} \cup \Gamma_{\mathrm{out}}$. The normal vector is denoted by $n$ and the tangential vectors by $\tau$. The friction constant is given by $\tilde{\alpha}$.
The inflow rate is between $1 \frac{\mu \mathrm{l}}{\mathrm{min}}$ and $3 \frac{\mu \mathrm{l}}{\mathrm{min}}$ with an average of $2.4 \frac{\mu \mathrm{l}}{\mathrm{min}}$ during the day. With the computed area about $125\,\mathrm{mm}^2$ of the ciliary body in the simulation, the inflow velocity at the ciliary body is estimated by:

$$u_{\mathrm{in}}^{\mathrm{CB}} = \frac{1\mathrm{mm}^3}{\mathrm{min}} \cdot \frac{1}{100\mathrm{mm}^2} \approx 1.6 \cdot 10^{-4} \frac{\mathrm{mm}}{\mathrm{s}}.$$

The (dynamic) viscosity of the aqueous humor is about $\frac{0.7g}{\mathrm{m} \cdot \mathrm{s}}$ [FJ09]. That means $\nu = 0.0007 \frac{\mathrm{kg}}{\mathrm{m} \cdot \mathrm{s}}$. The Stokes equation is a good approximation for the aqueous humor flow in the anterior chamber, since the Reynolds number is

$$\mathrm{Re} = \frac{\rho U L}{\nu} = \frac{10^3 10^{-7} 10^{-3}}{7 \cdot 10^{-4}} << 1.$$

The resistance of the trabecular meshwork is computed as follows: $p_0 = \frac{1}{|\Omega_p|}\int_{\Omega_p} p(x)\,dx$, where $p(x)$ is the solution of the Darcy equation.
The flow in the trabecular meshwork is described by the Darcy equation:

$$\begin{aligned} -\nabla\cdot(\frac{K}{\nu}\nabla p) &= f_2 \text{ in } \Omega_p \\ \frac{K}{\nu}\nabla p\cdot n &= 0 \text{ on } \Gamma_{\text{wall}} \\ \frac{K}{\nu}\nabla p\cdot n &= u_{\text{in}}^{\text{TW}}\cdot n \text{ on } \Gamma_{\text{in}} \\ p &= p_{\text{out}} \text{ on } \Gamma_{\text{out}}. \end{aligned} \tag{9}$$

The domain $\Omega_p \subset \mathbb{R}^d$ with $d = 2, 3$ is illustrating the trabecular meshwork. In the equations above, $K$ is a permeability constant, $\nu$ the viscosity, $p$ the pressure and $f$ the gravitational force. The boundary $\Gamma_{\text{out}}$ describes the outflow boundary, $\Gamma_{\text{in}}$ the inflow boundary and $\Gamma_{\text{wall}}$ the non-permeable boundary. The boundary is given by $\Gamma_{\text{Darcy}} = \Gamma_{\text{wall}} \cup \Gamma_{\text{in}} \cup \Gamma_{\text{out}}$. The term $p_{\text{out}}$ describes the pressure of the episcleral veins at the outflow pathway and $u_{\text{in}}^{\text{TW}}$ describes the velocity at the inflow pathway of the trabecular meshwork. As in the previous case, $n$ denotes the normal vector.
The inflow rate is between $1\frac{\mu\text{l}}{\text{min}}$ and $3\frac{\mu\text{l}}{\text{min}}$ with an average of $2.4\frac{\mu\text{l}}{\text{min}}$ during the day. Assuming that the inflow area at the trabecular meshwork is about $14\,\text{mm}^2$, the average inflow velocity is approximated by $v = \frac{Q}{A}$, where $Q$ is the inflow rate, $A$ the area and $v$ the velocity. This leads to

$$u_{\text{in}}^{\text{TW}} = 0.85\cdot\frac{1\text{mm}^3}{\text{min}}\cdot\frac{1}{14\text{mm}^2} \approx 0.001\frac{\text{mm}}{\text{s}}.$$

The factor 0.85 is used due to the fact that only 85% of the inflow at the ciliary body leave the anterior chamber through the trabecular meshwork.
According to the overview of [SM11] and references of measurements therein as well as [S$^+$05], the pressure of episcleral veins is set as $p_{\text{out}} = 1200$ Pa (which is equivalent to about 9 mmHg). To compute the permeability $K$, following facts are observed:

- $K$ ranges between $10^{-13}$ and $10^{-15}$ for most connective tissues [Joh06].
- Sample porosities for normal eyes are presented in table 2 in [EK$^+$86]. (Two values in the table are $\epsilon = 0.177$ and $\epsilon = 0.246$).

Due to Carman Kozerny theory and the following two equations:

- $\frac{\Delta p}{L} = \frac{150\nu(1-\epsilon)^2}{\epsilon^3 D_p^2\phi_s^2}\cdot v_s$
- $v_s = -\frac{K\Delta p}{\nu L}$

a formula

$$K = \frac{\epsilon^3 D_p^2}{(1-\epsilon)^2}$$

is obtained (where $D_p$ denotes a pore size and $\epsilon$ a porosity). Using this formula, and assuming three cases for the pore size $D_p = 2 \cdot 10^{-5}$, $D_p = 5 \cdot 10^{-5}$ and $5 \cdot 10^{-6}$ as well as three cases for porosities $\epsilon = 0.15, 0.2, 0.25$, different values for $K$ are obtained: between $7.78 \cdot 10^{-16}$ and $3.3 \cdot 10^{-14}$.

Now the model is set up. Next, well posedness of the model and mathematical analysis are presented.

# 4 Mathematical Analysis

In the following section an overview of mathematical theory for Stokes and Darcy equations is given. At the very beginning a short explanation is given why finite element method is chosen to solve the Stokes and the Darcy equation and basics about the finite element method are explained. Then, Stokes equation is considered and main known results about existence and Galerkin approximation are introduced. After that, convergence result for Taylor Hood elements is presented and a test case in two dimensions is presented. In the second part, Darcy equation is considered and known results about existence and Galerkin approximation are given. Then, a test case for Darcy equation in two dimensions is shown. At the end of the section, existence and uniqueness of solutions is shown and Galerkin approximation is explained.

## Mathematical method

In fact there are many different methods to solve partial differential equations. To name the most common methods let recall finite difference (FD), finite volume (FV), spectral and finite element methods (SM and FEM) [GRS07], [Qua09]. Finite difference and finite volume methods consider a partition of the domain into numerous small pieces, although none of them consider a variational formulation of the problem at hand. Moreover, finite difference schemes are suited for simple and uniform geometries. Finite volume methods allow more freedom for meshes, offer totally flexible spatial discretization and there is no need for dependent variables to be differentiable everywhere, but in most cases engineers need to verify their finite volume computations in experimental ways since there is no mathematical theory for formal accuracy for this method. Spectral methods and finite element methods are closely related and built on the same ideas; the main difference between them is that spectral methods use basis functions that are nonzero over the whole domain, while finite element methods use basis functions that are nonzero only on small subdomains. In other words, spectral methods take on a global approach while finite element methods use a local approach. Spectral methods are computationally less expensive than finite element methods, but become less accurate for problems with complex geometries and discontinuous coefficients (which is the case in this thesis). In contrast to FD,FV, SM, finite element methods allow to deal with complicated meshes and take into account the weak formulation of the partial differential equation. Furthermore, there are strong theoretical mathematical tools to study the efficiency and convergence of those methods. On top of that, some finite volume and finite difference schemes can be seen as special cases of some discretization strategies of the finite element methods. From a computational point of view, boundary conditions are naturally taken into account in the space in the variational formulation and the meshes can be locally refined with a help of different refinement strategies. Thus, finite element methods are considered in this work. Next, the Finite Element method is introduced.

## 4.1 Finite element method

Since the current thesis is interdisciplinary and not every reader of this work, especially with medical background, is familiar with finite elements, basics concepts are quickly repeated. In order to explain how the Finite Element method works, Galerkin discretization is presented. This section gives a short summary of the fundamentals in numerical analysis which are explained in more detail in [GT17], [Qua09] and [GRS07].

### Galerkin approximation

Let $V$ be a real Hilbert space, the bilinear form $a : V \times V \to \mathbb{R}$ be continuous and coercive, and the linear form $F : V \to \mathbb{R}$ be continuous. Consider the problem

$$\text{Find } u \in V, \ \text{ such that } a(u, v) = F(v) \quad \forall v \in V \tag{A}$$

Let $V_h$ be a finite dimensional subspace of $V$. Let $h$ be a discretization parameter with the notion that the discrete solution will converge to the continuous solution as $h \to 0$. The standard Galerkin method consists of restricting the equation (A) to the finite dimensional space $V_h$. Consequently, the problem reads

$$\text{Find } u_h \in V_h, \ \text{ such that } a(u_h, v_h) = F(v_h) \quad \forall v_h \in V_h \tag{$A_h$}$$

Since conforming methods are applied in this work, it follows $V_h \subset V$. Therefore, coercivity of $a(\cdot, \cdot)$ on $V$ implies the coercivity of $a(\cdot, \cdot)$ on $V_h$. Moreover, the bilinear form $a(\cdot, \cdot)$ and $F(\cdot)$ are continuous on $V_h$. Thus, Lax Milgram theorem can be applied to the discretized problem and there exists a unique solution of the discrete problem. The best approximation result follows from the Cea's lemma:

**Theorem 4.1.** *Let $V$ be a Hilbert space. Suppose the bilinear form $a$ is coercive and continuous, and the linear form $F(\cdot)$ is continuous. Then, for the unique solutions $u$ and $u_h$ of (A) and ($A_h$) it holds*

$$||u - u_h||_V \leq \frac{\beta}{\alpha} \inf_{v_h \in V_h} ||u - v_h||_V$$

*Here, $\beta$ is the continuity constant and $\alpha$ the coercivity constant of $a(\cdot, \cdot)$.*

Next, it is shown that the problem $(A_h)$ is equivalent to a linear algebraic system of equations.

Let $\{\phi_i\}, i = 1, ..., N$ be a basis of $V_h$. Setting $v_h = \phi_i$ in $(A_h)$, it follows

$$a(u_h, \phi_i) = F(\phi_i), \quad i = 1, ..., N \tag{10}$$

Let $V = H_0^1(\Omega)$ and $V_h \subset V$ its discretization. Now, write the discrete solution $u_h$ and its gradient in terms of the basis of $V_h$ as

$$u_h(x) = \sum_{j=1}^{N} U_j \phi_j(x), \qquad \nabla u_h(x) = \sum_{j=1}^{N} U_j \nabla \phi_j(x), \tag{11}$$

where $U_j, j = 1, ..., N$ are the unknown coefficients to be determined. Substituting (11) in (10) leads to

$$\sum_{j=1}^{N} U_j a(\phi_j, \phi_i) = F(\phi_i),\ i = 1, ..., N$$

Setting $a_{ij} := a(\phi_j, \phi_i)$ and $f_i := F(\phi_i)$, the system of algebraic equations

$$AU = b$$

is obtained, where the stiffness matrix, the solution vector and the load vector, respectively, are given by

$$A = \begin{pmatrix} a_{11} & \cdots & a_{1N} \\ a_{21} & \cdots & a_{2N} \\ \vdots & \cdots & \vdots \\ a_{N1} & \cdots & a_{NN} \end{pmatrix}, \quad U = \begin{pmatrix} U_1 \\ U_2 \\ \vdots \\ U_N \end{pmatrix}, \quad b = \begin{pmatrix} f_1 \\ f_2 \\ \vdots \\ f_N \end{pmatrix}$$

Let $v_h \in V_h$ be arbitrary. Then, there is a representation

$$v_h = \sum_{i=1}^{N} V_i \phi_i$$

and consequently,

$$\begin{aligned} a(u_h, v_h) &= a(u_h, \sum_{i=1}^{N} V_i \phi_i) = \sum_{i=1}^{N} V_i a(u_h, \phi_i) = \sum_{i=1}^{N} V_i F(\phi_i) \\ &= F(\sum_{i=1}^{N} V_i \phi_i) = F(v_h). \end{aligned}$$

It follows, that the matrix $A$ is symmetric if the bilinear form $a(\cdot, \cdot)$ is symmetric. Moreover, the matrix $A$ is positive definite if $a(\cdot, \cdot)$ is coercive.

In applications, the discrete spaces $V_h \subset V$ have been designed by decomposing the computational domain $\Omega$ into a finite set of subdomains $K$ (triangles, quadrilaterals, tetrahedrons, hexahedrons, etc.) and considering a function space $\mathcal{P}_k$ (often polynomials of certain degree) defined on $K$. This motivates the definition of finite elements.

### Finite elements

**Definition 4.2.** *A* finite element *is a triple* $(K, \mathcal{P}, \Sigma_K)$ *satisfying*

- $K \subset \mathbb{R}^n$ *is a closed, convex, polyhedral set with a Lipschitz-continuous boundary and* $|K| \neq 0$.
- *The space of shape functions* $\mathcal{P}_K$ *is a finite dimensional linear function space with dimension* $d$ *on* $K$.
- *The set of degrees of freedom (dofs)* $\Sigma_K$ *consists of* $d$ *linear independent functionals* $\sigma_i, i = 1, ..., d$, *on* $\mathcal{P}_K$. *Each* $p \in \mathcal{P}_K$ *is uniquely determined by the* $d$ *values* $\sigma_i(p), i = 1, ..., d$.

To construct finite elements, a decomposition of the domain $\Omega$ is necessary. Let $\mathcal{T}_h$ be a decomposition of a polyhedral domain $\Omega$ into non-overlapping open cells $K \in \mathcal{T}_h$. In order to classify certain types of decompositions of $\Omega$, $h_K, \rho_K$ and $\sigma_K$ are defined.

**Definition 4.3.** $h_K = \inf\{diam(B), B \subset K \text{ is a ball }\}$
$\rho_K = 2\min_{1 \leq i \leq 2^d} \sup\{diam(B), S_i \subset B \text{ is a ball }\}$ *for a quadrilateral or hexahedral triangulation, where* $S_i$ *is the* $d-$*simplex spanned by* $d$ *neighboring edges of vertex* $a_i$
$\sigma_k = h_K/\rho_K \geq 1$

**Definition 4.4.** *A decomposition* $\mathcal{T}_h = \{K_i\}_{i=1,...,n}$ *of the domain* $\Omega$ *in finitely many elements* $K_i$ *satisfying*

$$\Omega = \cup_{i=1}^n K_i \tag{12}$$
$$h_K \leq h \quad \forall K \in \mathcal{T}_h \tag{13}$$

The triangulations, which are used in this work, satisfy the following regularity assumption.

**Definition 4.5.** *A triangulation* $\mathcal{T}_h$ *of* $\Omega$ *is* admissible *if the intersection between two distinct elements is empty, a common vertex, a common side* ($d \geq 2$) *or a common face* ($d = 3$).

**Definition 4.6.**
- *A family of triangulations is said to be* regular *if*

  $$\sigma_K \leq C_1 \quad \forall K \in \mathcal{T}_h$$

  *where* $C_1$ *is a constant independent of* $h$.

- *If in addition there exists a constant $C_2 \geq 0$ independent of $h$ such that*

$$C_2 h \leq h_K \leq C_1 \rho_K \quad \forall K \in \mathcal{T}_h$$

*then $\mathcal{T}_h$ is called uniformly regular or quasi-uniform.*

All triangulations in this thesis are supposed to be regular. On each finite element certain ansatz functions are used. In this thesis, quadrilateral and hexahedral elements are used. Therefore, product polynomial space is introduced.

**Definition 4.7.** *(Space of tensor product polynomials)*
*The* space of tensor product polynomials *of order $k \in \mathbb{N}_0$ on the reference cell $\hat{K} = [0,1]^d$ is defined by*

$$\mathcal{Q}_k = span\{\prod_{i=1}^{d} x_i^{\alpha_i} \ : \ \max_{i=1}^{d} \alpha_i \leq k\}$$

In order to define function spaces on arbitrary elements, a mapping from the reference cell is needed to transform the polynomial spaces. There exists exactly one invertible multilinear mapping $F_K \in \mathcal{Q}_1$ that maps the reference cell $\hat{K}$ to a generic quadrilateral or hexahedral element $K = \text{conv}\{a_i \in \mathbb{R}^d,\ 1 \leq i \leq 2^d\}$, where

$$F_K(e_i) = a_i, \quad 1 \leq i \leq 2^d.$$

The mapped ansatz spaces (for instance, polynomial spaces) $\mathcal{R}_k(K)$ are given by

$$\mathcal{R}_k = \{r = \hat{r} \circ F_K^{-1}, \hat{r} \in \mathcal{R}_k\},$$

where $\mathcal{R}_k$ is the space of tensor product polynomials $\mathcal{Q}_k$ and $F_K$, respectively, mapping from the reference cell. The mapped space $\mathcal{Q}_k$ is invariant under affine linear transformations. In the general case of quadrilateral or hexahedral elements, the mapped space is not a space of polynomials.

## 4.2 Stokes equation

In this chapter, Stokes equation is described. First, the existence and uniqueness of solutions is stated. After that, Galerkin approximation and the application of the finite element method to Stokes equation is explained.

### 4.2.1 Existence and uniqueness of solutions

#### Existence and uniqueness of solutions for homogeneous Dirichlet boundary conditions

To understand the proof of existence and uniqueness of solutions of the model, main results of Girault Raviart [GR86] for the Stokes equation with a homogeneous boundary conditions will be shortly repeated.

**Definition 4.8.** *Let $\Omega_f \subset \mathbb{R}^d$, $d \in \{2,3\}$ be a bounded domain with Lipschitz boundary $\partial\Omega_f$ denoted as $\partial\Omega_f = \Gamma_D$. $\Omega_f$ is representing a free flow domain. Let $f \in L^2(\Omega_f)$, $u$ a vector function representing the velocity of the fluid and $p$ a scalar function representing the pressure, which are defined in $\Omega_f$ and satisfy the following equations and boundary conditions*

$$\begin{aligned} -\nu\Delta u + \nabla p &= f \ \textit{in } \Omega_f \\ \nabla \cdot u &= 0 \ \textit{in } \Omega_f \\ u &= 0 \ \textit{on } \Gamma_D \end{aligned}$$

*or in the Cauchy stress form*

$$\begin{aligned} -\nabla \cdot \mathbb{T}(u,p) &= f \ \textit{in } \Omega_f \\ \nabla \cdot u &= 0 \ \textit{in } \Omega_f \\ u &= 0 \ \textit{on } \Gamma_D \end{aligned}$$

*with $\mathbb{T}(u,p) := 2\nu\mathbb{D}(u) - p\mathbb{I}$ being the Cauchy stress tensor, $\nu > 0$ the kinematic viscosity and $\mathbb{D}(u) = \frac{1}{2}(\nabla u + \nabla u^T)$ denoting the deformation velocity.*

A strong formulation may be used to construct some simple continuous solutions and construct examples for validation of numerical simulations. However, this formulation is not helpful for the study of existence results and numerical theory. Thus, a weak formulation of the Stokes equation is introduced. The weak formulation can be connected to theorems of functional analysis and with their help, existence of solutions of the Stokes equation is obtained. Let $\partial\Omega_\mathrm{f} = \Gamma_\mathrm{D}$ and $V := \{v \in (H^1(\Omega_\mathrm{f}))^d : v|_{\Gamma_D} = 0\}$. To derive a weak formulation, multiply

$$-\nabla \cdot \mathbb{T}(u,p) = f$$

with the test function $v \in V$ and obtain

$$-\int_{\Omega_\mathrm{f}} (\nabla \cdot (2\nu\mathbb{D}(u))) \cdot v \, dx + \int_{\Omega_\mathrm{f}} (\nabla p) \cdot v \, dx = \int_{\Omega_\mathrm{f}} f \cdot v \, dx. \tag{14}$$

The second term turns to

$$\begin{aligned}
\int_{\Omega_f} (\nabla p) v \, dx &= \int_{\Omega_f} \sum_{i=1}^{d} \frac{\partial p}{\partial x_i} v_i \, dx \\
&= \int_{\Omega_f} \sum_{i=1}^{d} \frac{\partial}{\partial x_i}(p v_i) - p \frac{\partial v_i}{\partial x_i} \, dx \\
&= \int_{\Omega_f} \nabla \cdot (pv) - p \nabla \cdot v \, dx \\
&= \int_{\partial\Omega_f} (pv) \cdot n \, ds - \int_{\Omega_f} p \nabla \cdot v \, dx,
\end{aligned}$$

and setting $M := 2\nu\mathbb{D}(u)$ the first term becomes:

$$\begin{aligned}
-(\nabla \cdot (2\nu\mathbb{D}(u))) \cdot v &= -(\nabla \cdot M) \cdot v \\
&= -\sum_{i=1}^{d} \sum_{j=1}^{d} \frac{\partial M_{ij}}{\partial x_j} v_i \\
&= \sum_{i=1}^{d} \sum_{j=1}^{d} M_{ij} \frac{\partial v_i}{\partial x_j} - \frac{\partial (M_{ij} v_i)}{\partial x_j} \\
&= \sum_{i=1}^{d} \sum_{j=1}^{d} M_{ij} \frac{\partial v_i}{\partial x_j} - \frac{\partial (M_{ji} v_j)}{\partial x_j} \\
&= M : \nabla v - \nabla \cdot (Mv).
\end{aligned}$$

$M : \nabla v$ can be rewritten in the following way

$$\begin{aligned}
M : \nabla v &= \sum_{i=1}^{d} \sum_{j=1}^{d} M_{ij} \cdot \frac{\partial v_i}{\partial x_j} \\
&= \sum_{i=1}^{d} \sum_{j=1}^{d} \frac{1}{2}(M_{ij} + M_{ji}) \cdot \frac{\partial v_i}{\partial x_j} \\
&= \sum_{i=1}^{d} \sum_{j=1}^{d} \frac{1}{2} M_{ij} \cdot (\frac{\partial v_j}{\partial x_i} + \frac{\partial v_i}{\partial x_j}) \\
&= \sum_{i=1}^{d} \sum_{j=1}^{d} 2\nu(\mathbb{D}(u))_{ij} \cdot \frac{1}{2}(\frac{\partial v_j}{\partial x_i} + \frac{\partial v_i}{\partial x_j}) \\
&= 2\nu\mathbb{D}(u) : \mathbb{D}(v).
\end{aligned}$$

Putting all terms together into equation (14) leads to

$$2\nu \int_{\Omega_f} \mathbb{D}(u) : \mathbb{D}(v) \, dx - \int_{\Omega_f} p \nabla \cdot v \, dx - \int_{\partial\Omega_f} (2\nu\mathbb{D}(u)v - pv) \cdot n \, ds = \int_{\Omega_f} f \cdot v \, dx.$$

Now multiply

$$\nabla \cdot u = 0$$

with the test function $q \in L^2(\Omega_\mathrm{f})$ and obtain

$$\int_{\Omega_\mathrm{f}} \nabla \cdot uq \, dx = 0.$$

Summarizing the test functions in a vector $(v,q) \in V \times L^2(\Omega_\mathrm{f})$ leads to

$$2\nu \int_{\Omega_\mathrm{f}} \mathbb{D}(u) : \mathbb{D}(v) \, dx - \int_{\Omega_\mathrm{f}} p \nabla \cdot v \, dx - \int_{\partial\Omega_\mathrm{f}} (2\nu \mathbb{D}(u)v - pv) \cdot n \, ds + \int_{\Omega_\mathrm{f}} \nabla \cdot uq \, dx = \int_{\Omega_\mathrm{f}} f \cdot v \, dx.$$

Note, that $u = 0$ on the boundary $\Gamma_\mathrm{D}$, thus, the boundary term vanishes. Consequently, the weak formulation in the definition below is obtained

**Definition 4.9.** *Let $\Omega_f \subset \mathbb{R}^d$, $d \in \{2,3\}$ be a bounded domain with Lipschitz boundary $\partial\Omega_f$ denoted as $\partial\Omega_f = \Gamma_D$ and $V := \{v \in (H^1(\Omega_f))^d \, : \, v|_{\Gamma_D} = 0\}$.*
*Find $(u,p) \in V \times L^2(\Omega_f)$ such that for all $v \in V$ and for all $q \in L^2(\Omega_f)$ it holds*

$$\begin{aligned} a(u,v) + b(v,p) &= (f,v)_{L^2(\Omega_f)} \\ b(u,q) &= (\nabla \cdot u, q)_{L^2(\Omega_f)}, \end{aligned}$$

*where*

$$\begin{aligned} b(v,q) &= -(\nabla \cdot v, q)_{L^2(\Omega_f)}, \\ a(u,v) &= (2\nu \mathbb{D}(u), \mathbb{D}(v))_{\Omega_f}. \end{aligned}$$

Next, suitable norms, spaces and bilinear forms are constructed. Then, the weak formulation is transformed in a variational formulation. The obtained variational formulation is a helpful step to explain the proof for existence of solutions.
Let $X$ and $M$ denote two real Hilbert spaces with norms $||\cdot||_X$ and $||\cdot||_M$ respectively. Let $X'$ and $M'$ be their corresponding dual spaces and $||\cdot||_{X'}$ and $||\cdot||_{M'}$ denote their dual norms.
Let

$$a(\cdot,\cdot) : X \times X \to \mathbb{R}, b(\cdot,\cdot) : X \times M \to \mathbb{R},$$

be continuous bilinear forms with norms

$$\begin{aligned} ||a|| &= \sup_{u,v \in X, u \neq 0, v \neq 0} \frac{a(u,v)}{||u||_X ||v||_X} \\ ||b|| &= \sup_{v \in X, \nu \in M, v \neq 0, \nu \neq 0} \frac{b(v,\nu)}{||v||_X ||\nu||_M}. \end{aligned}$$

Consider the variational problem:

For $l$ given in $X'$ and $\chi$ in $M'$, find a pair $(u, \lambda)$ in $X \times M$ such that:

$$a(u,v) + b(v,\lambda) =< l, v > \ \forall v \in X$$
$$b(u,\lambda) =< \chi, \lambda > \ \forall \nu \in M. \tag{Q}$$

Associate $a$ and $b$ with two continuous, linear operators:
$A \in \mathcal{L}(X; X')$ and $B \in \mathcal{L}(X; M')$ defined by

$$\begin{aligned} < Au, v > &= a(u,v) \, \forall u, v \in X \\ < Bv, \nu > &= b(v,\nu) \, \forall v \in X, \, \forall \nu \in M. \end{aligned}$$

Let $B' \in \mathcal{L}(M; X')$ be the dual operator of $B$, i.e

$$< B'\nu, v >=< Bv, \nu >= b(v,\nu) \, \forall \nu \in M, \forall v \in X.$$

It holds:

$$||A||_{\mathcal{L}(X;X')} = ||a||, \; ||B||_{\mathcal{L}(X;M')} = ||b||.$$

Using the operators, the variational problem is given by

$$\begin{aligned} Au + B'\lambda &= l \ \text{ in } X' \\ Bu &= \chi \ \text{ in } M'. \end{aligned}$$

Set $V = \ker B$ in $X$. For each $\chi \in X'$ define:

$$V(\chi) = \{v \in X \, : \, Bv = \chi\}.$$

The following problem is associated with the model problem:
Find $u$ in $V(\chi)$ such that

$$a(u,v) =< l, v > \ \forall v \in V. \tag{P}$$

If $(u, \lambda) \in X \times M$ is a solution of (Q), then $u \in V(\chi)$ and $u$ is a solution of (P). The goal is to show the converse of this statement. For this, define

$$V^0 = \{g \in X' \, ; \, < g, v >= 0 \qquad \forall v \in V\}.$$

**Lemma 4.10.** *The following properties are equivalent:*

- *There exists a constant $\beta > 0$ such that*

$$\inf_{\nu \in M} \sup_{v \in X} \frac{b(v,\nu)}{||v||_X ||\nu||_M} \geq \beta.$$

- *The operator $B'$ is an isomorphism from $M$ onto $V^0$ and*

$$||B'\nu||_{X'} \geq \beta||\nu||_M \qquad \forall \nu \in M.$$

- *The operator $B$ is an isomorphism from $V^T$ onto $M'$ and*

$$||Bv||_{M'} \geq \beta||v||_X \qquad \forall v \in V^T.$$

*Proof.* See [GR86]. □

The lemma from above shows the equivalent properties to the inf sup condition. Moreover, this lemma can be used as a definition of the inf sup condition. With this result, a theorem with a general abstract setting for existence of solutions is obtained:

**Theorem 4.11.** *If the following assumptions hold,*

- *There exists a constant $\alpha > 0$ such that*

$$a(v, v) \geq \alpha||v||_X^2 \qquad \forall v \in V.$$

- *The bilinear form b satisfies the inf-sup condition.*

*then the problem (P) has a unique solution $u$ in $V(\chi)$ and there exists a unique $\lambda$ in $M$ such that the pair $(u, \lambda)$ is the unique solution of problem (Q).*

*Proof.* See [GR86]. □

From the theory of elliptic partial differential equations it is known, that Lax Milgram theorem (or Riesz representation theorem in simple cases) may be applied to prove the existence and uniqueness of solutions of the problem (P). With the help of this strategy, existence and uniqueness of solutions for saddle point problems (Q) like Stokes equation is obtained.

**Theorem 4.12.** *The Stokes equation with a homogeneous Dirichlet boundary condition has one and only one solution.*

*Proof.* The proof follows from the application of the previous theorem. Thus, it suffices to show the coercivity and the inf-sup condition.
*Coercivity*: (with the use the first Korn's inequality [Kor09], for extension of the first

Korn's inequality for incompatible tensor fields see [NPW15])

$$\begin{aligned} a(v,v) &= (2\nu\mathbb{D}(v),\mathbb{D}(v))_{L^2(\Omega)} \\ &= \nu\int_\Omega \sum_{i,j=1}^{d} \frac{1}{2}(\frac{\partial v_i}{\partial x_j}+\frac{\partial v_j}{\partial x_i})^2 \\ &\geq \frac{\nu}{\kappa}||v||^2_{H^1(\Omega)} \\ &\geq C\frac{\nu}{\kappa}||v||^2_V \end{aligned}$$

*Inf-Sup Condition*:
There exists a constant $c > 0$ such that:

$$\sup_{v\in H_0^1(\Omega)^n} \frac{(\phi,\nabla\cdot v)}{|v|_{H^1(\Omega)}} \geq c||\phi||_{L^2(\Omega)} \quad \forall\phi\in L_0^2(\Omega)$$

The proof follows from the statement, that there exists a function $v \in V^T$ such that $\phi = \nabla\cdot v$ and $|v|_{H^1(\Omega)} \leq c||\phi||_{L^2(\Omega)}$ (Lemma 3.2 in [GR86]).

□

#### Existence and uniqueness of solutions for mixed boundary conditions

Recall the weak formulation of the Stokes equation in the anterior chamber: Using

$$\begin{aligned} \Gamma &:= \partial\Omega_\mathrm{f} = \Gamma_\mathrm{D}\cup\Gamma_\mathrm{N} \\ H^1_\phi(\Gamma_\mathrm{D},\Omega_\mathrm{f}) &:= \{v\in H^1(\Omega_\mathrm{f}) \,:\, v=\phi \text{ on } \Gamma_\mathrm{D}\}, \\ Q_\mathrm{S} &:= L^2(\Omega_\mathrm{f}) \\ H^{\frac{1}{2}}_{00}(\Gamma_\mathrm{N}) &:= \{v\in L^2(\Gamma_\mathrm{N});\, \exists w\in H^1(\Omega_\mathrm{f}) \,:\, w_{|\Gamma_\mathrm{D}}=0,\, w_{|\Gamma_\mathrm{N}}=v\} \end{aligned}$$

Find $(u,p)\in H^1_\phi(\Gamma_\mathrm{D},\Omega_\mathrm{f})\times Q_\mathrm{S}$ such that it holds for all $(v,q)\in H^1_\phi(\Gamma_\mathrm{D},\Omega_\mathrm{f})\times Q_\mathrm{S}$

$$\begin{aligned} a_\mathrm{f}(u,v)+\sum_{i=1}^{d-1}(\frac{1}{\alpha}u\cdot\tau_i, v\cdot\tau_i)_{L^2(\Gamma)} + b_\mathrm{f}(v,p) &= (f,v)_{L^2(\Omega_\mathrm{f})} - (p_\mathrm{D}, v\cdot n)_{L^2(\Gamma)} \\ b_\mathrm{f}(u,q) &= 0, \end{aligned}$$

Now, apply a lifting method and convert the problem to a problem with a homogeneous Dirichlet boundary condition and $\tilde{u}\in H^1_0(\Gamma_\mathrm{D},\Omega_\mathrm{f})$. The boundaries $\partial\Omega_\mathrm{f}$ of the domain are piecewise $C^2$ and thus locally lipschitzian. Consequently, similar arguments to [Gal11] (theorem 1.1, chapter IV, p.188) apply.
Let there be given $f\in D_0^{1,2}(\Omega_\mathrm{f})$ (see the definition of the space in [Gal11], in the application $f$ is supposed to be constant, thus it also holds that $f\in H^{-1}(\Omega_\mathrm{f})$) and $\phi\in H^{\frac{1}{2}}(\Gamma)$ such that

$$0=\int_\Gamma \phi\cdot n\, d\Gamma.$$

According to [Gal11], there exists a solenoidal extension $u_0 \in H^1(\Omega_\mathrm{f})$ of $\phi$ with

$$||u_0||_{H^1(\Omega_\mathrm{f})} \leq c||\phi||_{H^{\frac{1}{2}}(\Gamma)}.$$

Consequently, by assumption and partial integration, it holds

$$\int_\Gamma \phi \cdot n \, d\Gamma = \int_{\Omega_\mathrm{f}} (\nabla \cdot u_0) \, dx = 0.$$

Setting $\tilde{u} = u - u_0$ the non-homogeneous Stokes problem reduces to a homogeneous problem

$$\begin{aligned} a_\mathrm{f}(\tilde{u}, v) + \sum_{i=1}^{d-1} (\frac{1}{\alpha} \tilde{u} \cdot \tau_i, v \cdot \tau_i)_{L^2(\Gamma)} + b_\mathrm{f}(v, p) &= (\tilde{f}, v)_{H^{-1}(\Omega_\mathrm{f})} - (\tilde{w}, v \cdot n)_{L^2(\Gamma)} \\ b_\mathrm{f}(\tilde{u}, q) &= 0, \end{aligned}$$

where $\tilde{u} \in H_0^1(\Gamma_\mathrm{D}, \Omega_\mathrm{f})$, $\tilde{w} \in H_{00}^{\frac{1}{2}}(\Gamma)$ is defined by

$$\tilde{w} = (\tilde{w} \cdot \tau)\tau + (\tilde{w} \cdot n)n$$

with

$$\tilde{w} \cdot n := p_\mathrm{D} - 2\nu n \mathbb{D}(u_0) n \qquad \text{and} \qquad \tilde{w} \cdot \tau := u_0 \tau - 2\nu n \mathbb{D}(u_0)\tau$$

as well as

$$\tilde{f} := f - \nu \nabla \cdot \mathbb{D}(u_0) \in H^{-1}(\Omega_\mathrm{f})^d.$$

Now consider the Stokes problem with mixed boundary conditions. One of the boundaries is given by a homogeneous Dirichlet boundary condition and the other part of the boundary by a Robin boundary condition. Both boundaries are piecewise $C^2$. The Robin and Dirichlet boundary are not separated. Moreover, the angle at the border between the Dirichlet and the Robin boundary is less than $2\pi$.

**Theorem 4.13.** *Let $f \in H^{-1}(\Omega_f)^d$. Let $a_f$ be coercive and $b_f$ fulfill the inf-sup condition. Let*

$$A(u, v) := a_f(\tilde{u}, v) + \sum_{i=1}^{d-1} (\frac{1}{\alpha} \tilde{u} \cdot \tau_i, v \cdot \tau_i)_{L^2(\Gamma)}$$

*Then, the two following problems are equivalent:*

- *variational mixed boundary Stokes problem : to find $(\tilde{u}, p) \in H_0^1(\Gamma_D, \Omega_f) \times L^2(\Omega_f)$ such that*

$$\begin{aligned} A(\tilde{u}, v) + b_f(v, p) &= (\tilde{f}, v)_{H^{-1}(\Omega_f)} - (\tilde{w}, v)_{L^2(\Gamma)} \\ b_f(\tilde{u}, q) &= 0 \end{aligned} \tag{$Q^*$}$$

- *elliptic problem : to find* $u \in H_0^1(\Gamma_D, \Omega_f)$ *such that*

$$A(u, v) =< l_1, v > + << l_2, v >> \tag{$P^*$}$$

*where*

$$< l_1, v >:= (\tilde{f}, v)_{H^{-1}(\Omega_f)}$$

*and*

$$<< l_2, v >>:= -(\tilde{w}, v)_{L^2(\Gamma)}.$$

*Proof.* $A(u, v)$ is coercive, since the bilinear form $a_\mathrm{f}(u, v)$ is coercive (due to Korn's inequality) and the fact that

$$\sum_{i=1}^{d-1} (\frac{1}{\alpha} v \cdot \tau_i, v \cdot \tau_i)_{L^2(\Gamma)} \geq 0$$

Since the pressure is now uniquely determined due to the Neumann condition (and not up to a constant like in a homogeneous case of the Stokes problem with homogeneous Dirichlet boundary conditions), the inf-sup condition mentioned in Girault Raviart [GR86] doesn't apply any more. Manouzi [Man90] has shown, that inf-sup condition holds also in the case with mixed boundary condition:

$$\sup_{v \in H_0^1(\Gamma_\mathrm{D}, \Omega_\mathrm{f})} \frac{|\int_{\Omega_\mathrm{f}} q \nabla \cdot v|}{||v||_{H^1(\Omega_\mathrm{f})}} \geq C||q||_{L^2(\Omega_\mathrm{f})}.$$

Thus, $(Q^*)$ is equivalent to $(P^*)$ similar to arguments from Girault Raviart. □

The problem $(P^*)$ has a unique solution due to Lax Milgram theorem. In order to apply Lax Milgram, the assumptions are checked.

- The left side is the same as in the case of the Stokes equation with homogeneous Dirichlet boundary conditions, thus the Korn's inequality applies and the coercivity is fulfilled. Moreover, $a(u, v)$ is bounded in $H_0^1(\Omega_\mathrm{f})$.

- $< l_1, v >= (\tilde{f}, v)_{H^{-1}(\Omega_\mathrm{f})}$ and thus, this term is bounded by Cauchy Schwarz inequality in $H^1(\Omega_\mathrm{f})$.

- $<< l_2, v >>= (\tilde{w}, v)_{L^2(\Gamma)}$. The discussion of boundedness of this term is similar to [AHC10]. Since $H^{\frac{1}{2}}(\Gamma_\mathrm{N}) = \rho H^1(\Omega_\mathrm{f})$, there exists $v_0 \in H^1(\Omega_\mathrm{f})$ such that $\rho v_0 = v$ [LM72]. Similarly, there exists $\tilde{g}_0 \in H^1(\Omega_\mathrm{f})$ such that $\rho \tilde{g}_0 = \tilde{w}$. The restriction $\rho : H^1(\Omega_\mathrm{f}) \to H^{\frac{1}{2}}(\partial\Omega_\mathrm{f})$ is continuous [McL00], and the embedding $\iota : H^{\frac{1}{2}}(\partial\Omega_\mathrm{f}) \hookrightarrow L^2(\partial\Omega_\mathrm{f})$ is compact [McL00]. Denote by $l_g$ the continuous mapping

$$u \to \int_{\partial\Omega_\mathrm{f}} u(x) g(x)\, dx, \quad u \in L^2(\partial\Omega_\mathrm{f})$$

Writing $l_2 = l_g \circ \iota \circ \rho$, it is obtained that $l_2$ is bounded in $H^1(\Omega_\mathrm{f})$.

Now, it is shown, that the Stokes problem with mixed boundary conditions has a unique solution. Next, the Galerkin approximation and discretizations of the Stokes equation are explained.

### 4.2.2 Discretization

The Stokes equation is considered as a mixed problem. The Galerkin approximation of mixed problems is analogous to elliptic problems. First, discrete subspaces are chosen and a best approximation property similar to Cea's lemma in the case of Poisson equation is constructed. Then, suitable discrete spaces and finite elements are chosen. Finally, convergence results are obtained. Following [GR86], introduce the discrete setting:
Let $h$ denote a discretization parameter tending to zero and, for each $h$, let $X_h$ and $M_h$ be two finite dimensional spaces such that

$$X_h \subset X, \quad M_h \subset M$$

A problem (Q) is approximated by: Find a pair $(u_h, \lambda_h)$ in $X_h \times M_h$ satisfying

$$\begin{aligned} a(u_h, v_h) + b(v_h, \lambda_h) &= < l, v_h > \quad \forall v_h \in X_h \\ b(u_h, \mu_h) &= < \chi, \mu_h > \quad \forall \mu_h \in M_h \end{aligned} \tag{$Q_{hh}$}$$

For each $\chi \in M'$ define the finite dimensional analogue of $V(\chi)$:

$$V_h(\chi) = \{v_h \in X_h\,; b(v_h, \mu_h) = 0 \quad \forall \mu_h \in M_h\}$$

In general, $X_h \subset X$ and $V_h(\chi) \subset V(\chi)$ do not always hold.
Like in the continuous case, the problem $(Q_{hh})$ is associated with the following problem: Find $u_h \in V_h(\chi)$ such that

$$a(u_h, v_h) = < l, v_h > \quad \forall v_h \in V_h \tag{$P_h$}$$

It follows that the first component of solution $u_h$ of any solution $(u_h, \lambda_h)$ of problem $Q_h$ is also a solution of $(P_h)$. The converse statement holds under assumptions in the next theorem:

**Theorem 4.14.** • *Assume that the following conditions hold:*

*(i)* $V_h(\chi)$ *is not empty.*

*(ii) There exists a constant* $\alpha^* > 0$ *such that:*

$$a(v_h, v_h) \geq \alpha^* ||v_h||_X^2 \quad \forall v_h \in V_h$$

*Then problem ($P_h$) has a unique solution $u \in V_h(\chi)$ and there exists a constant $C_1$ depending only upon $\alpha^*, ||a||$ and $||b||$ such that the error bound holds*

$$||u - u_h||_X \leq C_1 \cdot ( \inf_{v_h \in V_h(\chi)} ||u - v_h||_X + \inf_{\mu_h \in M_h} ||\lambda - \mu_h||_M).$$

- *Assume that hypothesis (ii) holds and, in addition that*

$$\sup_{v_h \in X_h} \frac{b(v_h, \mu_h)}{||v_h||_X} \geq \beta_* ||\mu_h||_M \forall \mu_h \in M_h$$

*Then $V_h(\chi) \neq \emptyset$ and there exists a unique $\lambda_h$ in $M_h$ so that $(u_h, \lambda_h)$ is the only solution of ($Q_{hh}$). Furthermore, there exists a constant $C_2$ depending only upon $\alpha^*, \beta^*, ||a||$ and $||b||$ such that*

$$||u - u_h||_V + ||\lambda - \lambda_h|| \leq C_2( \inf_{v_h \in X_h} ||u - v_h||_X + \inf_{\mu_h \in M_h} ||\lambda - \mu_h||_M).$$

*Proof.* See [GR86]. □

In the case of elementary elliptic problems, the coercivity condition and thus the Lax Milgram lemma for discretized spaces is inherited from the continuous case. For mixed problems it is not the case, because discrete inf-sup condition can not be inherited from the continuous case. Thus, inf sup condition becomes an additional requirement on the choice of $V_h$ and $Q_h$.

This general setting can be applied for Stokes equation. The discretized formulation of the Stokes equation with Robin boundary is given by:

**Definition 4.15.** *Let $\partial\Omega_f = \Gamma_D \cup \Gamma_N$ and $V_h \subset V := \{v \in (H^1(\Omega_f))^d \, : \, v_h|_{\Gamma_D} = 0\}$. Find $(u_h, p_h) \in V_h \times Q_h$ such that for all $v \in V_h$ and for all $q \in Q_h \subset L^2(\Omega_f)$ it holds*

$$a(u_h, v) + \sum_{i=1}^{d-1} (\frac{1}{\alpha} u_h \cdot \tau_i, v \cdot \tau_i)_{L^2(\Gamma)} + b(v, p_h) = (f, v)_{L^2(\Omega_f)} - (g, v)_{H^{-\frac{1}{2}}(\Gamma_N)}$$
$$b(u_h, q) = 0,$$

*where*

$$b(v, p_h) = -(\nabla \cdot v, p_h)_{L^2(\Omega_f)}$$
$$a(u_h, v) = (2\nu \mathbb{D}(u_h), \mathbb{D}(v))_{L^2(\Omega_f)}.$$

The situation is different to [GR86] in two aspects. First, the right hand side has a special term. Moreover, $Q_h \subset L^2(\Omega_\mathrm{f})$ and not $Q_h \subset L^2_0(\Omega_\mathrm{f})$ like in [GR86].
The term on the right hand side is bounded in the continuous case and thus, in the discrete case. Thus, existence and uniqueness of the problem follow from the Lax Milgram

theorem and equivalence of problems $P_h$ and $Q_h$ since $V_h \subset V$ and $Q_h \subset Q := L^2(\Omega_\mathrm{f})$. The next step is to construct such discrete spaces and to find finite elements which satisfy the assumptions of the approximation theorem. The Taylor Hood finite elements lead to good convergence and stability results in applications.

### Convergence results for Taylor Hood elements

The family of the Taylor Hood elements is defined below:

**Definition 4.16.** *The family of Taylor-Hood elements on quadrilaterals and hexahedra (for the choices $d = 2, 3$) for polynomial degrees $k \geq 1$ consists of the pairs*

$$V_h = \{v \in H_0^1(\Omega_f)^d \,|\, v_{|K} \in \mathcal{Q}_k(K)^d,\ K \in \mathcal{T}_h\}$$

*and*

$$P_h = \{p \in L^2(\Omega_f) \cap C(\Omega_f) \,|\, p_{|K} \in \mathcal{Q}_{k-1}(K),\ K \in \mathcal{T}_h\}.$$

Using macroelement technique [Ste90], it can be shown that the spaces $V_h$ and $P_h$ fulfill the discrete inf-sup condition. Thus, it holds:

**Theorem 4.17.** *For the solution $(u_h, p_h)$ of the discrete Stokes equation with $v_h \in V_h$ and $p_h \in P_h$, it holds*

$$||u - u_h||_{H^1(\Omega_f)} + ||p - p_h||_{L^2(\Omega_f)} \leq Ch^k(||u||_{H^{k+1}(\Omega_f)} + ||p||_{H^k(\Omega_f)}).$$

*For a convex domain $\Omega_f$, it holds*

$$||u - u_h||_{L^2(\Omega_f)} \leq Ch^{k+1}(||u||_{H^{k+1}(\Omega_f)} + ||p||_{H^k(\Omega_f)}).$$

The proof for two dimensions for triangles and quadrilaterals can be found in [Ste90]. The proof for tetrahedra in three dimensions can be found in [BBF$^+$06] (especially, it is shown, that the chosen spaces fulfill the discrete inf-sup condition). The proof in three dimensions for hexahedral elements follows the idea in the master thesis of Arndt [Arn13] and it is presented here.

**Definition 4.18.** *A macroelement $M$ is a polytope which is the union of adjacent elements. Two macroelements $M, \hat{M}$ are said to be equivalent if there exists a mapping $F_M : \hat{M} \to M$ such that*

*(1) $F_M$ is continuous and invertible*

*(2) $\hat{M} = \cup_{j=1}^m$ where $\hat{K}_j$ are the elements defining $\hat{M}$, then $K_j = F_M(\hat{K}_j)$ are the elements of $M$.*

*(3) $F_M|K_j = F_{K_j} \circ F_{\hat{K}_j}^{-1} \forall j \in \{1, ..., m\}$ $F_k$ denotes the affine mapping from the reference element to a generic element $K$*

Further define

$$V_{0,M} := \{v \in H^1_0(M)^d \,:\, \exists w \in V_h \quad v = w_{|M}\}$$

$$Q_M := \{q_{|M} \text{ with } q \in Q_h\}$$

Moreover, the space of spurious pressure modes is given by

$$N_M := \{q \in Q_M \mid \int_M q \nabla \cdot v \, dx = 0, \quad \forall v \in V_{0,M}\} \tag{15}$$

The following theorem:

**Theorem 4.19.** *Let $M_h$ be a macroelement partition of the elements of $\mathcal{T}_h$ such that*

*(H1) For each $M \in \mathcal{M}_h$ the space $N_M$ is one-dimensional and consists of functions which are constant on $M$*

*(H2) Each $M \in \mathcal{M}_h$ belongs to an equivalence class of macroelements*

*(H3) The number of equivalence classes of macroelements is finite and independent of $h$*

*(H4) Each element $K \in \mathcal{T}_h$ is contained in a finite number $N$ of macroelements $M \in \mathcal{M}_h$, with $N$ independent of $h$*

*(H5) The inf-sup condition between $V_h$ and the space of elementwise constant functions $\mathcal{Q}_0$ holds true.*

*Then, the choice of the spaces $V_h$ and $Q_h$ satisfies the inf-sup condition.*

*Proof.* See [BBF+06]. □

Let

$$V_h = \{v \in H^1_0(\Omega_\mathrm{f})^d \,|\, v_{|K} \in \mathcal{Q}_k(K)^d,\, K \in \mathcal{T}_h\}$$

and

$$P_h = \{p \in L^2(\Omega_\mathrm{f}) \cap C(\Omega_\mathrm{f}) \,|\, p_{|K} \in \mathcal{Q}_{k-1}(K),\, K \in \mathcal{T}_h\}$$

**Theorem 4.20.** *Define a macroelement partition $\mathcal{M}_h$ by grouping together, for each internal vertex $x_0$, those vertex elements that touch $x_0$. then, for the three-dimensional case the space of spurious pressure modes $N_M$ is one-dimensional, consisting of globally constant functions in $M$ for each $M \in \mathcal{M}_h$.*

*Proof.* First, consider a polynomial $\tilde{w} = 4x(1-x)(1-y)(1-z) \in \mathcal{Q}_2$ on the reference cell. Following observations can be made immediately:

(P1) The value of $\tilde{w}$ on the plane $\{y = 0\}$ just depends on $x$ and $y$.

(P2) On the plane $\{z=0\}$, $\tilde{w}$ only varies with $x$ and $y$,

(P3) The function vanishes on the four planes $\{x=0\},\{x=1\},\{y=1\}$ and $\{z=1\}$,

(P4) $\tilde{w}$ is linear with respect to $y$ and $z$ individually,

(P5) $\tilde{w}(x,y,z)\geq 0\ \forall(x,y,z)\in[0,1]^3$,

(P6) $\tilde{w}(x,y,z)=\tilde{w}(x,z,y) \quad \forall(x,z)\in[0,1]^2$.

Consider a generic macroelement $M\in\mathcal{M}_h$ associated to the internal vertex $x_0$. Let $K_0\in\mathcal{T}_h$ be a hexahedron of $M$, then $x_0$ belongs also to their elements of $M$. There are three edges $e_i, i=1,2,3$ of $k_0$ meeting at $x_0$. Now, a coordinate system is chosen, such that $e_1$ is lying on the x-axis.
The goal is to prove, that $\nabla p$ vanishes on $K_0$. Thus, consider $\mathcal{A}=\{K_0,...,K_n\}$ of elements in $\mathcal{T}_h$ that share $e_1$. Obviously, each $K\in\mathcal{A}$ has exactly two faces with other elements in $\mathcal{A}$ in common. Moreover, denote by $F_i$ an invertible bilinear mapping from $K_i$ to the reference cell that satisfies:

- the two faces of $K_i$ which are in common with other elements in $\mathcal{A}$ are mapped to $\{z=0\}$ and $\{y=0\}$ plane.
- $F_i$ is the identity on $e_1$.
- Vertices are mapped onto vertices.

Next, a polynomial for a given $q\in Q_M$ is constructed such that the following property holds:

$$\begin{aligned} w_{|K_i} &= ((\tilde{w}\circ F_i^{-1})\frac{\partial p}{\partial x}|_{K_i},0,0) \quad i=1,...,n,\\ w_{|K} &= 0 \quad \forall K\in\mathcal{T}_h\backslash\mathcal{A}. \end{aligned}$$

Due to properties (P1)-(P3) the constructed polynomial is continuous in $K_i\cup(M\backslash\mathcal{A})$ and the polynomial vanishes in $M\backslash\mathcal{A}$. The continuity of $\nabla p$ on the faces between elements in $\mathcal{A}$ in all tangential directions then ensures together with properties (P1) and (P2) the continuity of $w$ on these interfaces and finally in the whole set $M$.
Since $F_i$ preserves the $x-$direction, $\frac{\partial p}{\partial x}\circ F_i$ is of the form

$$\frac{\partial p}{\partial x}\in\operatorname{span}\{x^r y^s z^t, 0\leq r\leq k-1, 0\leq s,t\leq k\}$$

in $K_i$. The function $\tilde{w}\circ F_i^{-1}\circ F_i=\tilde{w}$ is quadratic in $x$ and linear in $y$ and z due to property (P4). Thus,

$$((\tilde{w}\circ F_i^{-1})\frac{\partial p}{\partial x}|K_i)\circ F_i\in\operatorname{span}\{x^r y^s z^t, 0\leq r,s,t\leq k+1\}=\mathcal{Q}_{k+1}$$

Consequently, it follows that $w \in V_{0,M}$. Now, this function may be tested with the macroelement condition (15) and it holds

$$\begin{aligned} 0 &= \int_M q\nabla \cdot w\, dx = \sum_{i=1}^{n}\left(\int_{\partial K_i} qw \cdot n\, dx - \int_{K_i} \nabla q \cdot w\, dx\right) && (16)\\ &= \sum_{i=1}^{n} \int_{K_i} ((\tilde{w} \circ F_i^{-1})(\frac{\partial p}{\partial x}|K_i)^2) && (17) \end{aligned}$$

where $\int_{\partial K_i} qw \cdot n\, dx$ disappears due to the choice of $w$. The function $(\tilde{w} \circ F_i^{-1})$ is non-negative in $K_i$ for all $i = 1, ..., n$ because of (P5). Therefore, the first component of $\nabla q$ vanishes. The same argumentation may be applied to the edges $e_2$ and $e_3$. Consequently, $\nabla q_k|_{K_i}$ disappears and q is elementwise constant.
Since $q$ is continuous, $q$ is constant on $M$. This finishes the proof of the proposition. □

**Theorem 4.21.** *The family of Taylor-Hood elements on hexahedra for polynomial degrees $k \geq 1$*

$$V_h = \{v \in H_0^1(\Omega_f)^d \,|\, v_{|K} \in \mathcal{Q}_k(K)^d,\, K \in \mathcal{T}_h\}$$

*and*

$$P_h = \{p \in L^2(\Omega_f) \cap C(\Omega_f) \,|\, p_{|K} \in \mathcal{Q}_{k-1}(K),\, K \in \mathcal{T}_h\}$$

*fulfills the discretized inf-sup condition.*

*Proof.* Applying the previous theorem, hypotheses (H1)-(H5) need to be checked. The previous proposition states that (H1) is fulfilled. (H2) and (H4) hold because of the choice of macroelements, (H3) is a consequence of the regularity assumptions. Since $\mathcal{Q}_0 \subset \mathcal{P}_k(K)\, \forall k \in \mathbb{N}_0$, the inf-sup condition between $V_h$ and constant pressure functions $\mathcal{Q}_0$ follows from [MT02]. Since all hypotheses are fulfilled, the inf-sup condition for Taylor-Hood elements is fulfilled. □

Since $V_h \subset V$ and $Q_h \subset Q$, the convergence theorem may be applied and results from Stenberg follow.
Before discussing the implementation, it is important to remark, that Taylor Hood finite elements are only globally mass conservative, i.e the condition

$$\int_{\Omega_\mathrm{f}} \nabla \cdot v_h = 0$$

holds in $\Omega_\mathrm{f}$, however, this condition is in general not true any more on the cell level, i.e the condition

$$\int_K \nabla \cdot v_h = 0$$

doesn't hold for a cell K. Since the main interest of this work is the mean intraocular pressure inside the whole domain $\Omega_\mathrm{f}$ (anterior chamber in the application), the mass conservation property of Taylor Hood finite elements is sufficient for the purpose of this thesis.

Moreover, it is important to remark, that there are reentrant corners (with an angle of 270 degrees) in the geometry of the anterior chamber. Moreover, Dirichlet and Robin boundary conditions are not separated. Consequently, an angle of 180 degrees between these boundary conditions is assumed for the computation using singularity analysis. Thus, [BR80] predicts a slower convergence rate than in theorem 4.17. For the velocity, the energy error is about $O(h^{0.544})$ for the case of homogeneous Dirichlet boundary conditions on the geometry with the reentrant corner. Expecting, that the dual problem has the same behavior at the singularity, the order of the $L^2$-error is about $O(h^{1.088})$ according to Aubin Nitsche trick. The change of boundary conditions leads to the same prediction of the convergence order which is about $O(h)$.

### 4.2.3 Implementation

The test case for the Stokes equation was implemented using Finite Element library deal.II. [BHK07],[BHH+15]. Especially, step−56 from the documentation of the library was adapted to the following model. The code of the step−56 was changed, such that mixed boundary conditions may be included. The discretization used in the code is given in definition 4.17. The discretization can be written as an algebraic system with a saddle point structure

$$\begin{pmatrix} A & B^T \\ B & 0 \end{pmatrix} \begin{pmatrix} U \\ P \end{pmatrix} = \begin{pmatrix} F \\ 0 \end{pmatrix}. \tag{18}$$

In order to solve this algebraic system efficiently, the strategy of Timo Heister [Hei11] is helpful. First, a block preconditioner $P$ needs to be found such that the matrix

$$\begin{pmatrix} A & B^T \\ B & 0 \end{pmatrix} P^{-1}$$

is easier to invert. In this case the iterative solver will converge within few iterations. Using the Schur complement $S = BA^{-1}B^T$ [ESW05], write

$$P^{-1} = \begin{pmatrix} A & B^T \\ 0 & S \end{pmatrix}.$$

Consequently, $P^{-1}$ would be a good choice for a preconditioner.
Let $\tilde{A}^{-1}$ be an approximation of $A^{-1}$ and $\widetilde{S^{-1}}$ of $S^{-1}$. Then,

$$P^{-1} = \begin{pmatrix} A^{-1} & 0 \\ 0 & I \end{pmatrix} \begin{pmatrix} I & B^T \\ 0 & -I \end{pmatrix} \begin{pmatrix} I & 0 \\ 0 & S^{-1} \end{pmatrix} \approx \begin{pmatrix} \widetilde{A^{-1}} & 0 \\ 0 & I \end{pmatrix} \begin{pmatrix} I & B^T \\ 0 & -I \end{pmatrix} \begin{pmatrix} I & 0 \\ 0 & \widetilde{S^{-1}} \end{pmatrix}.$$

Since $P$ is a preconditioner, the approximations on the right hand side are used.
Due to the saddle point structure, the matrix is not symmetric anymore. Thus, conjugate gradient method [HS52] is not directly applicable in this case. Consequently, a solver for more general matrices coming from Galerkin approximation is needed. One of such solvers is GMRES method [SS86]. Following [Qua09], the idea of this method is shortly described below. First, rewrite $Ax = b$ to $Cx = Cx - Ax + b$, and then to $x = (I - C^{-1}A)x + C^{-1}b$, where $C$ is a regular matrix. Then, an iteration is given by

$$x^{(k)} = (I - C^{-1}A)x^{(k-1)} + C^{-1}b.$$

Denote the residual at step $k$ as

$$r^{(k)} = b - Ax^{(k)}.$$

The residual at the $k$-th step can be related to the initial residual for the Richardson method as

$$r^{(k)} = \prod_{j=0}^{k-1}(I - \alpha_j A)r^{(0)} = p_k(A)r^{(0)}, \tag{19}$$

where $p_k(A)$ is a polynomial in $A$ of degree $k$. Introducing the space (which is called *Krylov space* of order $m$, associated with a matrix $A$ and a vector $v$)

$$K_m(A; v) = span\{v, Av, A^2v, ..., A^{m-1}v\}, \tag{20}$$

it follows from 19 that $r^{(k)} \in K_{k+1}(A; r^{(0)})$. Similarly, the iterate $x^{(k)}$ is given by

$$x^{(k)} = x^{(0)} + \sum_{j=0}^{k-1} \alpha_j r^{(j)},$$

whence

$$x^{(k)} \in W_k = \{v = x^{(0)} + y, y \in K_k(A; r^{(0)})\}.$$

The idea of GMRES method is to compute $x^{(k)} \in W_k$ minimizing the Euclidean norm of the residual $||r^{(k)}||_2$, i. e

$$||b - Ax^{(k)}||_2 = \min_{v \in W_k} ||b - Av||_2.$$

Since at each step a least-squares problem of size $k$ needs to be solved, the GMRES method will be more effective, the smaller is the number of iterations. Moreover, GMRES method has the finite termination property, that it terminates at most after $n$ iterations, yielding the exact solution. An algorithm of preconditioned GMRES method is described in [Qua09] (which is used for computation in step-56).

In deal.ii, a variable preconditioner $P_k$ (from the right side) is used at the $k$-th

Initialize $x^{(0)}, Pr^{(0)} = f - Ax^{(0)}, \beta = ||r^{(0)}||_2, x^{(1)} = \frac{r^{(0)}}{\beta}$
Iterate:
**for** $j = 1, ..., k$ **do**
  $Pw^{(j)} = Ax^{(j)}$
  **for** $i = 1, ..., j$ **do**
    $g_{ij} = (x^{(i)})^T w^{(j)}$
    $w^j = w^{(j)} - g_{ij} x_i$
  **end**
  $g_{j+1,j} = ||w^{(j)}||_2$
  **if** $g_{j+1,j} = 0$ **then**
    set $k = j$ and Goto (1)
  **end**
  $x^{j+1} = w^{(j)}/g_{j+1,j}$
**end**
$V_k = [x^{(1)}, ..., x^{(k)}]$, $\hat{H}_k = \{g_{ij}\}$, $1 \leq j \leq k, 1 \leq i \leq j+1$;
(1) Compute $z^{(k)}$, the minimizer of $||\beta e_1 - \hat{H}_k z||$
$x^{(k)} = x^{(0)} + V_k z^{(k)}$

**Algorithm 1:** preconditioned GMRES method

iteration. This method is called flexible GMRES or FGMRES. As a preconditioner an incomplete LU decomposition (ILU) is used. Next, the idea of ILU is shortly described. Choose $M$ as a preconditioning matrix to be an incomplete LU decomposition of $A$. Let $P_{sp}$ be a set of pairs of indices $(i, j), 1 \leq i, j \leq n$ representing the desired sparsity pattern (non-zeros of M). An incomplete LU factorization may then be obtained by performing Gaussian elimination on $A$, rejecting all fill-in entries $(k, l)$ if $(k, l) \notin P_{sp}$. A common choice is $P = \{(i, j) \,|\, A_{i,j} \neq 0\}$ (by $A_{i,j} \neq 0$ the entries in $A$ are meant that are not trivially equal to zero on the basis of the discretization method and the nodal numbering). This choice leads to ILU preconditioner where all fill-in entries are rejected. Uniqueness and existence of ILU factorization is shown for M-matrices in [MV77], stability of the ILU factorization for non-symmetric systems has been discussed in [Etm86]. Algorithms realizing ILU may be found in [Lan89] and [MAK03].

### 4.2.4 Test Case

Consider $\Omega_\mathrm{f} = [0, 1] \times [0, 1]$. Let $\Gamma_\mathrm{wall} = \{(x, y) \in [0, 1] \times [0, 1] \,|\, x = 0 \text{ and } x = 1\}$, $\Gamma_\mathrm{in} = \{(x, y) \in [0, 1] \times [0, 1] \,|\, y = 0\}$ and $\Gamma_\mathrm{out} = \{(x, y) \in [0, 1] \times [0, 1] \,|\, y = 1\}$.

The test case is given by the Stokes equation

$$
\begin{aligned}
-\nabla \cdot \mathbb{T}(u,p) &= (0, \pi^2 \sin(\pi x))^T \text{ in } \Omega_\mathrm{f} \\
\nabla \cdot u &= 0 \text{ in } \Omega_\mathrm{f} \\
u &= (0, \sin(\pi x))^T \text{ on } \Gamma_\mathrm{in} \\
u &= 0 \text{ on } \Gamma_\mathrm{wall} \\
-n \cdot \mathbb{T}(u,p) \cdot n &= 10 \text{ on } \Gamma_\mathrm{out} \\
-n \cdot \mathbb{T}(u,p) \cdot \tau &= -\pi \cos(\pi x) \text{ on } \Gamma_\mathrm{out}.
\end{aligned}
$$

The artificial function which fulfills the Stokes equation is given by

$$u(x,y) = (0, \sin(\pi x))^T,$$

$$p(x,y) = 10.$$

This example covers all the boundary conditions and represents a simplified situation in 2D.

| Error | velocity $L^2$ | pressure $L^2$ | Mean pressure |
|---|---|---|---|
| 16 cells | 1.6e-3 | 2.6e-3 | 1.9e-3 |
| 64 cells | 2e-4 | 2.5e-4 | 1.6e-4 |
| 256 cells | 2.6e-5 | 2.7e-5 | 1.3e-5 |
| 1024 cells | 3.2e-6 | 3.1e-6 | 1.1e-6 |
| 4096 cells | 4e-7 | 4e-7 | 8.96e-8 |
| 16384 cells | 5.6e-8 | 3.3e-6 | 1.1e-7 |

There are small singularities at the corners in the solution of the pressure. This table confirms the convergence order $O(h^k)$ with $k = 2.96$ for the velocity in the $L^2$-norm. Since the pressure in the example is constant, it lies in the ansatz space of Taylor Hood finite elements. Due to discretization theory, the error of the pressure and the error of the velocity depend on each other. Consequently, the convergence order of the pressure is approximately the same as for the velocity, $O(h^k)$ with $k = 3$. Because the mathematical model of the aqueous humor flow also describes the flow in a porous medium, Darcy equation is considered in the next chapter.

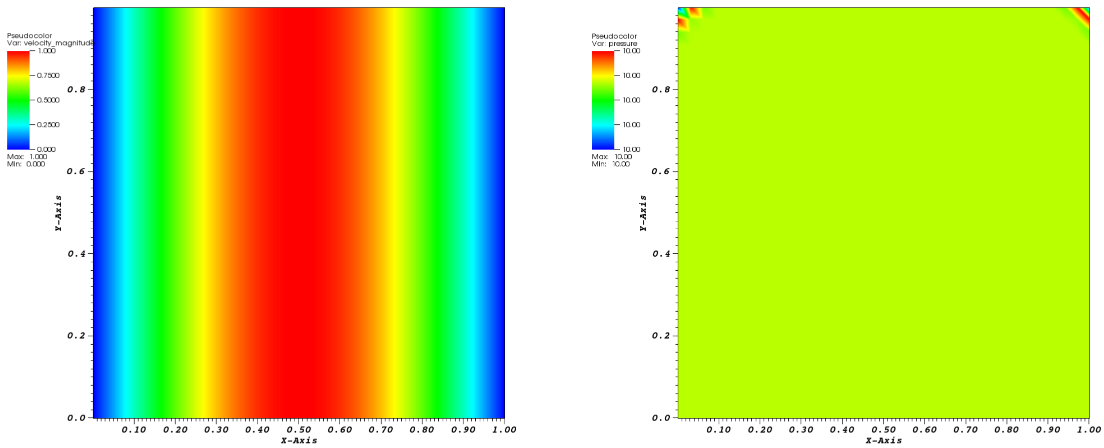


(a) Solution of the velocity

(b) Solution of the pressure

## 4.3 Darcy equation

The following chapter discusses the mathematical analysis of the Darcy equation. To be able to apply results from functional analysis, weak formulation of the Darcy equation is described and finally, existence of solutions for Darcy equation is shown. The second part of this chapter deals with Galerkin approximation and discretization of the Darcy equation. Because the structure of the primal formulation of the Darcy equation differs by a constant from the Poisson equation, the standard results for Poisson equation may be applied here.

### 4.3.1 Existence and uniqueness of solutions

In the strong formulation, the Darcy model reads

$$\begin{aligned}
-\nabla \cdot (\frac{K}{\nu}\nabla p_{\mathrm{D}}) &= f_2 \text{ in } \Omega_{\mathrm{p}} \\
\frac{K}{\nu}\nabla p_{\mathrm{D}} \cdot n &= 0 \text{ on } \Gamma_{\mathrm{wall}} \\
\frac{K}{\nu}\nabla p_{\mathrm{D}} \cdot n &= u_{\mathrm{in}}^{\mathrm{TW}} \cdot n \text{ on } \Gamma_{\mathrm{in}} \\
p_{\mathrm{D}} &= p_{\mathrm{out}} \text{ on } \Gamma_{\mathrm{out}}
\end{aligned}$$

Summarizing $\partial\Omega_{\mathrm{p}} = \Gamma_{\mathrm{out}} \cup \Gamma_{\mathrm{N}}$ and the Neumann boundary to $\Gamma_{\mathrm{N}} = \Gamma_{\mathrm{wall}} \cup \Gamma_{\mathrm{in}}$ and defining the function $\phi$ on $\Gamma_{\mathrm{N}}$ with $\phi = 0$ on $\Gamma_{\mathrm{wall}}$ and $\phi = u_{\mathrm{in}}^{\mathrm{TW}}$ on $\Gamma_{\mathrm{in}}$ leads to

$$\begin{aligned}
-\nabla \cdot (\frac{K}{\nu}\nabla p_{\mathrm{D}}) &= f_2 \text{ in } \Omega_{\mathrm{p}} \\
\frac{K}{\nu}\nabla p_{\mathrm{D}} \cdot n &= \phi \cdot n \text{ on } \Gamma_{\mathrm{N}} \\
p_{\mathrm{D}} &= p_{\mathrm{out}} \text{ on } \Gamma_{\mathrm{out}}
\end{aligned} \tag{21}$$

With the lifting method (21) and introducing $p_{\text{hom}} = p_{\text{D}} - p_{\text{out}}$ with inhomogeneous Dirichlet boundary conditions can be written as a Darcy equation with homogeneous boundary conditions

$$\begin{aligned} -\nabla \cdot (\frac{K}{\nu} \nabla p_{\text{hom}}) = f_2 - \nabla \cdot \frac{K}{\nu} \nabla p_{\text{out}} \in H^{-1} \\ \frac{K}{\nu} \nabla p_{\text{hom}} \cdot n = \phi \cdot n - \frac{K}{\nu} \nabla p_{\text{out}} \cdot n \text{ on } \Gamma_{\text{N}} \\ p_{\text{hom}} = 0 \text{ on } \Gamma_{\text{out}} \end{aligned} \tag{22}$$

Green formula and integration by parts lead to the weak formulation of the Darcy equation.

**Definition 4.22.** *Let $p_{hom} = p - \tilde{p}$. The weak formulation reads:*
*Find $p_{hom} \in H_0^1(\Omega_p)$ such that for all $\xi \in H_0^1(\Omega_p)$, it holds*

$$a(p_{hom}, \xi) = (\tilde{f}, \xi)_{L^2(\Omega_p)} - ((u_{in}^{TW} - \frac{K}{\nu} \nabla p_{out}) \cdot n, \xi)_{L^2(\partial\Omega_p)},$$

*where*

$$\begin{aligned} (\tilde{f}, \xi)_{L^2(\Omega_p)} &= (f, \xi)_{L^2(\Omega_p)} - (\nabla \cdot (\frac{K}{\nu} \nabla p_{out}), \xi)_{L^2(\Omega_p)} \\ a(p_{hom}, \xi) &= (\frac{K}{\nu} \nabla p_{hom}, \nabla \xi)_{L^2(\Omega_p)}. \end{aligned}$$

Defining $\tilde{g} := (u_{\text{in}}^{\text{TW}} - \frac{K}{\nu} \nabla p_{\text{out}}) \cdot n \in H^{\frac{1}{2}}(\partial\Omega_{\text{p}})$, the weak formulation has a similar form like the problem $(P^*)$:

$$a(p_{\text{hom}}, \xi) = (\tilde{f}, \xi)_{L^2(\Omega_{\text{p}})} - (\tilde{g}, \xi)_{L^2(\partial\Omega_{\text{p}})}.$$

Consequently, the proof for existence and uniqueness of solutions for Darcy equation can be given by the application of Lax Milgram theorem.

**Theorem 4.23.** *The Darcy problem with $\tilde{f} \in H^{-1}(\Omega_p), (K\nabla\tilde{p}) \cdot n \in H^{-\frac{1}{2}}(\Gamma_{wall})$ and $\tilde{p} \in H^{\frac{1}{2}}(\Gamma_D)$ has one and only one solution.*

*Proof.* It suffices to show boundedness and coercivity of $a(\cdot,\cdot)$ due to Lax Milgram theorem.

- $|a(p_{\text{hom}}, \xi)| = K|(\nabla p_{\text{hom}}, \nabla \xi)_{L^2(\Omega_{\text{p}})} \leq K||p_{\text{hom}}||_V ||\xi||_V$
- $|a(\phi, \phi)| = |(K\nabla\phi, \nabla\phi)_{L^2(\Omega_{\text{p}})}| = K(\phi, \phi)_V = K||\phi||_V^2$

The right hand side is bounded as in the argumentation for the problem $(P^*)$. □

Now, existence and uniqueness of solutions for Darcy equation is shown and numerical investigations are considered.

### 4.3.2 Discretization

Since the Darcy model differs by a constant from the Poisson equation, standard results are recalled.

**Definition 4.24.** *The weak formulation of the Darcy equation reads: Find $p_h \in H_0^1(\Omega_p)$ such that for all $\xi_h \in V_h \subset H_0^1(\Omega_p)$, it holds*

$$a(p_h, \xi_h) = (\tilde{f}, \xi_h)_{L^2(\Omega_p)} - ((u_{in}^{TW} - \frac{K}{\nu}\nabla p_{out}) \cdot n, \xi_h)_{L^2(\partial\Omega_p)},$$

*where*

$$\begin{aligned}(\tilde{f}, \xi_h)_{L^2(\Omega_p)} &= (f, \xi_h)_{L^2(\Omega_p)} - (\nabla \cdot (\frac{K}{\nu}\nabla p_{out}), \xi_h)_{L^2(\Omega_p)},\\ a(p_h, \xi_h) &= (\frac{K}{\nu}\nabla p_h, \nabla \xi_h)_{L^2(\Omega_p)}.\end{aligned}$$

Due to Lax Milgram theorem, discretized Darcy equation has a unique solution. The best approximation result follows from the Cea's lemma (theorem 4.1). Following finite elements are used for discretization.

**Definition 4.25.** *Lagrange elements on quadrilaterals and hexahedra (for the choices $d = 2, 3$) for polynomial degrees $k \geq 1$ are given by*

$$V_h = \{v \in H_0^1(\Omega_p)^d \,|\, v_{|K} \in \mathcal{Q}_k(K)^d,\ K \in \mathcal{T}_h\}$$

Using this elements, it holds $V_h \subset H_0^1(\Omega_\mathrm{p})$ and supposing $u \in H_0^1(\Omega_\mathrm{p}) \cap H^{k+1}(\Omega_\mathrm{p})$, following $L^2$ error estimate holds (Aubin Nitsche, see for example [GT17]):

$$||u - u_0||_{L^2(\Omega_\mathrm{p})} \leq Ch^{k+1}||u||_{H^{k+1}(\Omega_\mathrm{p})}.$$

### 4.3.3 Implementation

The Darcy equation with mixed boundary conditions was implemented using Finite Element library deal.II. [BHK07],[BHH$^+$15]. Especially, step$-$4 from the documentation of the library was adapted to the following model.
Then, the code of the step$-$4 was changed, such that mixed boundary conditions may be included. Moreover, mean pressure value in the whole domain is computed.
The discretization used in the code is given by:

$$(\frac{K}{\nu}\nabla p_h, \nabla \xi_h)_{L^2(\Omega_\mathrm{p})} = (f, \xi_h)_{L^2(\Omega_\mathrm{p})}.$$

The discretization can be written as an algebraic system $AU = F$. This algebraic system is solved using a conjugate gradient (CG) method ([HS52], and the algorithm explained in [Bra07]) in deal.ii. The idea of the CG method is to find a minimum of the function

$$f(x) = \frac{1}{2}x'Ax - b'x,$$

since the solution of this equation leads to a solution of $Ax = b$ (where $A$ is symmetric positive definite). The algorithm of the CG method is given by:

**Definition 4.26.** *Choose $x_0 \in \mathbb{R}^n$. Set $d_0 = -g_0 = b - Ax_0$ and compute for $k = 0, 1, 2, ...$*

*(1) $d\alpha_k = \frac{g_k' g_k}{d_k' A d_k}$*

*(2) $x_{k+1} = x_k + \alpha_k d_k$*

*(3) $g_{k+1} = g_k + \alpha_k A d_k$*

*(4) $\beta_k = \frac{g_{k+1}' g_{k+1}}{g_k' g_k}$,*

*(5) $d_{k+1} = -g_{k+1} + \beta_k d_k$, as long as $d_k \neq 0$.*

**Theorem 4.27.** *For all $x_0 \in \mathbb{R}^n$ it holds for the CG method*

$$||x_k - x^*||_A \leq 2(\frac{\sqrt{\kappa} - 1}{\sqrt{\kappa} + 1})^k ||x_0 - x^*||_A.$$

*Proof.* see [Bra07]. □

This inequality describes the case, where all eigenvalues are equally distributed between the smallest eigenvalue of $A$ $\lambda_{min}$ and the greatest eigenvalue $\lambda_{max}$. However, eigenvalues occur in groups. Consequently, there are gaps in the eigenvalue spectrum and therefore, this estimate may be improved in certain situations. (see [Bra07] and citations therein)

### 4.3.4 Test Case

Consider $\Omega_\mathrm{p} = [0,1]\times[0,1]$. Let $\Gamma_\mathrm{wall} = \{(x,y) \in [0,1] \times [0,1] \,|\, x = 0 \text{ and } x = 1\}$, $\Gamma_\mathrm{in} = \{(x,y) \in [0,1] \times [0,1] \,|\, y = 0\}$ and $\Gamma_\mathrm{out} = \{(x,y) \in [0,1] \times [0,1] \,|\, y = 1\}$.
The test case for the Darcy equation with $K = 1$ and $\nu = 1$ is defined by

$$\begin{aligned} -\Delta p &= 2\pi^2 \sin(\pi x)\cos(\pi y) \text{ in } \Omega_\mathrm{p} \\ \nabla p \cdot n &= u_\mathrm{in}^\mathrm{TW} \cdot n \text{ on } \Gamma_\mathrm{in} \\ p &= \sin(\pi x)\cos(\pi y) \text{ on } \Gamma_\mathrm{wall} \text{ and } \Gamma_\mathrm{out}. \end{aligned}$$

The artificial function fulfilling the Darcy equation is given by

$$p(x,y) = \sin(\pi x)\cos(\pi y).$$

Set

$$u_\mathrm{in}^\mathrm{TW} \cdot n = -\pi \sin(\pi x)\sin(\pi y).$$

This example covers mixed boundary conditions for the Darcy equation (Laplace equation) on a square. The table demonstartes $L^2$ convergence. Since the function in the example has a mean value zero, the mean pressure converges right away.

| Degrees of freedom | pressure $L^2$ | Mean pressure |
|---|---|---|
| 25 | 4e-2 | 4e-17 |
| 81 | 1e-2 | 7e-17 |
| 289 | 2e-3 | 6e-18 |
| 1089 | 6e-4 | 5e-17 |
| 4225 | 1.5e-4 | 3e-18 |
| 16641 | 3.85e-5 | 3.5e-16 |

This data confirms the convergence order $O(h^k)$ with $k = 2$ in the $L^2$-norm.

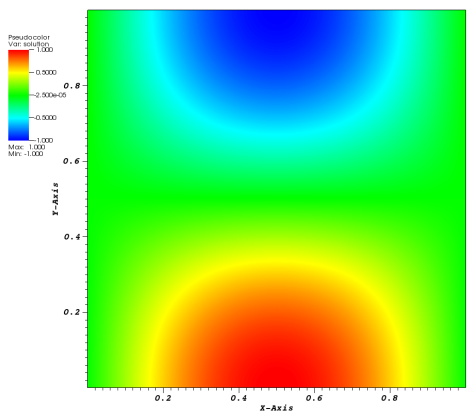


(a) Solution of the pressure

## 4.4 Application of theoretical results to the model

First, a weak formulation of the model is recalled:

**Definition 4.28.** *Let* $\partial\Omega_f = \Gamma_D \cup \Gamma_N$*,* $\partial\Omega_p = \Gamma_{ND} \cup \Gamma_{out}$ *and*
$V_S := \{v \in (H^1(\Omega_f))^d \, : \, v|_{\Gamma_D} = v_0\}$.
*Find* $(u,p) \in V_S \times L^2(\Omega_f)$ *such that for all* $v \in V_S$ *and for all* $q \in L^2(\Omega_f)$ *it holds*

$$a_f(u,v) + \sum_{i=1}^{d-1}(\frac{1}{\alpha}u \cdot \tau_i, v \cdot \tau_i)_{L^2(\Gamma_N)} + b_f^T(v,p) = (f_S, v)_{L^2(\Omega_f)} - (v \cdot n, p_0)_{L^2(\Gamma_N)}$$
$$b_f(u,q) = 0,$$

*where*

$$\begin{aligned} b_f(v,p) &= -(\nabla \cdot v, p)_{L^2(\Omega_f)}, \\ a_f(u,v) &= 2\nu(\mathbb{D}(u), \mathbb{D}(v))_{L^2(\Omega_f)}, \\ p_0 &= \frac{1}{|\Omega_p|}\int_{\Omega_p} p_D(x)\, dx, \end{aligned}$$

*where* $p_D$ *is the solution of the* Darcy equation*:*
*Find* $p_D \in V_D := \{p_D \in (H^1(\Omega_p)) \, : \, p_D|_{\Gamma_{out}} = p_{out}\}$ *such that:*

$$a_p(p_D, \xi) = (f_D, \xi)_{L^2(\Omega_p)} - (u_{in}^{TW} \cdot n, \xi)_{L^2(\Gamma_{ND})} \qquad \forall \xi \in V,$$

*where*

$$a : V \times V \to \mathbb{R},\, a(p_D, \xi) = (K\nabla p_D, \nabla\xi)_{L^2(\Omega_p)}$$

**Theorem 4.29.** *There exists a unique solution for the model.*

*Proof.* Darcy equation has a unique solution. Thus, the value $p_0$ in the Robin boundary condition of the Stokes equation is uniquely determined. Since Stokes equation with mixed boundary conditions has a unique solution, the whole model has a unique solution. □

## Discretization

The discretized weak formulation of the model is given by:

**Definition 4.30.** *Let $\partial\Omega_f = \Gamma_D \cup \Gamma_N$, $\partial\Omega_p = \Gamma_{ND} \cup \Gamma_{out}$ and let $V_{Sh}$ and $Q_{Sh}$ fulfill the assumptions of the theorem 4.14. Find $(u_h, p_h) \in V_{Sh} \times Q_{Sh}$ such that for all $v_h \in V_{Sh}$ and for all $q_h \in Q_{Sh}$ it holds*

$$a_f(u_h, v_h) + \sum_{i=1}^{d-1}(\frac{1}{\alpha}u_h \cdot \tau_i, v_h \cdot \tau_i)_{L^2(\Gamma_N)} + b_f^T(v_h, p_h) = (f_S, v_h)_{L^2(\Omega_f)} - (v_h \cdot n, p_0)_{L^2(\Gamma_N)}$$
$$b_f(u_h, q_h) = 0,$$

*where*

$$\begin{aligned} b_f(v_h, p_h) &= -(\nabla \cdot v_h, p_h)_{L^2(\Omega_f)}, \\ a_f(u_h, v_h) &= 2\nu(\mathbb{D}(u_h), \mathbb{D}(v_h))_{L^2(\Omega_f)}, \\ p_0 &= \frac{1}{|\Omega_p|}\int_{\Omega_p} p_{Dh}(x)\, dx, \end{aligned}$$

*where $p_{Dh}$ is the solution of the discretized* Darcy equation*:*
*Find $p_{Dh} \in V_{Dh}$ such that:*

$$a_p(p_{Dh}, \xi_h) = (f_D, \xi_h)_{L^2(\Omega_D)} - (u_{in}^{TW} \cdot n, \xi_h)_{L^2(\Gamma_{ND})} \qquad \forall \xi_h \in V_{Dh},$$

*where*

$$a : V_{Dh} \times V_{Dh} \to \mathbb{R},\ a(p_{Dh}, \xi_h) = (K\nabla p_{Dh}, \nabla\xi_h)_{L^2(\Omega_p)}.$$

**Theorem 4.31.** *There exists a unique solution for the discretized model.*

*Proof.* Discretized Darcy equation has a unique solution. Thus, the value $p_0$ in the Robin boundary condition of the Stokes equation is uniquely determined. Since discretized Stokes equation with mixed boundary conditions has a unique solution, the whole model has a unique discrete solution. □

Choosing for $V_{\mathrm{Sh}}$ and $Q_{\mathrm{Sh}}$ Taylor Hood finite elements and for $V_{\mathrm{Dh}}$ Lagrange finite elements, convergence results from previous sections apply on each region. Thus, the model is well posed in numerical sense.
Following strategy is applied to solve the model for the chosen parameters:

- Solve Darcy equation and compute the mean pressure value in the Darcy domain
- Solve the Stokes equation with the Robin boundary using the mean pressure value from above

# 5 Results

In this section simulation results in 3D are presented. First, the geometry of the eye is shown. Then, rescaling of the equations, the generation of results and the implementation are explained. Then, results are illustrated. In particular, following dependencies are considered:

- Impact of the position of the patient (lying prone, lying supine, lying on the right or left side, standing or sitting) on the IOP
- Impact of the inflow rate on the IOP
- Impact of the porosity on the IOP
- Impact of the episcleral venous pressure on the IOP
- Impact of the radius of the pupil on the IOP
- Impact of the thickness of the natural lens on the IOP
- Impact of the viscosity on the IOP

On the other hand, following medical applications are considered:

- IOP for patients wearing scleral lenses
- IOP after cataract surgery
- IOP after glaucoma operations like trabeculectomy or stent insertion

Moreover, there are people who already have been through a surgery. To estimate how the IOP has changed after exchange of the lens in the case of cataract surgery and how IOP has changed after trabeculectomy or stent insertion, some model cases are considered.

## 5.1 Geometry

The geometry of the anterior chamber is a part of a patent [FDO18]. Thus, this chapter summarizes information concerning the parameters and roughly describes the geometry.

### Anterior Chamber

Based on measurements of [RKA06], [BR13], [HKM$^+$12] and [MO17] it is assumed that the depth of the anterior chamber is about 3 mm. Moreover, the horizontal internal radius of the anterior chamber is approximately 6.1 mm (at the position where the lens is and where zonules are), see [WBS$^+$10] and [BJB05]. In the current model it is assumed that the ciliary body has a spread of approximately 1 mm. (Thus, internal radius of 7 mm is chosen.) The geometrical form of the anterior chamber is assumed to be a semi-ellipsoid.

## Iris

First, a case of a *healthy iris* is considered. The pupil is represented as a cylinder. According to measurements [NHF+11] and [KYK+14] distance between the lens and the iris (which is called lens vault) is assumed to be 0.3 mm for a healthy eye. In comparison, the model of [Kum03] supposed that the lens vault is about 0.25 mm. The thickness of the iris is about 0.4 mm [MVMP00], [HYSL16] and [IGC+15] and varies in different regions between 0.2 and 0.6 mm for patients with closed-angle glaucoma [SDC+17], [LHP+13]. This value may be taken as a height of the cylinder representing the pupil.
Furthermore, two special cases are interesting - the eye by daylight, that means that the radius of the pupil is about 1 or 2 mm as well as the eye at night, when it is dark, that means that pupil can reach the radius about 9 mm [MVMP00]. $R$ (the radius of the cylinder) can be set to any number mentioned here.
According to data from [MRK14], [MZZ+14] and [BR13], the anterior chamber depth varies between 3 and 4 mm in the healthy case and 1.5 to 2.2 mm in the case of open angle glaucoma. These data was used to construct a curved iris (for patients tending to develop closed-angle glaucoma).

## Natural ocular lens

The part of the ocular lens which is needed for the geometry takes a form of a semi-ellipsoid. The diameter of the lens varies between 6.5 and 9 mm according to measurements [RDF+06] and [MSG+08]. The thickness of the lens varies between 3.5 and 5 mm and changes with age [MVMP00], [MZZ+14], [MO17].

## Artificial lens

Artificial lens is given by a cylinder with a height of 0.5 mm and the radius 3 mm. These parameters are common in industry (see for instance parameters of lenses Alcon SA60AT, SN60WF, Cova PU6A).

## Trabecular meshwork

The trabecular meshwork is modeled as a thin tube around the anterior chamber. In order to be able to solve the model for realistic parameters, rescaling is explained in the next section.

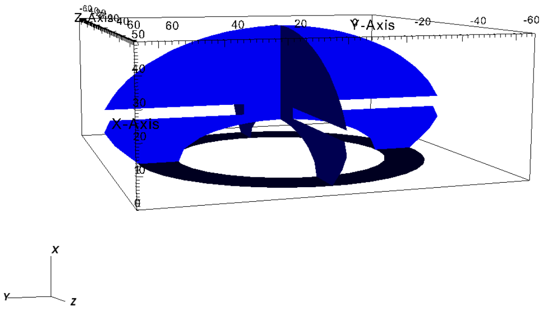


(a) Healthy eye with a natural ocular lens

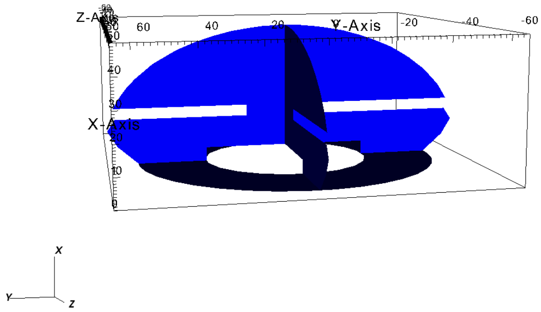


(b) Healthy eye with an artificial lens

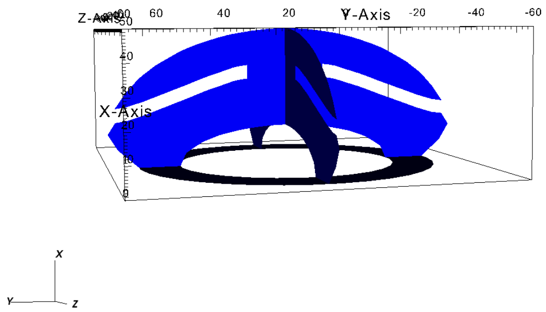


(c) Pathological eye with a natural ocular lens

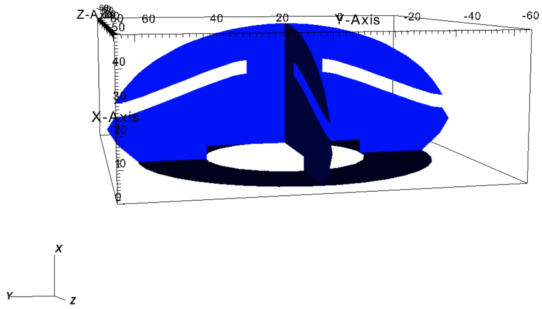


(d) Pathological eye with an artificial lens

Figure 3: Anterior chamber

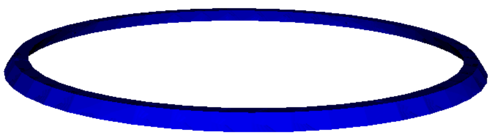

Figure 4: Trabecular meshwork

## 5.2 Rescaling

Due to great differences in the magnitude of the parameters, the matrices built by the finite element method might be ill posed. To improve the condition of this matrix (and to make the problem well posed), the rescaling technique is used.
The Stokes equation is given by

$$\begin{aligned} -\nabla \cdot \mathbb{T}(u,p) &= \rho g e_z \\ \nabla \cdot u &= 0 \\ u_{\text{in}} &= u_0 \text{ on } \Gamma_{\text{in}} \\ u &= 0 \text{ on } \Gamma_{\text{wall}} \\ -n \cdot \mathbb{T}(u,p) \cdot n &= p_0 \text{ on } \Gamma_{\text{out}} \\ -\tau \cdot \mathbb{T}(u,p) \cdot n &= \tilde{\alpha} u \cdot \tau \text{ on } \Gamma_{\text{out}}. \end{aligned}$$

Now, apply the rescaling argument

$$\bar{x} = \frac{x}{L}, \quad \bar{y} = \frac{y}{L}, \quad \bar{z} = \frac{z}{L}, \quad \bar{u} = \frac{u}{u_c}, \quad \bar{p} = \frac{p}{p_c},$$

where $L$ is a unit length, $u_c$ a unit velocity and $p_c$ unit pressure.
Applying the chain rule, the first derivative transforms as

$$\frac{\partial u(x)}{\partial x} = \frac{\partial(u_c \cdot \bar{u}(\bar{x}))}{\partial \bar{x}} \cdot \frac{\partial \bar{x}}{\partial x} = \frac{u_c}{L} \frac{\partial \bar{u}(\bar{x})}{\partial \bar{x}}.$$

Consequently, it implies

$$\frac{\partial^2 u(x)}{\partial^2 x} = \frac{u_c}{L^2} \frac{\partial^2 \bar{u}(\bar{x})}{\partial^2 \bar{x}}.$$

Thus, it holds

$$\begin{aligned} \nabla p(x) &= \frac{p_c}{L} \bar{\nabla} \bar{p}(\bar{x}), \\ \Delta u(x) &= \frac{u_c}{L^2} \bar{\Delta} \bar{u}(\bar{x}), \\ \nabla \cdot \mathbb{D}(u(x)) &= \frac{u_c}{L^2} \nabla \cdot \mathbb{D}(\bar{u}(\bar{x})), \\ \nabla \cdot u(x) &= \frac{u_c}{L} \bar{\nabla} \cdot \bar{u}(\bar{x}), \\ \bar{u_0} &= \frac{u_0}{u_c}. \end{aligned}$$

The nondimensional equation reads

$$
\begin{aligned}
-2\nu\frac{u_c}{L^2}\nabla\cdot\mathbb{D}(\bar{u}(\bar{x}))+\frac{p_c}{L}\bar{\nabla}\bar{p} &= \rho g e_z\\
\bar{\nabla}\cdot\bar{u} &= 0\\
\bar{u_{\text{in}}} &= \bar{u_0} \text{ on } \Gamma_{\text{in}}\\
\bar{u} &= 0 \text{ on } \Gamma_{\text{wall}}\\
-n\cdot(2\nu\frac{u_c}{L}\mathbb{D}(\bar{u})-p_c\bar{p})\cdot n &= \bar{p_0} \text{ on } \Gamma_{\text{out}}\\
-\tau\cdot(2\nu\frac{u_c}{L}\mathbb{D}(\bar{u})-p_c\bar{p})\cdot n &= \tilde{\alpha}u_c\bar{u}\cdot\tau \text{ on } \Gamma_{\text{out}}.
\end{aligned}
\tag{23}
$$

According to the model parameters the scaling is given by $L\approx 10^{-4}$, $U\approx 10^{-2}$ and $\nu\approx 10^{-4}$. Choosing the parameters for the model, the coefficients range is

$$
\begin{aligned}
\nu\frac{u_c}{L^2} &\approx 10^2,\\
\frac{p_c}{L}=\frac{\rho u_c^2}{L} &\approx 10^3,\\
g\rho\cdot e_z &\approx 9810\cdot e_z,
\end{aligned}
$$

where $p_c=\rho U^2$ (here $\rho\approx 1000\frac{kg}{m^3}$) is a common pressure scale in fluid mechanics, arising from Bernoullis equation

$$
p+\frac{1}{2}\rho u\cdot u = const.
$$

The equation which is implemented in deal.ii looks

$$
\begin{aligned}
-1.4\nabla\cdot\mathbb{D}(\bar{u}(\bar{x}))+\bar{\nabla}\bar{p} &= -9.81e_x\\
\bar{\nabla}\cdot\bar{u} &= 0\\
\bar{u_{\text{in}}} &= 0.15 \text{ on } \Gamma_{\text{in}}\\
\bar{u} &= 0 \text{ on } \Gamma_{\text{wall}}\\
-n\cdot\mathbb{T}(\bar{u},\bar{p})\cdot n &= 10p_0 \text{ on } \Gamma_{\text{out}}\\
-\tau\cdot\mathbb{T}(\bar{u},\bar{p})\cdot n &= 0.1\tilde{\alpha}\bar{u}\cdot\tau \text{ on } \Gamma_{\text{out}}.
\end{aligned}
$$

Next, compute the rescaling of the Darcy equation. Since both equations are solved separately, each equation may be adjusted to its own scale.

The Darcy equation is given by

$$
\begin{aligned}
-\nabla \cdot (\frac{K}{\nu}\nabla p) &= -\rho g \\
(\frac{K}{\nu}\nabla p) \cdot n &= u_{\text{in}}^{\text{TW}} \cdot n \text{ on } \Gamma_{\text{in}} \\
(\frac{K}{\nu}\nabla p) \cdot n &= 0 \text{ on } \Gamma_{\text{wall}} \\
p_{out} &= 1200 \text{ on } \Gamma_{\text{out}}.
\end{aligned}
$$

It is given

$$
\begin{aligned}
\rho g &= 9810\,\frac{\text{kg}}{\text{m}^2\text{s}^2}, \\
\nu &= 0.0007\,\frac{\text{kg}}{\text{ms}}, \\
K &= 10^{-15}\,\text{m}^2.
\end{aligned}
$$

Converting the scale from $m$ to $mm$ leads to

$$
\begin{aligned}
\rho g &= 0.00981\,\frac{\text{kg}}{\text{mm}^2\text{s}^2}, \\
\nu &= 0.0000007\,\frac{\text{kg}}{\text{mms}}, \\
K &= 10^{-9}\,\text{mm}^2, \\
p_{in} &= 1.2\,\frac{\text{kg}}{\text{mms}}.
\end{aligned}
$$

Thus, it follows

$$
\frac{K}{\nu} = 10^{-2} \cdot \frac{1}{7} \approx 0.00143.
$$

Using the new scale, following equation is implemented:

$$
\begin{aligned}
-\nabla \cdot (\frac{K}{\nu}\nabla p) &= -0.00981 \\
(\frac{K}{\nu}\nabla p) \cdot n &= u_{\text{in}}^{\text{TW}} \cdot n \text{ on } \partial\Gamma_{\text{wall}} \\
(\frac{K}{\nu}\nabla p) \cdot n &= 0 \text{ on } \Gamma_{\text{wall}} \\
p_{\text{out}} &= 1.2 \text{ on } \Gamma_{\text{out}}.
\end{aligned}
$$

Using this rescaling technique both equations can be solved.

## 5.3 Implementation

First, the Darcy equation is solved and a mean pressure is computed. After Darcy equation is solved, mean value of the pressure in the Darcy equation is incorporated into the Stokes equation. Then, the Stokes equation is solved and the IOP and the flow of the aqueous humor is computed.
The Darcy equation with mixed boundary conditions was implemented using Finite Element library deal.II. [BHK07],[BHH$^+$15]. Especially, step$-4$ from the documentation of the library was adapted to the model in this thesis.
The geometry of the trabecular meshwork was constructed with a help of GMSH [GR09] (see results section for further details). Since GMSH generates tetrahedral finite elements in three dimensions and deal.II library only works with hexahedral finite elements, the GMSH grid was converted to hexahedrals using the program ./tethex [Art15].
The details about the algebraic solvers and discretization of the Darcy equation can be found in section 3 (Darcy equation, discretization, test case).
The inflow velocity in the trabecular meshwork was modeled using polar coordinates and *arctan*-function. It is assumed that the inflow is rotational symmetric in $y$ and $z$ coordinates and that the inflow function is continuous. First, the angle is computed, to guarantee that the inflow in the trabecular meshwork is oriented contrary to the center of natural lens in the anterior chamber.

$$\phi = \begin{cases} \arctan(\frac{z}{y}) & y > 0 \\ \arctan(\frac{z}{y}) + \pi & y < 0 \text{ and } z \geq 0 \\ \arctan(\frac{z}{y}) - \pi & y < 0 \text{ and } z < 0 \\ \frac{\pi}{2} & y = 0 \text{ and } z > 0 \\ -\frac{\pi}{2} & y = 0 \text{ and } z < 0 \end{cases}$$

Using this values, components of the inflow velocity are defined:

$$\begin{aligned} u_{\text{in},x} &= 0 \\ u_{\text{in},y} &= 2 \cdot 0.032 \cdot (x-2) \cdot (x-2.4) \cdot \cos(\phi) \\ u_{\text{in},z} &= 2 \cdot 0.032 \cdot (x-2) \cdot (x-2.4) \cdot \sin(\phi) \end{aligned}$$

The boundary segment $\Gamma_{\text{wall}}$ is defined by the unification of the intersections of the planes $x = 2.4$ and $x = 2$ with the geometry of the trabecular meshwork. The boundary segment $\Gamma_{\text{in}}$ is given by the intersection of the geometry of the trabecular meshwork and the surface of the semi-ellipsoid

$$\{(x, y, z) \in \mathbb{R}^3_+ \,|\frac{x^2}{25} + \frac{y^2}{49} + \frac{z^2}{49} = 1\}.$$

The segment $\Gamma_{\text{out}}$ is denoted by the intersection of the geometry of the trabecular meshwork and the surface of the semi-ellipsoid

$$\{(x,y,z) \in \mathbb{R}^3_+ \,|\frac{x^2}{25} + \frac{y^2}{7.5^2} + \frac{z^2}{7.5^2} = 1\}.$$

The quadratic function leads to a smooth continuation between the segment $\Gamma_{\text{wall}}$, where $\frac{K}{\nu}\nabla p \cdot n = 0$ holds, and $\Gamma_{\text{in}}$, where $\frac{K}{\nu}\nabla p \cdot n = u_{\text{in}}^{\text{TW}} \cdot n$. The maximum of the quadratic function is computed such that it holds $u_{\text{in}}^{\text{TW}} = 0.85 \cdot u_{\text{in}}^{\text{CB}}$, where $u_{\text{in}}^{\text{CB}} = 4 \cdot 10^{-7} \frac{\text{m}}{\text{s}}$ (inflow rate $2\frac{\mu\text{l}}{\text{min}}$). At the segment $\Gamma_{\text{out}}$, it holds $p = p_0$, where $p_0 = 1200$ Pa.
The Stokes equation with Robin boundary condition was implemented using Finite Element library deal.II. [BHK07],[BHH+15]. Especially, step−56 from the documentation of the library was adapted to the following model.
Similarly to Darcy, the geometry of the anterior chamber was constructed with a help of GMSH [GR09] and the grid was converted to hexahedrals using the program ./tethex [Art15]. The results are visualized using the open source software VisIt [CBW+12]. The plots are produced using Matlab [MAT09].
The inflow velocity in the ciliary body was modeled using polar coordinates and *arctan*-function. It is assumed that the inflow is rotational symmetric in $x$ and $y$ coordinates and that the inflow function is continuous. In order to obtain $u = 0$ near the iris and $u = 0$ near the zonules, the inflow velocity $u$ is fitted, such that the boarderlines between the $\Gamma_{\text{wall}}$ and $\Gamma_{\text{in}}$ boundaries are continuous. Following formulas are used:
First, the angle is computed, to guarantee that the inflow is oriented towards the center of natural lens in the anterior chamber.

$$\phi = \begin{cases} \arctan(\frac{y}{x}) & x > 0 \\ \arctan(\frac{y}{x}) + \pi & x < 0 \text{ and } y \geq 0 \\ \arctan(\frac{y}{x}) - \pi & x < 0 \text{ and } y < 0 \\ \frac{\pi}{2} & x = 0 \text{ and } y > 0 \\ -\frac{\pi}{2} & x = 0 \text{ and } y < 0 \end{cases}$$

After this, compute $\text{rad} = \sqrt{x^2 + y^2}$ and choose the scaling $\text{sc} = 10$. Using this values, components of the inflow velocity are defined:

$$\begin{aligned} u_{\text{in},x} &= (5.5 \cdot \text{sc} - \text{rad}) \cdot \cos(\phi) \\ u_{\text{in},y} &= (5.5 \cdot \text{sc} - \text{rad}) \cdot \sin(\phi) \\ u_{\text{in},z} &= 0 \end{aligned}$$

The boundary segment $\Gamma_{\text{in}}$ is the boundary of the geometry for the points $0 < z < 1.64$. On this part, it holds $u = u_{\text{in}}$. The segment $\Gamma_{\text{out}}$ is the boundary for the geometry for points $2.05 < z < 2.45$. On this part, the Robin boundary condition $n\mathbb{T}(u,p)n = p_0$ and $n\mathbb{T}(u,p)\tau = \tilde{\alpha} u \tau$ holds. The rest part of the boundary is $\Gamma_{\text{wall}}$ on which $u = 0$

holds.
Then, the code of the step−56 was changed, such that mixed boundary conditions may be included. Moreover, mean pressure values were computed in the region between the iris and the lens (posterior chamber) and in the region between the cornea and the iris (anterior chamber) as well as the mean pressure in the whole front part of the eye.
The details about algebraic solvers and discretization can be found in section 4 (Stokes equation, discretization, test case.)

## 5.4 Changes of specific parameters

On the one hand, one specific parameter in the model is changed and its impact on the IOP is computed. The mean IOP is computed in three regions of the front part of the eye: in the anterior chamber (denoted as IOP (AC)), a region between the cornea and the iris, in the posterior chamber (denoted as IOP (PC)), a region between the zonules and the iris, and the IOP in the whole front part of the eye (IOP). Following parameters are fixed in the simulations (if not stated otherwise)

- Inflow velocity is about $u_{\text{in}} = 4 \cdot 10^{-7} \frac{\text{m}}{\text{s}}$ (inflow rate $2 \frac{\mu \text{l}}{\text{min}}$)
- The permeability is given by $K = 0.35 \cdot 10^{-15}\,\text{m}^2$.
- Episcleral venous pressure $p_{\text{out}} = 1200$ Pa.
- The outflow boundary condition is set for the surface of the geometry with $2.05 < x < 2.45$.
- The inflow boundary condition is set for the surface of the geometry with $0 < x < 1.64$ and the radius in the $y - z$ plane $r > 5.5$.
- No slip condition $u = 0$ is set in the remaining parts.
- The radius of the pupil is 1.5 mm.
- The width (noted as $w$) of the natural lens lense is supposed to be 8 mm and the height of the half of the lens (noted as $h$) is 1.4 mm.
- the viscosity is chosen as $\nu = \frac{0.7\text{g}}{\text{m} \cdot \text{s}}$.
- The force is given by $f = (-g, 0, 0)$ (the patient is lying supine).

### Inflow Rate and IOP

Inflow rate of the aqueous humor may change due to circadian rhythm, operations in the ciliary body, secondary glaucoma and many other reasons [G+10].

| Inflow Rate | Pressure TW | IOP |
|---|---|---|
| 1 | 2002 | 2001.94 |
| 2 | 2002.13 | 2002.07 |
| 3 | 2002.27 | 2002.21 |
| 4 | 2002.41 | 2002.35 |
| 5 | 2002.54 | 2002.48 |

Since the velocity of the aqueous humor is very small in the front part of the eye, there is no significant change in IOP caused by inflow rate of the aqueous humor according to the model. The table shows a tendency that the IOP increases if the aqueous humor (AH) production increases. However, the AH inflow rate should be thousand times greater to cause a significant effect on the IOP.

### Thickness of the lens and IOP

Once individuals get older, the shape of their lenses changes [DH01].

| Lens parameters | IOP | IOP (AC) | IOP (PC) |
|---|---|---|---|
| $h = 1.35$ $w = 3.5$ | 2002.78 | 1994.09 | 2014.56 |
| $h = 1.4$ $w = 4$ | 2002.07 | 1994.11 | 2013.78 |
| $h = 1.45$ $w = 4.5$ | 2002.04 | 1994.15 | 2014.84 |
| $h = 1.5$ $w = 5$ | 2001.21 | 1994.2 | 2014.16 |

Table shows that there is no significant change in IOP (only about 0.1%) if the lens thickness (or general shape) changes.

### Opening of the pupil and IOP

Due to light conditions or different emotional states, the size of the pupil changes ([KSS18] and citations therein). In this section, the dependence between the radius of the pupil and the IOP is shown.

| Radius (Pupil) | IOP | IOP (AC) | IOP (PC) |
|---|---|---|---|
| 1.5 | 2002.33 | 1994.2 | 2014.23 |
| 2 | 2002.4 | 1994.34 | 2014.32 |
| 2.5 | 2002.54 | 1994.4 | 2014.59 |
| 3 | 2002.69 | 1994.5 | 2014.82 |
| 5 | 2002.95 | 1995.12 | 2014.59 |

The following table shows that there is no significant dependence between the pupil radius and the intraocular pressure. The mean IOP variation is about 0.62 Pa between the simulations with the radius of the pupil $r = 1.5$ and $r = 5$ mm.

### Permeability and IOP

Permeability is a parameter representing the occlusion in the pores in the trabecular meshwork. The figure 5 shows the dependence between the permeability and the IOP.

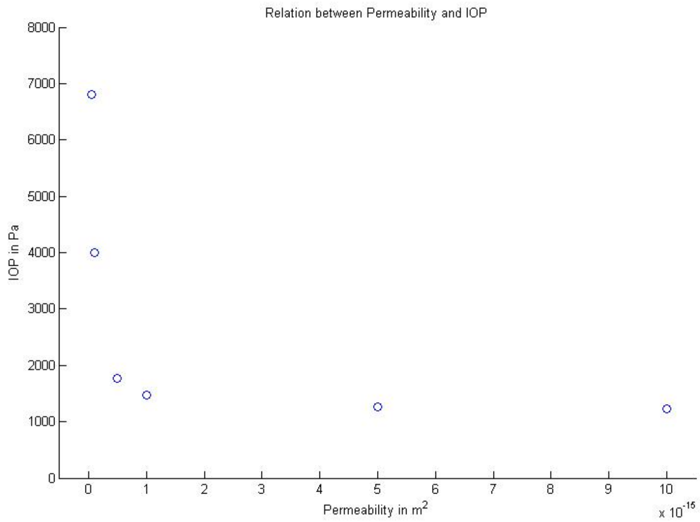


Figure 5: Relation between permeability and IOP

If the permeability of the tissue gets smaller, the IOP in the anterior chamber increases. Once pores get very small, meaning that the permeability becomes $10^{-16}$, there is a greater increase in IOP. Comparing this results to increase of IOP due to variations in the inflow rate, it can be seen, that the permeability has a stronger impact on the change of the IOP than the inflow rate according to the model.

### Episcleral venous pressure (EVP) and IOP

Elevated episcleral venous pressure (EVP) is one of the risk factors for glaucoma. In particular, due to Sturge Weber Syndrome EVP increases [SAY$^+$12],[JG87]. This leads to an increase in IOP. The increased IOP leads to glaucoma. The figure 6 shows the dependence between the episcleral venous pressure (EVP) and the IOP. If the EVP increases the IOP increases. According to the results, there is a linear dependence between those two quantities:

$$IOP = EVP + 802\text{Pa}$$

Moreover,the table illustrates that the IOP is slightly less than the mean pressure $p_0$ in the trabecular meshwork. Like in the previous observations, the IOP in the posterior chamber is slightly greater than in the area between the cornea and the iris.

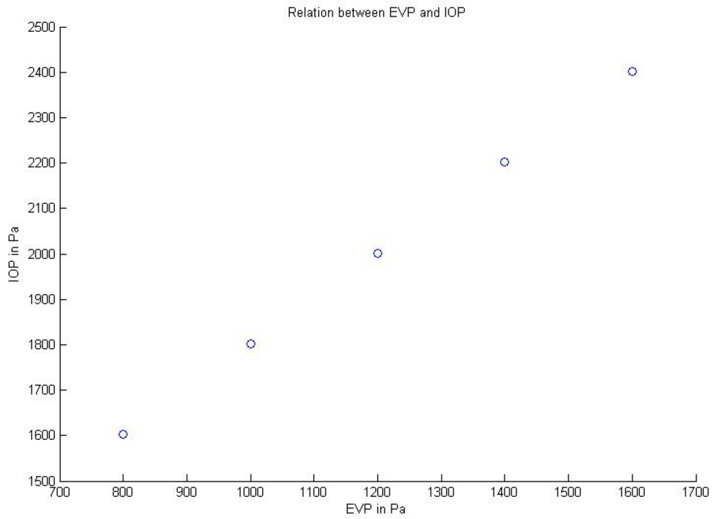


Figure 6: Relation between EVP and IOP

### Viscosity and IOP

The viscosity changes once secondary glaucoma occur. Moreover, it is common, that after operations (or treatment with medication) viscosity of the aqueous humor changes [V+04]. Next, the dependence of viscosity on the mean IOP is illustrated.

Increase of viscosity by 0.1 leads to an increase of mean IOP about approximately 114

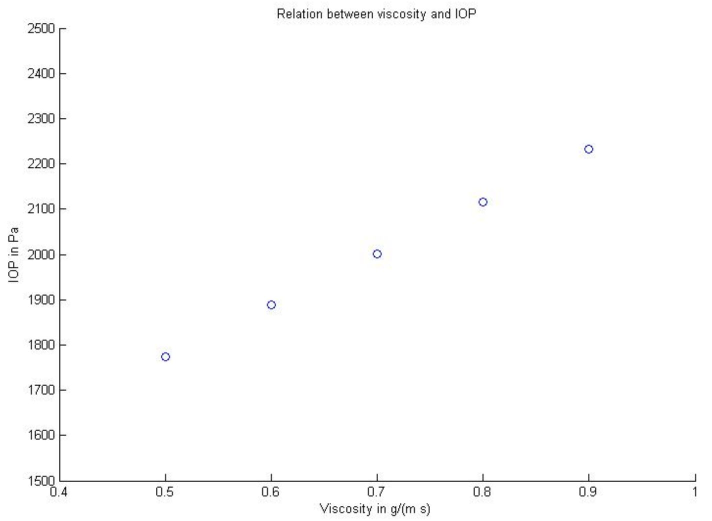


Figure 7: Relation between viscosity and IOP

Pa. A difference between viscosity for $\nu = 0.4$ and $\nu = 0.9$ is about 458 Pa (approximately 3.43 mmHg). Since realistic viscosity parameters lie in the range between 0.6 and 0.9 [V+04], pressure difference about 344 Pa (approximately 2.58 mmHg) results between two extreme points. The relative pressure difference is about 17.2% (taking 2000 Pa as 100%). According to the model, one option to heal glaucoma at an early stage is to decrease the viscosity of the aqueous humor.

## 5.5 Medical applications

### 5.5.1 Position of the patient and IOP

Since an individual performs different tasks during a day, he/she takes different body postures throughout the day. If you study, you often sit on a chair or at the table. If you rest and listen to music, you maybe lie supine. To be able to see how the posture influences the mean IOP, following parameters are considered: EVP values are set according to experiments [BTP01], [AMHS17]:

- Sitting: $6.4 \pm 1.4$ mmHg (866.6666 Pa is chosen in the simulation)
- Inclined: $7.7 \pm 1.7$ mmHg (1040 Pa is chosen in the simulation)
- Lying supine: 10 mmHg (1346.666 Pa is chosen in the simulation)

The direction of the gravitation force is changed due to the position of the patient. Choose the force term $f$ as follows:

- Standing/Sitting/inclined: $f = (0, -g, 0)$
- Lying Supine: $f = (-g, 0, 0)$

| Position | EVP | Pressure (TW) | IOP |
|---|---|---|---|
| Sitting | 866.6 | 1668.13 | 1668.17 |
| Inclined | 1040 | 1842.13 | 1842.12 |
| Lying supine | 1346.6 | 2148.13 | 2148.03 |

According to the results of the model, IOP depends on body posture. Lying supine leads to the greatest increase in both EVP (3.6 mmHg according to [BTP01] in comparison with the sitting position) and IOP (3.6 mmHg according to computations). Sitting position leads to lowest EVP and IOP values.

### 5.5.2 Cataract surgery

There a many cases when patients are suffering from multiple diseases. Sometimes, glaucoma and cataract occur at once. Cataract is a clouding of the lens in the eye which can cause blindness or visual impairment [Gre12]. One of the options to treat cataract is the removal of the natural lens and insertion of an artificial intraocular lens on its place [Gre12]. To understand, what impact the exchange of the lens has on the IOP, following simulation is performed. Let the following parameters be fixed:

- $K = 1.7 \cdot 10^{-16}\,\mathrm{m}^2$
- The inflow velocity is about $u_{\mathrm{in}} = 4 \cdot 10^{-7} \frac{\mathrm{m}}{\mathrm{s}}$ (inflow rate $2 \frac{\mu\mathrm{l}}{\mathrm{min}}$).
- The force is given by $f = (-g, 0, 0)$ (patient is lying supine).

- The outflow boundary condition is set for the surface of the geometry with $2.05 < x < 2.45$.
- The inflow boundary condition is set for the surface of the geometry with $0 < x < 1.64$ and the radius in the $y - z$ plane $r > 5.5$.
- No slip condition $u = 0$ is set in the remaining parts.
- The radius of the pupil is 1.5 mm.

The first simulation uses the natural lens of semi-ellipsoidal shape with the width $w = 8$ mm and the height of the half of the lens $h = 1.4$ mm. In this case, mean IOP in the whole front part of the eye is about 1994.11 Pa, the mean IOP in the posterior chamber is 2013.78 Pa and the mean IOP in the anterior segment between the cornea and the iris is 2002.33 Pa.
The second simulation uses artificial lens of cylindrical shape with the radius $r = 3$ mm and the height $h = 0.5$ mm. In this case, mean IOP in the whole front part of the eye is about 1995.17 Pa, the mean IOP in the posterior chamber is 2016.56 Pa and the mean IOP in the anterior segment between the cornea and the iris is 2005.05 Pa. IOP increases approximately about 0.15% after the operation for the case with a plane iris. This IOP change is not significant.
The third and forth simulations use curved geometry for the iris. Other parameters are the same as in the previous case. In this case, mean IOP in the anterior chamber and posterior chamber has no significant difference. (2002.9 Pa in the case with a natural lens and 2002.9 Pa in the case with artificial lens).
This results show that there is only a very tiny change in the overall IOP inside of the eye if the lens is exchanged (not significantly dependent on the form of the iris). Consequently, according to computations, cataract surgery does not effect the IOP such that it has dangerous consequences. It can also be observed, that the IOP is distributed equally in the case of the artificial lens in the front part and the posterior part while there is a slightly higher IOP in the case of the natural lens in the posterior chamber than in the region between the cornea and the iris. In [LY$^+$18] the changes of the IOP after cataract surgery are measured. The authors observe the increase of IOP during the first day after cataract surgery. Then, after thirty days after cataract surgery, the IOP is lower than before the operation. Finally, after ninety days after the operation, the IOP is higher than the IOP after thirty days, however lower than the preoperative IOP. In [ZB15] it is estimated that the mean reduction of the IOP is about 1.46 mmHg in a long term after cataract surgery.
Comparing results of the model with measurements, it may be seen that not all factors during the surgery are described by the model accurately. For example, the current model does not incorporate any information about inflammation, neural regeneration after surgery. This model describes only the change of the geometry and its influence

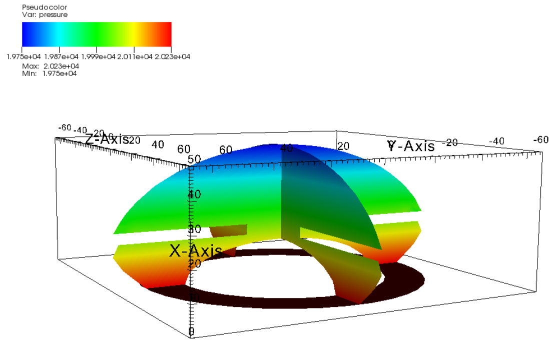


(a) Healthy eye with a natural ocular lens

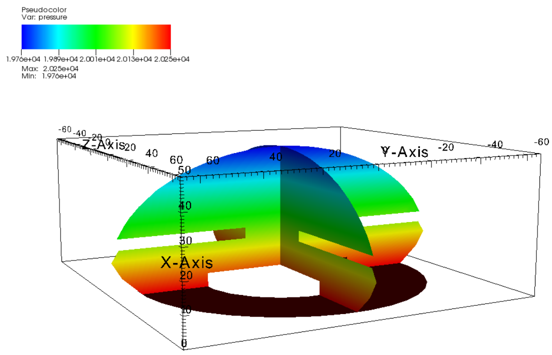


(b) Healthy eye with an artificial lens after cataract surgery

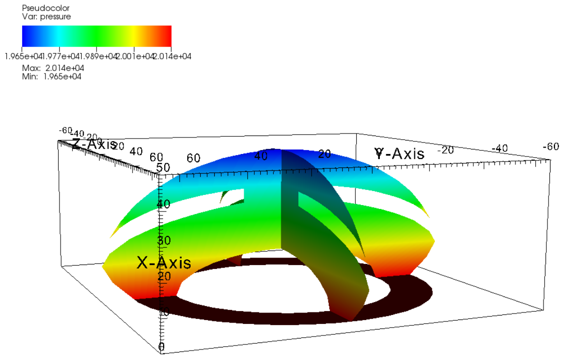


(c) Healthy eye with curved iris and a natural lens

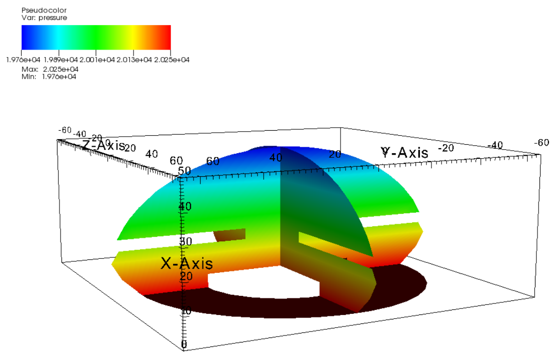


(d) Healthy eye with deformed iris and an artificial lens after cataract surgery

on the IOP. Thus, it needs to be extended to predict the IOP change after cataract surgery more accurately.

### 5.5.3 Scleral lens

Scleral lenses are large-diameter gas permeable contact lenses that are supported by a tear reservoir, rest on the conjunctival tissue overlying the sclera, and vault the cornea and limbus. These lenses maintain a fluid reservoir between the back surface of the contact lens and the front surface of the eye. Scleral lenses are used to treat ocular surface disease, corneal irregularity and uncomplicated refractive error ([HS18] and citations therein).

At the current moment, medical doctors are dealing with the question whether the scleral lens has an impact on the IOP or not. The idea of the following simulation arose from the cooperation with Young Hyun Kim from the University of California, Berkeley. The model in this thesis may predict the IOP change which is caused by deformation of the sclera and limbus caused by wearing the scleral lens (see forces described in [PJGM14]). To do this, only geometry of the anterior chamber is modified while other parameters are fixed. Since the scleral lens is covering cornea, limbus and sclera and the deformation properties of cornea, limbus and sclera are different, these regions are considered separately. The width of the limbus is around 1 to 2 mm. ([C$^+$17] and citations therein) In the geometry, 1 mm is supposed to belong to corneal region and 1 mm to scleral region. According to [P$^+$16], limbal distance from the iris (depth of the limbus) is supposed to be around 1 mm. Since the geometry of the anterior chamber doesn't include sclera, this part is not considered here. The deformation of the cornea

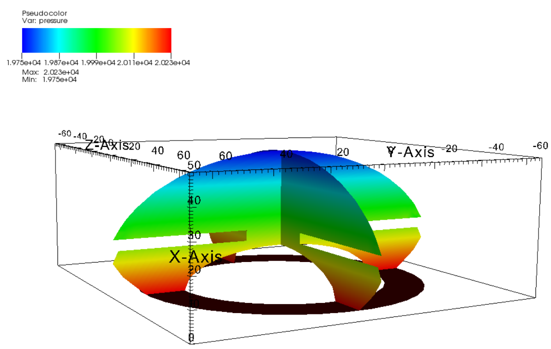


(a) Pressure before deformation

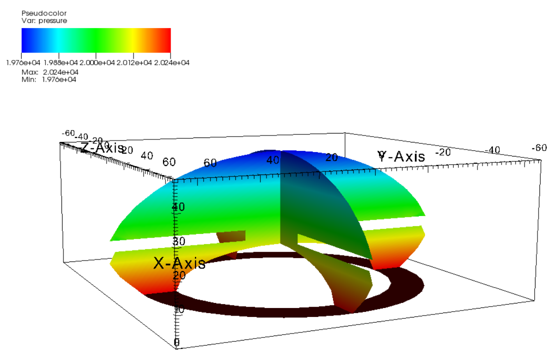


(b) Pressure after deformation

is supposed to be 15 $\mu$m at the top. The deformation of the limbus is supposed to be 1 $\mu$m. Using these parameters, following values are obtained:

- Mean IOP of 2002.07 Pa before deformation
- Mean IOP of 2002.06 Pa after deformation

This means, that the scleral lens has no impact on the mean IOP in the simulation (less than 0.01 Pa).

### 5.5.4 Glaucoma operations

To model the situation of trabeculectomy or insertion of stents, the following strategy is applied:

- Build a cut of the anterior chamber geometry with the $y-z$ plane at the position of the iridocorneal angle and obtain a circle in the $y-z$ plane.
- The circumference of this circle is given by $U = 2\pi r$, where $r$ is the radius.

- The width of the stent $w_s$ is usually between 0.5 and 2 mm.
- Build the ratio of the width of the stent and the circumference. This ratio represents an angle $\alpha$ according to the formula

$$\frac{\alpha}{360} = \frac{w_s}{2\pi r}$$

  which is used in simulations.
- Choose the position where the stent is inserted (or where the cut for trabeculectomy takes place). Denote the insertion point with the coordinates $(x_0, y_0, z_0)$. The angle $\phi$ is computed between the points at the outflow boundary (only components $y, z$ are considered for computation, $x$ is coordinate representing the depth of the anterior chamber) and this starting point.
- Subdivide the outflow domain in two parts with a help of the angle $\phi$.
  - $\phi \leq \alpha$: Set $p_0(\phi) = f(\phi)$.
  - $\phi \geq \alpha$: Set $p_1(x) = p_0$ (mean pressure which is obtained from the Darcy equation).

The function $f$ is given by

$$f(\phi) = \alpha_1 - \beta_1 \cdot \exp(-\frac{(\phi - \frac{\alpha}{2})^8}{\alpha^8}),$$

where $\beta_1 = \frac{p_0 - p_{\mathrm{EVP}}}{1-\exp(-0.5^8)}$ and $\alpha_1 = p_{\mathrm{EVP}} + \beta_1$. $p_{\mathrm{EVP}} = 9$ mmHg ($= 1200$ Pa).
In the following simulations, following parameters are chosen:

- The inflow velocity is about $u_{\mathrm{in}} = 4 \cdot 10^{-7} \frac{\mathrm{m}}{\mathrm{s}}$ (inflow rate $2 \frac{\mu\mathrm{l}}{\mathrm{min}}$).
- $K = 10^{-16}\,\mathrm{m}^2$ (generating IOP of 30mmHg) and $K = 5 \cdot 10^{-17}\,\mathrm{m}^2$ (generating IOP of 50 mmHg)
- $\nabla p \cdot n = \frac{K}{\nu} u_{\mathrm{in}} \cdot n$.
- The force is set $f = (-g, 0, 0)$ (the patient is lying supine).
- The outflow boundary condition is set for the surface of the geometry with $2.05 < x < 2.55$.
- The inflow boundary condition is set for the surface of the geometry with $0 < x < 1.64$ and the radius in the $y - z$ plane $r > 5.5$.
- No slip condition $u = 0$ is set in the remaining parts.
- The radius of the pupil is 1.5 mm.

- The width of the natural lens lense is supposed to be 8 mm and the height of the half of the lens is 1.4 mm.

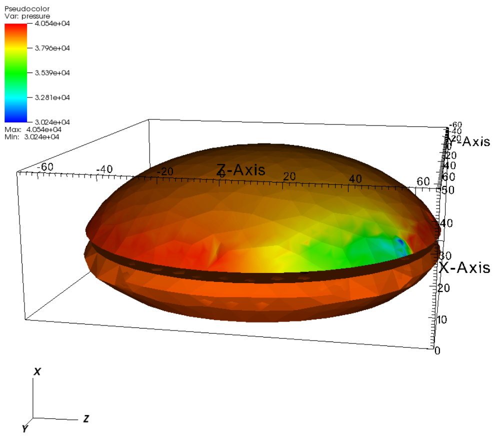

(a) Pressure (after trabeculectomy/stent insertion)

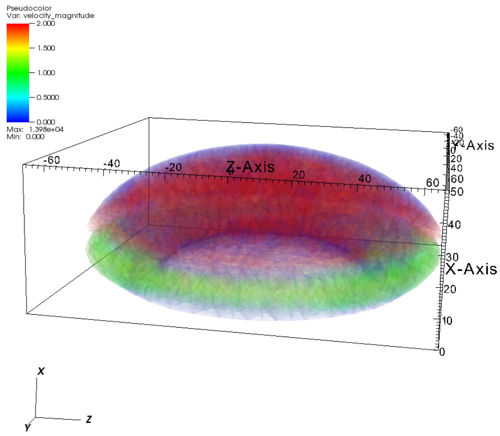

(b) Velocity (after trabeculectomy/stent insertion)

The simulation lead to the result: Insertion of a stent leads to the pressure drop of approximately 1.5 to 2 percent (for patients with high IOP between 30 and 50 mmHg). In order to be able to differentiate between stent insertion and trabeculectomy, prediction of the pressure in the treated segment (in the case of trabeculectomy) and in the stent (in the case of stent insertion) are considered.

### Trabeculectomy

To predict pressure drop due to trabeculectomy in the operated segment, following model is applied:

$$
\begin{aligned}
-\nabla \cdot \mathbb{T}(u,p) &= f_1 \text{ in } \Omega_{\text{TRAB}} \\
\nabla \cdot u &= 0 \text{ in } \Omega_{\text{TRAB}} \\
u &= u_0 \text{ on } \Gamma_{in} \\
n \cdot \mathbb{T}(u,p) \cdot n &= p_0 \text{ on } \Gamma_{\text{TW}} \\
n \cdot \mathbb{T}(u,p) \cdot \tau &= \tilde{\alpha} u \cdot \tau \text{ on } \Gamma_{\text{TW}} \\
n \cdot \mathbb{T}(u,p) \cdot n &= p_{\text{EPI}} \text{ on } \Gamma_{\text{EPI}} \\
n \cdot \mathbb{T}(u,p) \cdot \tau &= \tilde{\alpha} u \cdot \tau \text{ on } \Gamma_{\text{EPI}},
\end{aligned}
\tag{24}
$$

where $\Omega_{\text{TRAB}} \subset \mathbb{R}^d$ with $d = 2, 3$ is the domain illustrating the treated tissue segment of the trabecular meshwork and where $u$ denotes the velocity, $p$ the pressure, $f_1$ the force, $u_0$ the inflow velocity, $p_0$ the pressure (resistance) of the trabecular meshwork, $p_{\text{EPI}}$ the pressure in the episcleral veins and $\nu$ the viscosity of the aqueous humor. The boundary segment $\Gamma_{\text{TW}}$ describes the outflow boundary (into the trabecular meshwork), $\Gamma_{\text{in}}$ the inflow boundary and $\Gamma_{\text{EPI}}$ the outflow boundary (into Schlemm canal and episcleral veins). The boundary is given by $\Gamma_{\text{Stokes}} = \Gamma_{\text{in}} \cup \Gamma_{\text{TW}} \cup \Gamma_{\text{EPI}}$. The vector $n$ denotes the normal vector, $\tau$ represents the tangential vectors and $I$ denotes the identity matrix.

- Assume that the treated tissue $\Omega_{\text{TRAB}}$ in the operation is a cube (with a length of a side between 2 to 3 mm).
- Since the sides of the treated tissue (the cube) boarder to the trabecular meshwork, the pressure at the sides is supposed to be the same as in the trabecular meshwork (for a pathological case about 4000 Pa).
- The pressure at the outflow boundary, at the episcleral veins is 1200 Pa.
- At the boundary contacting the anterior chamber, the mean velocity of the Stokes equation at the boundary is taken as the inflow velocity (about 1.5 $\frac{\text{mm}}{\text{s}}$).

The mean pressure in the removed segment drops from 4000 Pa to 2400 Pa. This pressure may be taken in previous considerations as $p_{\text{EVP}} = 2400$ Pa in the $f(\phi)$ function. Next, it is interesting to compare this result to the pressure inside of the stent.

### Stent insertion

To predict pressure drop due to stent insertion, following model is applied:

$$
\begin{aligned}
-\nabla \cdot \mathbb{T}(u,p) &= f_1 \text{ in } \Omega_{\text{ST}} \\
\nabla \cdot u &= 0 \text{ in } \Omega_{\text{ST}} \\
u &= u_0 \text{ on } \Gamma_{\text{in}} \\
u &= 0 \text{ on } \Gamma_{\text{wall}} \\
n \cdot \mathbb{T}(u,p) \cdot n &= p_{\text{EPI}} \text{ on } \Gamma_{\text{EPI}} \\
n \cdot \mathbb{T}(u,p) \cdot \tau &= \tilde{\alpha} u \cdot \tau \text{ on } \Gamma_{\text{EPI}},
\end{aligned} \tag{25}
$$

where $\Omega_{\text{ST}} \subset \mathbb{R}^d$ with $d = 2, 3$ is the domain illustrating stent and where $u$ denotes the velocity, $p$ the pressure, $f_1$ the force, $u_0$ the inflow velocity, $p_{\text{EPI}}$ the pressure in the episcleral veins and $\nu$ the viscosity of the aqueous humor. The boundary segment $\Gamma_{\text{in}}$ describes the inflow boundary, $\Gamma_{\text{EPI}}$ the outflow boundary (into Schlemm canal and episcleral veins), and $\Gamma_{\text{wall}}$ the no slip boundary of the stent. The boundary is given by $\Gamma_{\text{Stokes}} = \Gamma_{\text{in}} \cup \Gamma_{\text{wall}} \cup \Gamma_{\text{EPI}}$. The vector $n$ denotes the normal vector, $\tau$ represents the tangential vectors and the matrix $I$ denotes the identity matrix.

- Assume that the stent $\Omega_{\text{ST}}$ is a cylinder (with a radius of 0.5 mm).
- Since the sides of stent are impermeable, set $u = 0$ at the hull.

- The pressure at the outflow boundary, at the episcleral veins is 1200 Pa.
- At the boundary contacting the anterior chamber, the mean velocity of the Stokes equation at the boundary is taken as the inflow velocity (about $1.5\frac{\mathrm{mm}}{\mathrm{s}}$).

The mean pressure in the stent is 1201 Pa. This pressure may be taken in previous considerations as $p_{\mathrm{EVP}} = 1201$ Pa in the $f(\phi)$ function. Consequently, the pressure drop inside of the stent is greater than the pressure drop in the removed tissue after trabeculectomy. However, the trabeculectomy cut is often greater than the stent. Next, it is interesting to compare the pressure drop in the anterior chamber after stent insertion and after trabeculectomy with these predictions.

#### Comparison: Trabeculectomy and Stent insertion

The computed estimations for the mean pressure inside a stent and inside an operated segment as well as the choice of a cut about 3 mm is taken for trabeculectomy and a diameter of a stent is supposed to be 1 mm. It is assumed that the pressure before stent insertion or trabeculectomy is about 51.1 mmHg and that the trabecular meshwork is occluded equally at each position. Following results are obtained:

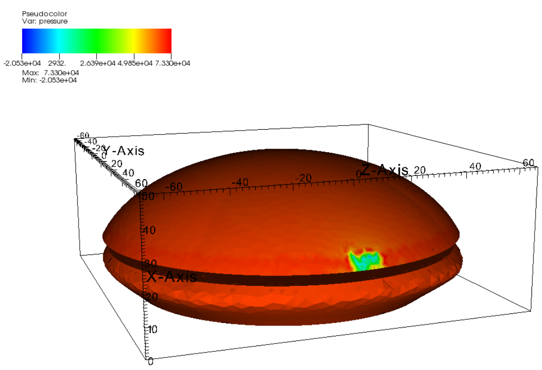


(a) IOP after stent insertion

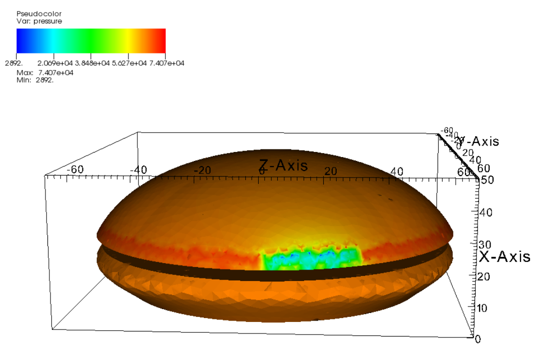


(b) IOP after trabeculectomy

- Mean IOP after stent insertion 50.15 mmHg
- Mean IOP after trabeculectomy 48.52 mmHg

Thus, the size of the cut during the operation has more impact on the decrease of the IOP than the pressure inside the operated segment or a stent. Although the pressure inside a stent is 1200 Pa, and in the operated segment caused by trabeculectomy 2400 Pa, the model predicts a greater decrease in IOP after trabeculectomy. However, equal occlusion of the trabecular meshwork is not common. It is more realistic, that some segments of the trabecular meshwork are clogged more than the other. This case is discussed in the next section.

### Effectiveness of operations

To model the effectiveness of operations and partial obstruction of the trabecular meshwork, the subdivision function is changed as follows:
Subdivide the outflow domain in two parts with a help of the angle $\phi$ (for a nasal region $\phi = 90$ degree)

- $\phi \leq \alpha$: Set $p_0(\phi) = f_1(\phi)$ (pressure in the occluded segment)
- $\phi \geq \alpha$: Set $p_0(\phi) = p_0$ (pressure in a healthy segment)

In case of treatment inside the occluded part, include in addition a function $f_2(\phi)$.

- $\phi \leq \alpha_1$: Set $p_0(\phi) = f_1(\phi)$ (pressure in the occluded segment)
- $\phi \geq \alpha_1$ and $\phi \leq \alpha_2$: Set $p_0(\phi) = f_2(\phi)$ (pressure in the operated segment)
- $\phi \geq \alpha_2$ and $\phi \leq \alpha$: Set $p_0(\phi) = p_{\text{occ}}$ (pressure in the occluded segment)
- $\phi \geq \alpha$: Set $p_0(\phi) = p_0$ (healthy segment)

The function $f_1$ is given by

$$f_1(\phi) = \alpha_1 + \beta_1 \cdot \exp\left(-\frac{(\phi - \frac{\alpha}{2})^8}{\alpha^8}\right),$$

where $\beta_1 = \frac{p_{\text{occ}} - p_0}{1 - \exp(-0.5^8)}$, $\alpha_1 = p_{\text{occ}} - \beta_1$, $p_{\text{occ}} = 10000$ Pa and $p_0 = 2000$ Pa. The function $f_2$ is given by

$$f_2(\phi) = \alpha_2 - \beta_2 \cdot \exp\left(-\frac{(\phi - \frac{\alpha}{2})^8}{\alpha^8}\right),$$

where $\beta_2 = \frac{p_{\text{occ}} - p_{\text{out}}}{1 - \exp(-0.5^8)}$, $\alpha_2 = p_{\text{out}} + \beta_1$ and $p_{\text{out}} = 2400$ Pa.
Suppose, the doctor finds out a segment, where there is the greatest occlusion in the eye and treats this segment. Let nasal region of an eye be clogged (about one fourth of the circumference of the trabecular meshwork). Before the operation, the mean IOP in the anterior chamber is about 28.37 mmHg. However, after trabeculectomy, the pressure drops to 23.17 mmHg. Consequently, the reduction of the mean IOP is about 18.32%. Thus, setting the stent in the occluded area of the trabecular meshwork leads to best results according to the model.

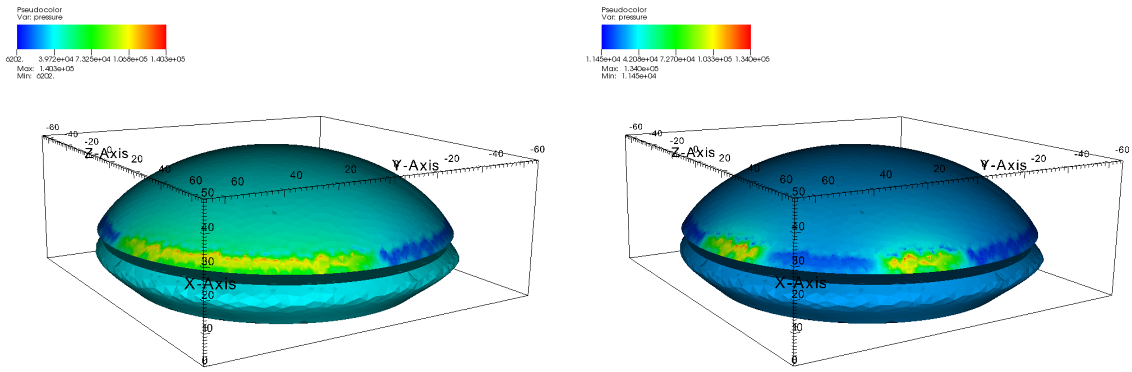


(a) IOP before operation or stent insertion (b) IOP after operation or stent insertion

# Conclusion

There are already some models about Stokes Darcy coupling and their applications in ophthalmology. However, most of them are based on engineering [VR+12], [Kum03] or the models are covering the two dimensional case only [FO+14],[CE13] . In this thesis, a new model is developed based on mathematical theory. Moreover, computations in three dimensions are performed and well posedness of the model is shown. In order to predict the increase of the intra-ocular pressure in the anterior chamber of the human eye, a model based on Stokes and Darcy equations was developed. The Stokes equation describes the aqueous humor flow in the anterior chamber and the Darcy equation describes the pressure behavior in the trabecular meshwork. The characteristic physical properties are given by the inflow rate of the aqueous humor at the ciliary body, the pressure of the episcleral veins and it is assumed that the cornea, the lens, the iris and the zonules are impermeable. To understand how the resistance in the trabecular meshwork influences IOP in the anterior chamber, following ansatz is proposed. Using permeability constant, the size of the pores in the trabecular meshwork can be modeled. The less the permeability constant, the greater the resistance. With the help of the Darcy equation, the pressure in the trabecular meshwork is computed. Then, the mean value of the pressure in the trabecular meshwork is obtained. This mean value is incorporated in the Robin boundary condition of the Stokes equation. Having solved the Stokes equation, the IOP and the flow of the aqueous humor in the anterior chamber are obtained. Existence and uniqueness of solutions and discretization of the model is studied. Moreover, test cases for Darcy and Stokes equation are presented. This proves that the model works. Using this model, following results are obtained:

- If the natural lens gets thicker, there is an increase in IOP up to 3.5%.
- The IOP decreases up to 0.3% once the pupil gets wider.

- IOP = EVP + const, where const is determined by the permeability in the trabecular meshwork.

- After cataract surgery, no significant change of the mean IOP is expected according to computations in this thesis.

- Trabeculectomy surgery or stent insertion leads to best results if doctors know where the occlusion takes place in the trabecular meshwork. Test case in this work show, that the IOP may be reduced about 18% in glaucoma with preoperative IOP about 28 mmHg.

- The smaller the permeability Per, the greater the pressure $p_{\mathrm{TW}}$ inside of the trabecular meshwork. The relation between the permeability and pressure in the trabecular meshwork is approximately $p_{\mathrm{TW}} = \mathrm{const} \cdot \frac{1}{\mathrm{Per}}$.

- The effect of the position of the patient (standing/lying prone/lying supine/lying on a side) leads to a change of the IOP. The model confirms the observations from medicine. In a lying posture, the IOP increases. In a standing/sitting posture the IOP decreases. The difference in IOP between standing and sitting posture is about 3.6 mmHg.

There are following advantages of the model of this thesis:

- The following method is a simplification of the well known Stokes Darcy coupling fulfilling mass conservation, balance of normal forces and the Beavers Joseph and Saffman condition.

- It is a decoupled method. Thus, both equations can be solved separately.

- Efficient numerical solvers are available for each equation.

- There is a solid mathematical theory about Stokes and Darcy equations.

- Instead of an interface, there is a boundary condition for the outflow (representing the obstruction of the trabecular meshwork) creating an alternative to do-nothing boundary conditions.

However, there are disadvantages and limitations of the model in this thesis:

- Pressure might vary on the borderline between the trabecular meshwork and the anterior chamber and be slightly smaller than the mean value (due to the tissue structure).

- This model is a simplification of the Stokes Darcy equation and this model is only usable for cases where the fluid domain is much larger than the porous domain.

The model of this thesis may be extended to Navier Stokes and Darcy equations. However, in this case existence and uniqueness of solutions in three dimensions is restricted to small data only. Consequently, verification with data from experiments is necessary in this extension. Moreover, the model may be extended to nonstationary Stokes and Darcy equations or a nonstationary Navier Stokes and Darcy coupling.
In addition, drug distribution in the anterior chamber may be considered. Modeling and simulation of drug distribution in the vitreous body is considered in [DFS17] and the motion of vitreous humor in a deforming eyeball is studied in [TSPF18]. In the end, all these results may be combined and the drug distribution in the whole human eye may be modeled.
Furthermore, there is an open question following from the perspective of application:

- How to develop a software out of this model to help doctors to predict at which position in the trabecular meshwork they could treat glaucoma with the greatest IOP decrease?

# Acknowledgment

In first place, I am grateful to my first supervisor, a member of the faculty of Mathematics and Computer Science at the Heidelberg University, Prof. Dr. Friedmann, who not only proposed the subject of this work, but also for her supervision and her effort.
I thank my second supervisor, Prof. Dr. med. Auffarth for helpful discussions concerning medical applications and geometry construction of the human eye and for the opportunity to watch vitrectomy and cataract surgery.
I would like to express my gratitude to Prof. Dr. Dr. h. c. Rannacher for reading my work and for fruitful discussions concerning numerical analysis of this thesis.
I am grateful for support of Prof. Dr. Kanschat, also a member of the faculty of Mathematics and Computer Science, who helped me with mathematical part of this thesis and for support with deal.ii library.
I would like to thank Prof. Dr. med. Dr. med. habil. Hengerer for explanation of medical terminology and for helping me with the search for medical studies and papers at the beginning of my doctoral studies.
I deeply thank Dr. Patrick Merz, Dr. Sonja Schickhardt and their team for support in the David J Apple Laboratory and for helpful discussions concerning artificial lenses and experiments with bowine and human autopsy-eyes.
I appreciate discussions concerning modeling with Dr. Thomas Carraro at the beginning of the project and that he taught me during his supervision of my master thesis how to write scientific articles. The knowledge I gained at that time was very helpful for my PhD.
I am grateful to Heidelberg Graduate School (HGS) for many interesting workshops, for annual colloquia and for scientific exchange with other PhD students.
I thank Klaus Tschira Stiftung for financial support of the PhD project.
The Numerical Analysis and Modeling and Simulation in Ophthalmology groups in Heidelberg always provided a most pleasant working atmosphere, for which I am grateful to all my colleagues. In particular, I am thankful to Dr. Daniel Arndt, Dr. Victoria Ponce, Simon Dörsam and Sven Wetterauer for explaining me basics about deal.ii library and their patience. I feel very grateful to Alexander Drobny for his idea to try GMSH for construction of the geometry. I am grateful for fruitful discussions concerning finite elements and analysis of PDEs with Simon Dörsam, Judith Stein, Dr. Stefan Frei and Felix Brinkmann. I also enjoyed free time activities and time spent with my working group during conferences.
I am also deeply grateful to my parents, to my sister and my aunt for supporting me during my PhD period.

# References


[ADF06] A. D. Fitt, G. G.: Fluid Mechanics of the Human Eye: Aqueous Humor Flow in the Anterior Chamber. In: *Bulletin of Mathematical Biology* (2006)

[AH74] Anderson, D. R. ; Hendrickson, A.: Effect of intraocular pressure on rapid axoplasmic transport in monkey optic nerve. In: *Investigative Ophthalmology* (1974)

[AHC10] Atkinson, K. ; Hansen, O. ; Chen, D.: A spectral method for elliptic equations: the Neumann problem. In: *Advanced Computational Mathematics* (2010)

[AMHS17] Arora, N. ; McLaren, J.W. ; Hodge, D. O. ; Sit, A. J.: Effect of body position on episcleral venous pressure in healthy subjects. In: *Investigative Ophthalmology and Visual Science* (2017)

[Arn13] Arndt, D.: Augmented Taylor-Hood Elements for Incompressible Flow. In: *Masterarbeit, University of Goettingen* (2013)

[Art15] Artemyev, M.: *Tethex*. `https://github.com/martemyev/tethex`. Version: 2015

[AS06] Avtar, R. ; Srivastava, R.: Modeling aqueous humor outflow through trabecular meshwork. In: *Applied Mathematics and Computation* (2006)

[BBF+06] Boffi, D. ; Brezzi, F. ; Fortin, M. et al.: *Mixed Finite elements, compatibility conditions and applications*. Springer Verlag, 2006

[BBF13] Boffi, D. ; Brezzi, F. ; Fortin, M.: *Mixed Finite Element Methods and Applications*. Springer Verlag, 2013

[BDQ10] Badea, L. ; Discacciati, M. ; Quarteroni, A.: Mathematical analysis of the Navier-Stokes/Darcy coupling. In: *Numerische Mathematik* (2010)

[BH07] Burman, E. ; Hansbo, P.: A unified stabilized method for Stokes' and Darcy's equations. In: *Journal of Computational and Applied Mathematics* (2007)

[BHH+15] Bangerth, W. ; Heiser, T. ; Heltai, L. et al.: *The deal-II Library, version 8.2*. 2015

[BHK07] Bangerth, W. ; Hartmann, R. ; Kanschat, G.: *deal-II A general-purpose object-oriented finite element library*. 2007

[BJ67] Beavers, G. S. ; Joseph, D.D.: Boundary conditions at a naturally permeable wall. In: *Journal of fluid mechanics* (1967)

[BJB05] Baikoff, G. ; Jodai, H. J. ; Bourgeon, G.: Measurement of the internal diameter and depth of the anterior chamber: IOLMaster versus anterior chamber optical coherence tomographer. In: *Journal of cataract and refractive surgery* (2005)

[BMB+07] Balaratnasingam, C. ; Morgan, W. H. ; Bass, L. et al.: Axonal transport and cytoskeletal changes in the laminar regions after elevated intraocular pressure. In: *Investigative Ophthalmology and Visual Science* (2007)

[Bor16] Borthwick, D.: *Introduction to Partial Differential Equations*. Springer International Publishing, 2016

[BR80] Blum, H. ; Rannacher, R.: On the Boundary Value Problem of the Biharmonic Operator on Domains with Angular Corners. In: *Mathematical Methods in Applied Sciences* (1980)

[BR13] Bhardwaj, V. ; Rajeshbhai, G. P.: Axial length, anterior chamber depth - a study in different age groups and refractive errors. In: *Journal of Clinical and Diagnostic Research* (2013)

[Bra07] Braess, D.: *Finite elements: theory, fast solvers and applications in solid mechanics*. Springer Verlag, 2007

[BTP01] Blondeau, P. ; Tétrault, J.-P. ; Papamarkakis, C.: Diurnal variation of episcleral pressure in healthy patients: a pilot study. In: *Journal of Glaucoma* (2001)

[C+17] Consejo, A. et al.: Mean shape of the human limbus. In: *Journal of Cataract and Refractive Surgery* (2017)

[CBW+12] Childs, Hank ; Brugger, Eric ; Whitlock, Brad ; Meredith, Jeremy ; Ahern, Sean ; Pugmire, David ; Biagas, Kathleen ; Miller, Mark ; Harrison, Cyrus ; Weber, Gunther H. ; Krishnan, Hari ; Fogal, Thomas ; Sanderson, Allen ; Garth, Christoph ; Bethel, E. W. ; Camp, David ; Rübel, Oliver ; Durant, Marc ; Favre, Jean M. ; Navrátil, Paul: VisIt: An End-User Tool For Visualizing and Analyzing Very Large Data. In: *High Performance Visualization–Enabling Extreme-Scale Scientific Insight*. 2012, S. 357–372

[CE13] Crowder, T. R. ; Ervin, V. J.: Numerical Simulations of Fluid Pressure in the Human Eye. In: *Applied Mathematics and Computation* (2013)

[CG02] Canning, C. R. ; Greaney, M. J.: Fluid flow in the anterior chamber of a human eye. In: *Journal of Mathematics Applied in Medicine and Biology* (2002)

[CGHW10] Cao, Y. ; Gunzburger, M. ; Hua, F. ; Wang, X.: Coupled Stokes-Darcy Model with Beavers-Joseph Interface Boundary Condition. In: *Communications in Mathematical Sciences* (2010)

[CGW10] Cao, Y. ; Gunzburger, M. ; Wang, X.: Coupled Stokes-Darcy model with Beavers-Joseph interface boundary condition. In: *Communications in Mathematical Sciences* (2010)

[CJW14] Caiazzo, A. ; John, V. ; Wilbrandt, U.: On classical iterative subdomain methods for the Stokes-Darcy problem. In: *Computational Geosciences* (2014)

[DFS17] Dörsam, S. ; Friedmann, E. ; Stein, J.: Modeling and Simulation of Drug Distribution in the Human Vitreous. In: *Topical Problems of Fluid Mechanics* (2017)

[DH01] Dubbelman, M. ; Heijde, G. L. V.: The shape of the aging human lens: curvature, equivalent refractive index and the lens paradox. In: *Vision Research* (2001)

[Dis05] Discacciati, M.: Iterative Methods for Stokes/Darcy coupling. In: *Domain Decomposition Methods in Science and Engineering* (2005)

[DMQ02] Discacciati, M. ; Miglio, E. ; Quarteroni, A.: Mathematical and numerical models for coupling surface and groundwater flows. In: *Applied Numerical Mathematics* (2002)

[DZ11] D'Angelo, C. ; Zunino, P.: Robust numerical approximation of coupled Stokes and Darcy's flows applied to vascular hemodynamics and biochemical transport. In: *Mathematical Modeling and Numerical Analysis* (2011)

[EGS17] European Glaucoma Society Terminology and Guidelines for Glaucoma, 4th Edition - Chapter 3: Treatment principles and options. In: *British Journal of Ophthalmology* (2017)

[EJS11] Ervin, V. J. ; Jenkins, E. W. ; Sun, S.: Coupling nonlinear Stokes and Darcy flow using mortar finite elements. In: *Applied Numerical Mathematics* (2011)

[EK+86] Ethier, C.R. ; Kamm, R. D. et al.: Calculations of flow resistance in the juxtacanalicular meshwork. In: *Investigations in Ophthalmology and Visual Science* (1986)

[ESP75] Ene, H. ; Sanchez-Palencia, E.: Equations et phénomènes de surface pour l' écoulement dans un modèle de milieu poreux. In: *Journal de Mécanique* (1975)

[ESW05] Elman, H. C. ; Silvester, D. J. ; Wathen, A. J.: Finite elements and fast iterative solvers: with applications in incompressible fluid dynamics. In: *Numerical Mathematics and Scientific Computation. Oxford University Press* (2005)

[Etm86] Etman, H. C.: A stability analysis of incomplete LU factorizations. In: *Mathematics of Computation* (1986)

[Eva15] Evans, Lawrence C.: *Partial Differential Equations, second edition.* American Mathematical Society, 2015

[FDO18] Friedmann, E. ; Dörsam, S. ; Olkhovskiy, V.: Test and optimization of medical treatments for the human eye. In: *European patent application ep 18000349* (2018)

[FJ09] Freddo, T. F. ; Johnson, M.: Aqueous Humor Outflow Resistance. In: *Current topics in Membranes, Elsevier, Volume 62* (2009)

[FO+14] Ferreira, J. A. ; Oliviera, P. D. et al.: Numerical simulation of aqueous humor flow: from healthy to pathologic situations. In: *Applied Mathematics and Computation* (2014)

[FPS03] Feiner, L. ; Piltz-Seymour, J.R.: Collaborative initial glaucoma treatment study: a summary of results to date. In: *Current Opinion in Ophthalmology* (2003)

[G+10] Goel, M. et al.: Aqueous Humor Dynamics: A Review. In: *Open Ophthalmology Journal* (2010)

[Gal11] Galdi, G. P.: *An Introduction to the Mathematical Theory of the Navier-Stokes equations*. Bd. 1. Springer Verlag, 2011

[GGZ74] Gajewski, H. ; Gröger, K. ; Zacharias, K.: *Nichtlineare Operatorgleichungen*. Akademie Verlag Berlin, 1974

[GHB+12] Gedde, S.J. ; Herndon, L.W. ; Brandt, J.D. et al.: Postoperative complications in the Tube versus Trabeculectomy study during five years of follow up. In: *American Journal of Ophthalmology* (2012)

[GOS11] Gatica, G.N. ; Oyarzua, R. ; Sayas, F.J.: Analysis of fully-mixed finite element methods for the Stokes-Darcy coupled problem. In: *Mathematics od Computation* (2011)

[GR86] Girault, V. ; Raviart, P.-A.: *Finite element approximations of the Navier Stokes equations*. Springer Verlag, 1986

[GR09] Geuzaine, C. ; Remacle, J.-F.: Gmsh: a three-dimensional finite element generator with built-in pre- and post-processing facilities. In: *International Journal for Numerical Methods in Engineering* (2009)

[Gre12] Grehn, F.: *Augenheilkunde*. Springer Verlag, 2012

[GRS07] Grossmann, C. ; Roos, H.-G. ; Stynes, M.: *Numerical treatment of partial differential equations*. Springer Verlag, 2007

[GSF+09] Gedde, S.J. ; Schiffmann, J.C. ; Feuer, W.J et al.: Three-year follow up of the tube versus trabeculectomy study. In: *American Journal of Ophthalmology* (2009)

[GT17] Ganesan, S. ; Tobiska, L.: *Finite elements, Theory and Algorithms*. Cambridge University Press, 2017

[HARCH18] Hengerer, F.H. ; Auffarth, G.U. ; Riffel, C. ; Conrad-Hengerer, I.: Prospective, Non-randomized, 36-Month Study of Second- Generation Trabecular Micro-Bypass Stents with Phacoemulsification in Eyes with Various Types of Glaucoma. In: *Ophthalmology and therapy* (2018)

[HARCH19a] Hengerer, F.H. ; Auffarth, G.U. ; Riffel, C. ; Conrad-Hengerer, I.: Comparison of Minimally Invasive XEN45 Gel Stent Implantation in Glaucoma Patients Without and With Prior Interventional Therapies. In: *Ophthalmology and therapy* (2019)

[HARCH19b] Hengerer, F.H. ; Auffarth, G.U. ; Riffel, C. ; Conrad-Hengerer, I.: Second Generation Trabecular Micro-Bypass Stents as Standalone Treatment for Glaucoma: A 36-Month Prospective Study. In: *Advances in therapy* (2019)

[HBT02] Heys, J.-J. ; Barocas, V. H. ; Taravella, M. J.: Modeling Passive Mechanical Interaction between Aqueous Humor and Iris. In: *Journal of Biomechanical Engeneering* (2002)

[Hei11] Heister, T.: A massively parallel finite element framework with application to incompressible flows. In: *Dissertation, University of Goettingen* (2011)

[HKM+12] Hashemi, I. H. ; Khabazkhoob, M. ; Miraftab, M. et al.: The distribution of axial length, anterior chamber depth, lens thickness, and vitreous chamber depth in adult population of Shahrood. In: *BMC Ophthalmology* (2012)

[HLB+02] Heijl, A. ; Leske, M C. ; Bengtsson, B. et al.: Reduction of IOP and glaucoma progression: results from the early manifest glaucoma trial. In: *Archives of Ophthalmology* (2002)

[HS52] Hestenes, M. R. ; Stiefel, E.: Method of Conjugate Gradients for solving linear systems. In: *Journal of Research of the National Bureau of Standards* (1952)

[HS18] Harthan, J. S. ; Shorter, E.: Therapeutic uses of scleral contact lenses for ocular sufrace disease: patient selection and special considerations. In: *Clinical Optometry* (2018)

[HWNW09] Hanspal, N. ; Waghode, A. ; Nassehi, V. ; Wakeman, R.: Development of a predictive mathematical model for coupled Stokes/Darcy flows in cross-flow membrane function. In: *Chemical Engeneering Journal* (2009)

[HYSL16] Hong, J. W. ; Yun, S.-C. ; Sung, K. R. ; Lee, J. E.: Clinical and anterior segment anatomical features in primary angle closure subgroups based on configurations of iris root insertion. In: *Korean Journal of Ophthalmology* (2016)

[IGC+15] Invernizzi, A. ; Giardini, P. ; Cigada, M. et al.: Three-dimensional morphometric analysis of the iris by swept-source anterior segment optical coherence tomography in a caucasian population. In: *Investigative Ophthalmology and Visual Science* (2015)

[JG87] Jørgensen, J. ; Guthoff, R.: Glaukom mit erhötem episkleralen Venendruck. In: *Klinische Monatsblätter für die Augenheilkunde* (1987)

[JM96] Jäger, W. ; Mikelić, A.: On the boundary conditions at the contact interface between a porous medium and a free fluid. In: *Annali della Scuola Normale Superiore di Pisa - Classe di Scienze 23.3* (1996)

[JM00] Jäger, W. ; Mikelić, A.: On the interface boundary conditions of Beavers, Joseph, and Saffman. In: *SIAM Journal on Applied Mathematics* (2000)

[JMG+05] Jampel, H.D. ; Musch, D.C. ; Gillespie, B.W. et al.: Perioperative complications of trabeculectomy in the collaborative initial glaucoma treatment study (CIGTS). In: *American Journal of Ophthalmology* (2005)

[Joh06] Johnson, M.: What controls aqueous humor resistance? In: *Experimental Eye Research* (2006)

[JT10] Johnson, M. ; Tamm, E.R.: Biomechanics of Aqueous Humor Outflow Resistance. In: *Beshare J. and Dana R. : Encyclopedia of the Eye* (2010)

[Kor09] Korn, A.: Über einige Ungleichungen, welche in der Theorie der elastischen und elektrischen Schwingungen eine Rolle spielen. In: *Bull. Intern. Cracov. Akad. Umiejet* (1909)

[KR09] Kanschat, G. ; Riviére, B.: A strongly conservative finite element method for the coupling of Stokes and Darcy flow. In: *Journal of Computational Physics* (2009)

[KSS18] Kret, M. E. ; Sjak-Shie, E. E.: Preprocessing pupil size data: Guidelines and code. In: *Behaviour Research Methods* (2018)

[Kum03] Kumar, S.: Numerical Solution of ocular fluid dynamics. In: *Dep. Mech. Eng. Louisiana State University, Diploma thesis* (2003)

[KYK+14] Kim, Y. K. ; Yoo, B. W. ; Kim, H. C. et al.: Relative lens vault in subjects with angle closure. In: *BMC Ophthalmology* (2014)

[Lan89] Langtangen, H. P.: Conjugate gradient methods and ILU preconditioning of non-symmetric matrix systems with arbitrary sparsity patterns. In: *International Journal of Numerical Methods in Fluids* (1989)

[Lax02] Lax, Peter D.: *Functional Analysis.* John Wiley and Sons, Inc., 2002

[Lev11] Levin, L. A.: *Adler's physiology of the eye.* Saunders, 2011

[LGG03a] Llobet, A. ; Gasull, X. ; Gual, A.: Understanding Trabecular Meshwork Physiology: A Key to the Control of Intraocular Pressure? In: *Physiology 18, Nr. 5, p. 205-209* (2003)

[LGG03b] Llobet, A. ; Gasull, X. ; Gual, A.: Understanding Trabecular Meshwork Physiology: A Key to the Control of the Intraocular Pressure? In: *News in physiological sciences* (2003)

[LHP+13] Lee, R. Y. ; Huang, G. ; Porco, T.C. et al.: Differences in iris thickness among african americans, caucasian americans, hispanic americans, chinese americans, and Filipino-Americans. In: *Journal of Glaucoma* (2013)

[LL+16] Lee, R. Y. ; Lin, S.C et al.: Association Between Trabecular Meshwork Anteroposterior Length and Anterior Chamber Angle Width. In: *American Journal of Ophthalmology* (2016)

[LM72] Lions, J-L. ; Magenes, E.: *Non-homogeneous boundary value problems and applications*. Springer Verlag, 1972

[LS17] Larsen, C.L. ; Samuelson, T.W.: Managing coexistent cataract and glaucoma with iStent. In: *Survey of Ophthalmology* (2017)

[LSP03] Levy, T. ; Sanchez-Palencia, E.: On boundary conditions for fluid flow in porous media. In: *International Journal of Engeneering Science* (2003)

[LSY03] Layton, W. J. ; Schieweck, F. ; Yotov, I.: Coupling fluid flow with porous media flow. In: *SIAM Journal on Numerical Analysis* (2003)

[LY+18] Lv, H. ; Yang, J. et al.: Changes of intraocular pressure after cataract surgery in myopic and emmetropic patients. In: *Medicine (Baltimore)* (2018)

[MAGA14] Modarreszadeh, S. ; Abouali, O. ; Gaffarieh, A. ; Ahmadi, G.: Physiology of aqueous humor dynamic in the anterior chamber due to rapid eye movement. In: *Physiology and Behaviour* (2014)

[MAK03] Mittal, R. C. ; Al-Kurdi, A. H.: An efficient method for constructing an ILU preconditioner for solving large sparse nonsymmetric linear systems by the GMRES method. In: *Computers and Mathematics with Applications 45* (2003)

[Man90] Manouzi, H.: The Stokes problem and the mixed boundary conditions. In: *C. R. Math. Rep. Academy Sciences Canada* (1990)

[MAT09] MATLAB: *version 7.8.0.347 (R2009a)*. Natick, Massachusetts : The MathWorks Inc., 2009

[MBJ77] Minckler, D. S. ; Bunt, A. H. ; Johanson, G.W.: Orthograde and retrograde axoplasmic transport during acute ocular hypertension in the monkey. In: *Investigative Ophthalmology and Visual Science* (1977)

[McL00] McLean, W.: *Strongly elliptic systems and boundary integral equations*. Cambridge University Press, 2000

[MH07] Merchant, B. M. ; Heys, J. J.: Effects of variable permeability on aqueous humor outflow. In: *Applied Mathematics and Computation* (2007)

[MMH+18] Myers, J.S. ; Masood, I. ; Hornbreak, D.M et al.: Prospective Evaluation of Two iStent® Trabecular Stents, One iStent Supra® Suprachoroidal Stent, and Postoperative Prostaglandin in Refractory Glaucoma: 4-year Outcomes. In: *Advances in therapy* (2018)

[MO17] Mashige, K. P. ; Oduntan, O. A.: Axial length, anterior chamber depth and lens thickness: Their intercorrelations in black South Africans. In: *African Vision and Eye Health* (2017)

[MRK14] Mitra, A. ; Ramakrishnan, R. ; Kader, M.A.: Anterior segment optical coherence tomography documentation of a case of topiramate induced acute angle closure. In: *Indian Journal of Ophthalmology* (2014)

[MSG+08] Martin, H. ; Stachs, O. ; Guthoff, R. et al.: In vivo determination of the human crystalline lens shape with clinically established measurement methods. In: *IFMBE Proceedings, volume 22* (2008)

[MT02] Matthies, G. ; Tobiska, L.: The inf-sup condition for the mapped $Q_k - P_{k-1}^{disc}$ element in arbitrary space dimensions. In: *Computing 69* (2002)

[MTW02] Mardal, K. ; Tai, X.C. ; Winther, R.: A robust finite element method for Darcy-Stokes flow. In: *SIAM Journal of Numerical Analysis* (2002)

[MV77] Meijerink, J. A. ; Vorst, H. A. V.: An iterative solution method for linear systems of which coefficient matrix is a symmetric M-Matrix. In: *Mathematics of Computation* (1977)

[MVMP00] Michelson, G. ; Viestenz, A. ; Müller, E. ; Pogorelov, P.: *Das Auge in Zahlen*. `https://www.onjoph.net/patinfo/funktion/zahlen.html`. Version: 2000

[MX07] Mu, M. ; Xu, J.: A two-grid method of a mixed Stokes-Darcy model for coupling fluid flow with porous media flow. In: *SIAM Journal of Numerical Analysis* (2007)

[MZZ+14] Mei, L. ; Zhonghao, W. ; Zhen, M. et al.: Lens thickness and position of primary angle closure measured by anterior segment optical coherence tomography. In: *Eye (The Scientific Journal of the Royal College of Ophthalmologists)* (2014)

[NHF+11] Nongpiur, M. E. ; He, M. ; Friedman, D.S. et al.: Lens vault, thickness and position in Chinese subjects with angle closure. In: *Ophthalmology* (2011)

[NMBW+95] Nouri-Mahdavi, K. ; Brigatti, L. ; Weitzmann, M. et al.: Outcomes of trabeculectomy for primary open-angle glaucoma. In: *Ophthalmology* (1995)

[NPW15] Neff, P. ; Pauly, D. ; Witsch, K.-J.: Poincare meets Korn via Maxwell: extending first Korn's inequality to incompatible tensor fields. In: *Journal of Differential Equations* (2015)

[ON07] Ooi, E.-H. ; Ng, E. Y.-K.: Simulation of aqueous humor hydrodynamics in human eye heat transfer. In: *Computers in Biology and Medicine* (2007)

[P+16] Pascu, A. T. et al.: Evaluations and geometrical measurements of the human eye in order to establish the design parameters for the customized contact lens. In: *IOP Conference series: Materials Science and Engineering* (2016)

[PJGM14] Philipp, E. ; Jiri, N. ; Günther, S. ; Michael, S.: Nanoidentation derived mechanical properties of the corneoscleral rim of the human eye. In: *Key Engineering Materials* (2014)

[PW17] Plange, N. ; Walter, P.: *Basiswissen Augenheilkunde*. Springer Verlag, 2017

[QB06] Quingley, H.A. ; Broman, A.T.: The number of people with glaucoma worldwide in 2010 and 2020. In: *British Journal of Ophthalmology* (2006)

[Qua09] Quarteroni, A.: *Numerical models for differential problems*. Springer Verlag Italia, Milan, 2009

[RA03] R. Adams, J. F.: *Sobolev spaces*. Academic Press, 2003

[Ran17] Rannacher, R.: *Numerik partieller Differentialgleichungen*. Heidelberg University Publishing, 2017

[RDF+06] Rosen, A. M. ; Denham, D. B. ; Fernandez, V. et al.: In vitro dimensions and curvatures of human lenses. In: *Vision Research* (2006)

[RKA06] Rabsilber, T. M. ; Khoramnia, R. ; Auffarth, G. U.: Anterior chamber measurements using Pentacam rotating Scheimpflug camera. In: *Journal of Cataract and Refractive Surgery* (2006)

[RY04] Riviére, B. ; Yotov, I.: Locally Conservative Coupling of Stokes and Darcy Flows. In: *SIAM Journal on Numerical Analysis* (2004)

[S+05] Selbach, J. M. et al.: Episcleral Venous Pressure in untreated primary open angle and normal tension glaucoma. In: *Ophthalmologica* (2005)

[Saf71] Saffman, P. G.: On the boundary condition at the surface of the porous medium. In: *Stud. Applied Mathematics* (1971)

[SAY+12] Shiau, T. ; Armogan, N. ; Yan, D. B. et al.: The role of EVP in glaucoma associated with Sturge-Weber syndrome. In: *Journal of AAPOS* (2012)

[SB11] Sharaawy, T. ; Bhartiya, S.: Surgical management of glaucoma: Evolving paradigms. In: *Indian Journal of Ophthalmology* (2011)

[SDC+17] Sun, X. ; Dai, Y. ; Chen, Y. et al.: Primary angle closure glaucoma: What we know and what we do not know. In: *Progress in retinal Eye Research* (2017)

[SE11] Siggers, J. H. ; Ethier, C. R.: Fluid mechanics of the Eye. In: *Annual Review on Fluid Mechanics* (2011)

[SM11] Sit, A. J. ; McLaren, J. W.: Measurement of episcleral venous pressure. In: *Experimental Eye Research* (2011)

[SS86] Saad, Y. ; Schultz, M. H.: A generalized minimal residual algorithm for solving nonsymmetric linear systems. In: *Journal on Scientific and Statistical Computing* (1986)

[Ste90] Stenberg, R.: A technique for analysing finite element methods for viscous incompressible flow. In: *International Jopurnal of Numerical Methods in Fluids* (1990)

[Tem77] Temam, R.: *Navier-Stokes equations, theory and numerical analysis.* American Mathematical Society, 1977

[TLW+14] Tham, Y.-C. ; Li, X. ; Wong, T.Y. et al.: Global prevalence of glaucoma and projections of glaucoma burden through 2040: a systematic review and meta-analysis. In: *Ophthalmology* (2014)

[TRS13] Thieme, H. ; Renieri, G. ; Schuart, C.: Allgemeine Substanzklassen und Pharmakologie bei Glaukom. In: *Ophthalmologe 2013* (2013)

[TSPF18] Tůma, K. ; Stein, J. ; Průša, V. ; Friedmann, E.: Motion of the vitreous humor in a deforming eye-fluid-structure interaction between a nonlinear elastic solid and viscoelastic fluid. In: *Applied Mathematics and Computation* (2018)

[UNGD08] Urquiza, J. ; N'Dri, D. ; Garon, A. ; Delfour, M.: Stokes and Darcy equations. In: *Applied Numerical Mathematics* (2008)

[V+04] Vass, C. et al.: Human aqueous humor viscosity in cataract, primary angle glaucoma and pseudoexfoliation syndrome. In: *IOVS an Arvo Journal* (2004)

[VR+12] Villamarin, A. ; Roy, S. et al.: 3D Simulation of the aqueous flow in the human eye. In: *Medical Engineering and Physics* (2012)

[WBS+10] Wilczynski, M. ; Bartela, J. ; Synder, A. et al.: Comparison of internal anterior chamber diameter measured with ultrabiomicroscopy with white-to-white distance measured using digital photography in aphakic eyes. In: *European Journal of Ophthalmology* (2010)

[WO16] Wang, W. ; Others: Fluid and structure coupling analysis of the interaction between aqueous humor and iris. In: *BioMedical Engeneering Online* (2016)

[XXX08] Xie, X. ; Xu, J. ; Xue, G.: Uniformly-stable finite element methods for Darcy-Stokes-Brinkman models. In: *Journal of Computational Mathematics* (2008)

[ZB15] Zetterström, C. ; Behndig, A.: Changes in IOP after cataract surgery: analysis of the Swedish National Cataract Register data. In: *Journal of Cataract and Refractive Surgery* (2015)